The influence of composition, processing and temperature on the Young's modulus of elasticity of carbon-bonded refractories

By the Faculty of Maschinenbau, Verfahrens- und Energietechnik
of the Technische Universität Bergakademie Freiberg

approved

Thesis

to attain the academic degree of

Doktor - Ingenieur
(Dr. - Ing.)

submitted by **Dipl. - Ing. Joern Werner**

born on the 1st December 1983 in Berlin

Assessor: Prof. Dr.-Ing. habil. Christos G. Aneziris
Prof. Dr.-Ing. habil. Horst Biermann

Date of the award:Freiberg, 3rd November 2014

Versicherung

Hiermit versichere ich, dass ich die vorliegende Arbeit ohne unzulässige Hilfe Dritter und ohne Benutzung anderer als der angegebenen Hilfsmittel angefertigt habe; die aus fremden Quellen direkt oder indirekt übernommenen Gedanken sind als solche kenntlich gemacht.

Die Hilfe eines Promotionsberaters habe ich nicht in Anspruch genommen. Weitere Personen haben von mir keine geldwerten Leistungen für Arbeiten erhalten, die nicht als solche kenntlich gemacht worden sind. Die Arbeit wurde bisher weder im Inland noch im Ausland in gleicher oder ähnlicher Form einer anderen Prüfungsbehörde vorgelegt.

03. November 2014 Dipl. - Ing. Joern Werner

Declaration

I hereby declare that I completed this work without any improper help from a third party and without using any aids other than those cited. All ideas derived directly or indirectly from other sources are identified as such.

I did not seek the help of a professional doctorate-consultant. Only those persons identified as having done so received any financial payment from me for any work done for me. This thesis has not previously been published in the same or a similar form in Germany or abroad.

3rd November 2014 Dipl. - Ing. Joern Werner

Acknowledgement

This work was carried out at the Institute of Ceramics, Glass and Construction Materials TU Bergakademie Freiberg.
First of all I would like to thank my supervisor Prof. Dr.-Ing.-habil. Christos G. Aneziris for the opportunity to carry out that study and for the dialogues. Furthermore, I would like to thank all my colleagues at the institute for the discussions and additional support. A special thanks I would like to address to Prof. Jose de Anchieta Rodrigues from the Federal University of Sao Carlos who supported my work from the very beginning with fruitful conversations.
Many thanks to my family and my friends who always supported me and without them I would not have been able to accomplish that work.
Finally, I would like to gratefully acknowledge the German Research Foundation (DFG) for supporting the Collaborative Research Center CRC 920 and the integrated MGK for offering a great variety of further education possibilities.

Contents

List of Symbols

Symbol	Units	Description
b	mm	Width of a rectangular bar
c_p	$\mathrm{J\,K^{-1}\,m^{-3}}$	Heat capacity per volume unit at constant pressure
d	mm	Diameter of a rod
d_max	mm	Maximum alumina particle size of an experimental composition
f_f	Hz / $\mathrm{s^{-1}}$	Flexural or torsional resonance frequency
f_t	Hz / $\mathrm{s^{-1}}$	Flexural or torsional resonance frequency
h	mm	Height of a rectangular bar
l	mm	Length of a rod or a rectangular bar
m	g	Mass of a specimen
v_l	$\mathrm{m\,s^{-1}}$	Propagation velocity of a longitudinal ultrasonic wave
v_t	$\mathrm{m\,s^{-1}}$	Propagation velocity of a transverse ultrasonic wave
C_1	$-$	Geometric constant of proportionality ≈ 1 for open cell foams
E	GPa	Young's modulus
E_0	GPa	Young's modulus either at 0 K, 0 porosity or without cracks
E_{ad}	GPa	Adiabatic Young's modulus
E_D	GPa	Dynamically determined Young's modulus
E_R	GPa	Young's modulus of a composite according to the Reuss boundary
E_S	GPa	Young's modulus of the strut material of an open cell foam
E_{St}	GPa	Statically determined Young's modulus
E_T	GPa	Isothermal Young's modulus

E_V	GPa	Young's modulus of a composite according to the Voigt boundary
E^*	GPa	Young's modulus of an open cell foam
F	N	Load in a load deflection experiment
G	GPa	Modulus of rigidity or shear modulus
G_f	$\mathrm{J\,m^{-2}}$	Specific fracture energy
K	GPa	Bulk modulus
L	mm	Distance between the supports in the three point bending test
P	–	Pore volume fraction
Q^{-1}	–	Damping of a vibration
R	K	Thermal shock resistance parameters
R'	K	Thermal shock resistance parameters
R''''	K	Thermal shock damage parameters
R_{st}	K	Thermal shock damage parameters
T	°C	Temperature
T_0	K	Temperature equal to 0 K
α	$\mathrm{K^{-1}}$	Linear thermal expansion coefficient
β	$\mathrm{K^{-1}}$	Volume thermal expansion coefficient
γ	–	Shear strain
δ	–	Logarithmic decrement of a vibration
ε	–	Strain
λ	$\mathrm{W\,m^{-1}\,K^{-1}}$	Thermal conductivity
ν	–	Poisson's ratio
π_P	%	Porosity (calculated) after pressing
π_a	%	Apparent porosity determined by water immersion
ρ_b	$\mathrm{g\,cm^{-3}}$	Bulk density
ρ_t	$\mathrm{g\,cm^{-3}}$	Theoretical density
ρ_S	$\mathrm{g\,cm^{-3}}$	Density of the strut material of an open cell foam
ρ^*	$\mathrm{g\,cm^{-3}}$	Density of an open cell foam
σ	$\mathrm{N/mm^2}$	Tensile stress or materials strength (e.g. in bending)
τ	$\mathrm{N/mm^2}$	Shear stress
ϕ	–	Volume fraction

List of Figures

List of Tables

1. Introduction

Refractory materials are of major interest for almost all industries. There are applications in primary industries like metallurgy (e.g. lining in iron and non-iron metallurgy) and energy industry (e.g. lining for fossil fuel power plants and fuel rods in nuclear power plants) [Semler, 2014; Lee, 2012]. Besides, there are also numerous applications in high technology industries like aerospace industry and automotive industry. They can be found in the thermal protection for space shuttles, in particle filters for cars and in rotors, blades and rings for gas turbines [Pierson, 1997; Paul et al., 2012]. For the design of these products structural information of the used materials is essential.

Therefore, mechanical, thermal and corrosion properties have to be provided by material scientists. Especially for high temperature application it is necessary to consider the material reaction on temperature changes. Opening and closing of a furnace during service, start and stop of turbines or insertion of a Lambda-sonde into a steel melt are only a few examples of this particular demand [Buchebner et al., 2008; Poirier et al., 2005].

This behavior is called thermal shock resistance and was firstly addressed by Kingery [Kingery, 1955] and Hasselman [Hasselman, 1969] in a fracture mechanics view. Kingery already defined the important material properties to resist a thermal shock as the materials strength σ, Poisson's ratio ν, Young's modulus E and the coefficient of thermal expansion α. He introduced the so called resistance parameter:

$$R = \frac{(1-\nu)\cdot\sigma}{E\cdot\alpha} \tag{1.1}$$

which can be regarded as the temperature range ΔT to be resisted by a particular structure.

Nowadays, these properties are still used as indicators for the thermal shock behavior of refractory material. However, virtually always they are measured at room temperature and are used for the thermal shock prediction, although the service temperature range

is mostly at elevated temperatures (e.g. 1200 to 1600°C for emptying a steel ladle) [Boccaccini et al., 2008; Aneziris et al., 2007].

Besides the engineering need for exact material properties like Young's modulus, there is more information to be gained out of the knowledge of elastic measurements. They are one of the most direct way of measuring the strength of chemical bonding. Therefore, the basic data for the calculation of the theoretical strength of crystals can be obtained by elastic measurements. Furthermore, microstructural analysis of materials can be carried out according to the results of the measurements. Elastic properties are also used for the interpretation of wave propagation in the earth as a basis for the fundamental understanding of its composition [Wachtman, 1969; Patapy et al., 2012; Luz et al., 2013; Werner et al., 2013].

This work deals with the elastic properties of carbon-bonded refractories. These materials are widely used for example in steel making. They can be found in linings of basic oxygen converters or as functional components, like submerged entry nozzles or mono bloc stoppers in continuous steel making. Knowledge about the room temperature and high temperature elasticity of this material could enable engineers and scientists to improve products (complete linings) and materials (composition change). The so called impulse excitation technique (IET) was used to determine the dynamic elastic constants. A broad range of factors influencing the microstructure of the material were investigated (e.g. graphite content, oxide particle size, bonding system, and more). Furthermore, the application of IET enabled Young's modulus measurements up to 1450°C, to address the lack of data regarding the thermal shock resistance. An overview of the gained information will be given. These results will be discussed by comparison to the literature and well known models from one phase oxide refractories. The results shown and discussed in this thesis are mainly based on own recent publications [Werner et al., 2013; Werner and Aneziris, 2013; Werner et al., 2014].

This work should be regarded as a starting point for a deeper understanding of the microstructure and thermal shock resistance of carbon-bonded refractories.

2. State of the art

The following chapter gives an overview of the elastic behavior of carbon-bonded alumina and its relationship to the materials microstructure. Therefore, at first an overview about the elasticity of ceramics will be given, followed by the microstructure and high temperature dependence of the elastic moduli. Furthermore, an overview of the elasticity measurement methods will be provided. Subsequently, the contribution of Young's modulus to the calculation and estimation of the thermal shock resistance will be discussed. Finally, a brief introduction of carbon-bonded alumina as the material investigated in this study will be given.

2.1. Elasticity of ceramics

2.1.1. Fundamentals

One of the biggest drawbacks of ceramics is their brittle fracture fail behavior. There is no actual plastic deformation for these materials. Hence, their application is reduced due to their poor impact resistance [Kingery et al., 1976].

Young's modulus is closely related to inter atomic bonding forces. By applying a stress to a crystal lattice, the distance of the atoms can be extended or decreased. This is the physical origin of Hooke's law, which the elastic deformation of ceramics follows [Carter and M.G.Norton, 2007a]. According to Hooke's law stress is directly proportional to the strain:

$$\sigma = E\epsilon \tag{2.1}$$

where σ is the stress (tensile), E is Young's modulus and ϵ the strain. Similarly, there is an expression for the shear stress:

$$\tau = G\gamma \tag{2.2}$$

Tab. 2.1.: Elastic properties of ceramic materials, taken from Salmang and Scholze [2007]; Pierson [1997]; McKee [1973]

Material	E	G	K	ν
	GPa			
Al_2O_3	410	165	255	0.23
MgO	310	130	155	0.17
ZrO_2	190	75	140	0.27
Porcelain	76	32	38	0.17
Mullite	100	42	56	0.2
SiC	480	200	240	0.17
Si_3N_4	295	115	235	0.29
Pyrolytic graphite	$28-31$	-	-	-
Glassy carbon	$14-33$	-	-	-

where G is the shear modulus or modulus of rigidity and γ the shear strain. The deformation of a sample due to a tension is connected to a change in thickness. A characterization of this change is the Poisson's ratio:

$$\nu = -\frac{\Delta d/d}{\Delta l/l} \tag{2.3}$$

It relates to the elastic moduli as follows:

$$\nu = \frac{E}{2G} - 1 \tag{2.4}$$

In case of isotropic pressure the elastic response is called bulk modulus K. There are several equations for the translation of the elastic constants into each other (e.g. $E \rightarrow G$). They can be found for example in Carter and M.G.Norton [2007b].

In Table 2.1 the elastic properties of some ceramic materials are shown. However, these are virtually theoretical values. Most of these materials are composed of a microstructure with defects (impurities, pores, grain boundaries). These microstructure variations have a strong impact on the elasticity.

Also characteristic for ceramic materials is a behavior called an-elasticity. Hereby, the deformation made to a body is not instantaneously fully recoverable after the removal of stress [Kingery et al., 1976]. This behavior especially can be observed at high temperatures due to grain boundary sliding and softening [Wachtman and Lam, 1959; Chang, 1959]. Moreover, there are several nonlinear effects which can not be explained by linear elastic theory. Therefore, researchers especially from the field of earth sciences

addressed this problem by the introduction of a "new" material class. Guyer and Johnson [2009] defined the so called "Nonlinear mesoscopic materials" as materials exhibiting "extreme/unusual elastic behaviors".

Materials like ceramics, rocks and soil should be regarded as a mortar-tile system in which the mortar is the weak bond between the stiff tiles. One of the key conclusions of this model is that the minor phase (mortar) determines the global properties of the whole system. For example in a carbon-bonded alumina or magnesia the Young's modulus ranges typically from 5 to 80 MPa [Manhart et al., 2005; Buchebner et al., 2008]. Considering the Young's modulus from Table 2.1, alumina and magnesia show a 3 to 5 times higher E. Apparently the graphite or the pyrolytic carbon obtained from the binder phase is determining the elastic properties of the composite.

Phenomena related to this material class are well known for refractory materials. For example the strain relaxation when an applied stress is removed or the shift of resonance frequency of a bar in dependence on the excitation energy [Pereira et al., 2010, 2011; Manhart and Harmuth, 2009]. A further example is the hysteresis in stress vs. strain curves of carbon-bonded materials [Schmitt et al., 2000]. All of these phenomena classify these materials as nonlinear. Therefore, one has to take into account, that ceramics and especially refractories do not exhibit exact linear elastic behavior. This is already a strong field of interest in the refractory research community and there is much work left to do [Belrhiti et al., 2013].

2.1.2. Microstructural dependence of elastic moduli

Talking about elastic constants one has to take into account that they are always related to isotropic bodies or more exactly to the materials lattice. However, defects like grain boundaries, crystalline structure and dislocations have to be considered interpreting experimental data.

> "Therefore, nearly the whole technique of engineering continuum mechanics is based on semi-intuitively defined effective properties of non-homogeneous materials." [Mileiko, 1997]

Most ceramics and virtually all refractories are two or more phase systems (considering porosity as a phase). For the computation and modeling of these microstructures, the literature provides a broad range of models and equations. The Young's modulus of a composite can be derived from the moduli of the pure elements. Composite constituents

aligned either parallel or perpendicular to an applied stress are the extreme cases. Two boundary models are established addressing these conditions.

Voigt [1889] assumed layers of each composite phase aligned parallel to the applied stress. A further assumption is an equal strain level in each constituent, hence the Young's modulus of the composite is:

$$E_V = \phi_2 E_2 + (1 - \phi_2) E_1 \tag{2.5}$$

where ϕ_2 is the volume fraction of phase two and E_2 its Young's modulus. The second boundary model by Reuss [1929] assumes a perpendicular alignment of the phases to the applied stress, which has to be equal in each constituent:

$$\frac{1}{E_R} = \frac{\phi_2}{E_2} - \frac{1 - \phi_2}{E_1} \tag{2.6}$$

A more precise approach was suggested by Hashin and Shtrikman [1963]. This set of bounds was shown to be the most precise for the determination of the elastic constants of a composite material with arbitrary phase geometry. However, its validity is limited to quasi-homogeneous and isotropic materials. For the bulk modulus the Hashin-Shtrikman bounds are given for $K_2 > K_1$ and $G_2 > G_1$,

$$K_L = K_1 + \frac{\phi_2}{1/(K_2 - K_1) + [3(1 - \phi_2)]/(3K_1 + 4G_1)} \tag{2.7}$$

$$K_U = K_2 + \frac{1 - \phi_2}{1/(K_1 - K_2) + 3\phi_2/(3K_2 + 4G_2)} \tag{2.8}$$

where K_U and K_L represent the upper and lower bounds [Kingery et al., 1976; Carter and M.G.Norton, 2007b]. Considering the composite nature of carbon-bonded alumina, these models will be discussed further in results and discussions. Reducing the amount of the second phase to zero would result in a model considering the porosity. In this case Young's modulus of the composite will be decreased remarkably ($E_2 = 0$), according to the introduced models.

There can be found a tremendous amount of models for $E(P)$ in the literature, either analytic or empirical. MacKenzie [1950] first addressed the problem of porosity in a solid body under the assumption of spherical pores. Coble and Kingery [1956] compared experimental results with MacKenzies model. It appeared to be valid for a porosity range of $0 - 0.5$ pore volume fraction.

Tab. 2.2.: Models describing $E(P)$ found in the literature; m, b and c are parameters to be fitted empirically, E^* and ρ^* are the properties of the foam

Model	Reference
$E = E_0 e^{-bP}$	Spriggs [1961]
$E = E_0(1-P)^m$	Phani and Niyogi [1986]
$E = E_0 \frac{(1-P^2)}{1+(c^{-1}-1)P}$	Nielsen [1984]
$\frac{E^*}{E_S} = C_1 \left(\frac{\rho^*}{\rho_S}\right)^2$	Gibson and Ashby [1997] for open cell foams

In the early 1960s several researchers found empirical models for the relationship of Young's modulus on the porosity. However, none of them recognized the pore shape as an influencing factor [Spriggs, 1961; Spriggs et al., 1962; Knudsen, 1962]. These models can basically be described as an exponential dependency of E on P as can be seen in Table 2.2. However, this equation does not meet the boarder conditions $P = 0 \rightarrow E = E_0$ and $P = 1 \rightarrow E = 0$ respectively.

Therefore, Nielsen [1984] and Phani and Niyogi [1986] suggested two different models. These satisfy the boundary conditions declared above and could be applied therefore in a broader range of porosity. Nielsen [1984] also took the influence of the pore shape into account as he introduced the shape factor c in his equation (see Table 2.2). More recent works improved this approach by adding several pore shape and orientation factors [Andersson, 1996; Boccaccini and Boccaccini, 1997].

The applicability of these models strongly depends on the porosity range. For reasonable small porosity ($0 < P < 0.5$) the exponential relationship matches the experimental data quite well. However, for porosity been higher than 0.5 other approaches have to be taken into account. As mentioned Phani and Niyogi [1986] proposed a power function for this correlation. Furthermore, Gibson and Ashby [1997] proposed and summarized models for cellular solids. They defined E as a function of relative density of the foam and the Young's modulus of its bulk material. In terms of open cell foams, which were investigated within this thesis, they proposed a model to be found in Table 2.2. Recent studies proved the validity of this model by experimental and analytic means [Knackstedt et al., 2005; Zhang et al., 2012; Bourret et al., 2013]. Gibson and Ashby [1997] suggested a value of approximately one for the geometric constant of proportionality C_1.

A further microstructural influence on E are microcracks. Their role in terms of crack propagation will be discussed in subsection 2.3. Stiffler and Hasselman [1983] assumed microcracks as extremely thin inclusions of zero stiffness. They proposed a model to

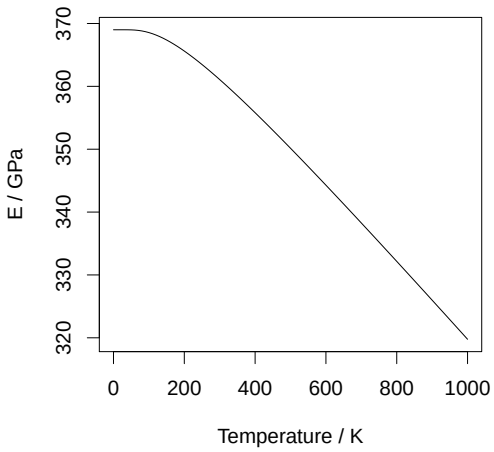

Fig. 2.1.: Temperature dependency of Young's modulus of alumina modeled according to equation 2.9, parameters taken from Wachtman et al. [1961]

compute the shear modulus of microcracked materials, in the form of the Hashin and Shtrikman [1963] equation introduced earlier. So microcracks can be regarded as a single phase in a composite or as porosity in terms of elasticity.

It was shown that the elastic properties of ceramics are strongly related to its crystal lattice as well as to its microstructure. Several models were introduced to give a brief overview of the existing prediction possibilities.

2.1.3. High temperature dependence of elastic moduli

Due to the mentioned relationship between the crystal lattice and the elastic properties of ceramics, one will expect a strong dependence of them on the temperature. The increase of kinetic energy due to a temperature increase contributes to an extension of the atomic distance. Hence, Young's modulus should decrease with increasing temperature. Several studies confirmed this relationship for one phase oxide ceramics [Schwartz, 1952; Wachtman and Lam, 1959; Spriggs et al., 1964; Soga and Anderson, 1966; Gerlich and Fisher, 1969]. Wachtman et al. [1961] suggested a model for this relationship which satisfies the linear decrease of E at high temperatures as well as the zero slope area at low temperatures (see Figure 2.1 as well):

$$E = E_0 - BTexp(-T_0/T) \tag{2.9}$$

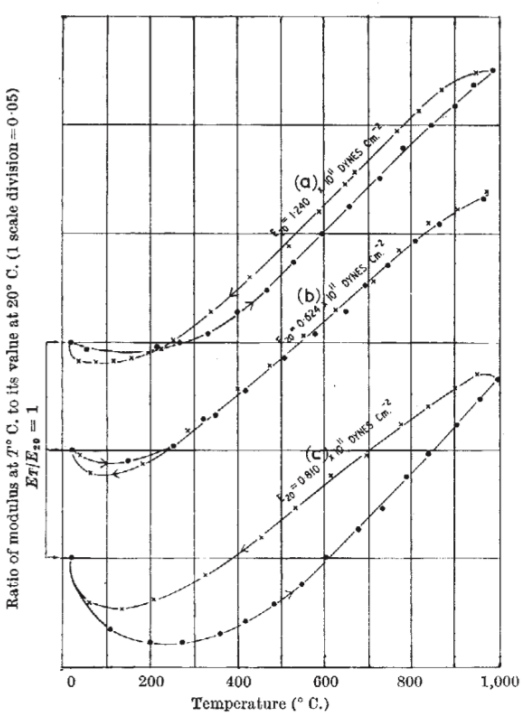

Fig. 2.2.: Temperature dependency of Young's modulus of graphite; Illustration taken from [Mason and Knibbs, 1960]

E_0 represents Young's modulus at 0 K and B is a material dependent constant. However, it was also observed that Young's modulus decreases nonlinear at higher temperatures (depending on the material e.g. $\sim 1000\,^{\circ}\mathrm{C}$ for alumina). There was no such behavior for single crystals (e.g. ruby) found. Therefore, this nonlinear decrease in polycrystalline oxide ceramics was attributed to a grain boundary slip [Wachtman and Lam, 1959; Chang, 1959].

Mason and Knibbs [1960] investigated the high temperature Young's modulus of graphite (see Figure 2.2) and found an increase instead of the expected decrease for $E(T)$. They attributed their result mainly to the strong expansion of the c-axes of graphite crystals. Thus, voids in the material could be filled resulting in a stiffening effect. They also reported a hysteresis effect during cooling and explained it with a plastic yielding due to a suppressed expansion of overcrowding neighbor crystals. This is of important interest for this study, since graphite is a main constituent of carbon-bonded refractories.

For composite materials and for materials undergoing phase transformations during heating or cooling, the relationship $E(T)$ is mostly not linear. Gault et al. [1985] showed this

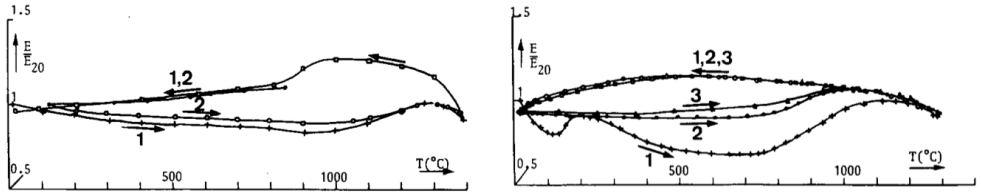

(a) Aliumina-zirconia-glassy phase composite (AZ) **(b)** Alumina-mullite-zirconia composite (AMZ)

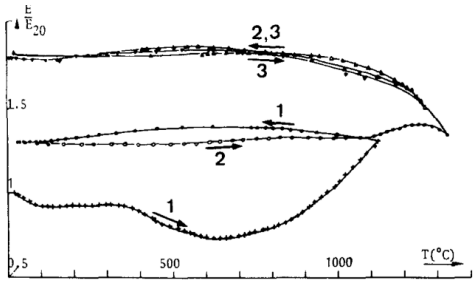

(c) Carbon-bonded alumina (CBA)

Fig. 2.3.: Young's modulus dependence of composite refractories on the temperature; Figures taken from [Gault et al., 1985]

nonlinear $E(T)$ behavior in their study. They investigated an alumina-mullite-zirconia composite (AMZ), an alumina-zirconia-silica composite (AZ), an alumina-chromium(III)oxide (AC) and a carbon-bonded alumina (CBA).

Besides the AC composite, which exhibited almost exact linear behavior, all composites showed nonlinear behavior. This behavior was attributed to microstructural changes during heating and cooling. For the zirconia containing composition there is a phase transformation from the monoclinic to the tetragonal crystal system, which is the denser one. They reported an increase of E in the temperature range from 950 to 1250 °C (shown in Figure 2.3a) and correlated this to dilatometry measurements showing the phase transformation in the same temperature range. However, a densification of one phase might also contribute to an increase in porosity of the composite, resulting in a lower E. Fogaing et al. [2006] showed a decreasing effect of this phase transformation for pure zirconia. Hence, the conclusion of Gault et al. [1985] regarding the observed increase of E might not be entirely correct. This stiffening effect could also be attributed to a thermal expansion mismatch of the constituents (zirconia, alumina, glassy phase). As described for graphite above, this could contribute to a void closing and therefore to an increase of E.

The $E(T)$ behavior of the alumina-mullite-zirconia composite (AMZ) is quite comparable

to AZ with an increase up to 1000 °C (see Figure 2.3b). A proper explanation for this behavior was not given by the authors. They attributed the hysteresis between cooling and heating to either the phase transformation in zirconia or a microcrack closure.

Moreover, the results for the carbon-bonded alumina were not explained properly by the authors. They attributed the "unstable and markedly irreversible increase" during heating to the carbon and/or to other elements, such as silicon. This conclusion reveals a main drawback of this study; the lack of information about the material they used. There was no hint regarding the initial condition of this material at the beginning of the measurements. Especially, the condition of the carbon phase (cured or already pyrolysed) would be of interest for the interpretation of these results.

A more recent study from Baudson et al. [1999] about carbon-bonded magnesia revealed similar results. The samples were pretreated in a pyrolysis up to 1000 °C in a CO atmosphere. They found a strong increase of E above 1100 °C and attributed this to a bridging of the magnesia particles. Furthermore, they revealed an oxidation of the pyrolytic carbon derived from the resin in the temperature range from 600 to 800 °C.

Manhart et al. [2005] as well as Buchebner et al. [2008] showed the transformation of resin and pitch into pyrolytic carbon in terms of carbon-bonded magnesia from 25 to 1500 °C. They observed a decrease of E from 350 to 600 °C. The overall amount of this decrease is influenced by the residual carbon content. This depression is caused by the release of volatile parts of the resin [Cowlard and Lewis, 1967]. The same was observed for pitch bonded material. At higher temperatures Young's modulus is slightly decreased. Furthermore, Buchebner et al. [2008] performed thermal cycles from 800 to 1400 ° at the in-situ cured samples (see Figure 2.4) to gather information regarding structural changes within the ladle lining. They observed a hysteresis but reversible behavior. During cooling E decreased significantly and increased at reheating respectively. In combination with modulus of rupture measurements they gained information for future magnesia-carbon brick development and life time prediction.

2.2. Measurement of elastic moduli

In general there are two ways to determine elastic moduli experimentally. They can be divided into quasi-static and dynamic methods. The terms static and dynamic are roughly bound to the applied strain rate. The static tests introduce large strains at low strain rates whereas for dynamic tests the opposite holds. This section will introduce

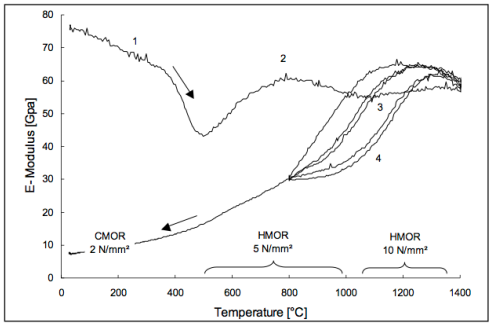

Fig. 2.4.: Young's modulus dependence of cured carbon-bonded magnesia refractories on the temperature (Cycling from 800 to 1400 °C); Figure taken from [Buchebner et al., 2008]

these methods and discuss their results in terms of comparability and applicability for engineering purposes [Wolfenden, 1990].

2.2.1. Quasi-static method

According to Hooke's law, Young's modulus is the slope of the stress strain curve. Thus, it should be easy to obtain any elastic constant (E, G, K and ν) out of a load-deflection test in which the load corresponds to the elastic constants.

For refractory materials the three point bending test is most common for obtaining tensile stress values. A load is subjected to the center of a bar which is mounted on two supports. At the load application point, a compression stress can be found while on the other side of the bar a tensile stress occurs. This outer fiber stress is defined as:

$$\sigma = \frac{3FL}{2bh^2} \tag{2.10}$$

where F is the load, L is the distance between the supports, b the width and h the height of the bar. The Young's modulus can be calculated according to the following equation:

$$E = \frac{FL^3}{4bh^3y} \tag{2.11}$$

where y represents the deflection. However, especially for refractory materials there are also contributions to this deflection of slow crack growth and other nonelastic behaviors. These effects actually increase y resulting in an underestimation of E due to the samples apparent bending behavior. Therefore, the determination and interpretation of Young's modulus, shear modulus or bulk modulus from mechanical load deflection should be

carried out under consideration of these effects [Bradt, 1993]. Typical standards for determining the Young's modulus from the load-deflection curve of refractory materials are ASTM C469 / C469M, ASTM E111 and DIN EN 843-2.

2.2.2. Dynamic methods

The so called dynamic methods are a nondestructive way to obtain the elastic moduli. The propagation of waves in a solid is the basic concept of these methods. They can be divided into the ultrasonic wave (or pulse) velocity method and the resonance frequency method.

Ultrasonic wave velocity method

This is the most accurate measurement method for the elastic moduli [Wachtman, 1969]. A plane wave is propagated in a specimen. Two types of waves are of special interest. A wave which vibration direction is equal to the propagation direction is called longitudinal, whereas a transverse wave is characterized by a perpendicular vibration direction to the propagation. Basically, the elastic moduli can be derived from the time a wave needs to transit through the material. Therefore, several equations have been proposed [Bancroft, 1941; Hudson, 1943; Davies, 1948; Stanford, 1950; Tu et al., 1955]. However one has to take into account the border conditions. An important influence on these equations have the specimen dimensions. For sufficient high frequencies of the excitation wave the specimen dimensions become infinite compared to the wavelength. In this case Young's modulus can be calculated by the following equation:

$$E = \rho v_l^2 \frac{(1+\nu)(1-2\nu)}{1-\nu} \tag{2.12}$$

where ρ represents the density (bulk density) of the material, v_l^2 is the longitudinal wave velocity and ν is the Poisson's ratio. For the shear modulus a similar equation can be applied using the transverse wave velocity:

$$G = \rho v_t^2 \tag{2.13}$$

Poisson's ratio can be derived from G and E.
The actual measurement is carried out by bonding a piezoelectric transducer to a specimen and measuring the transit time of the excited sound waves. From this time one

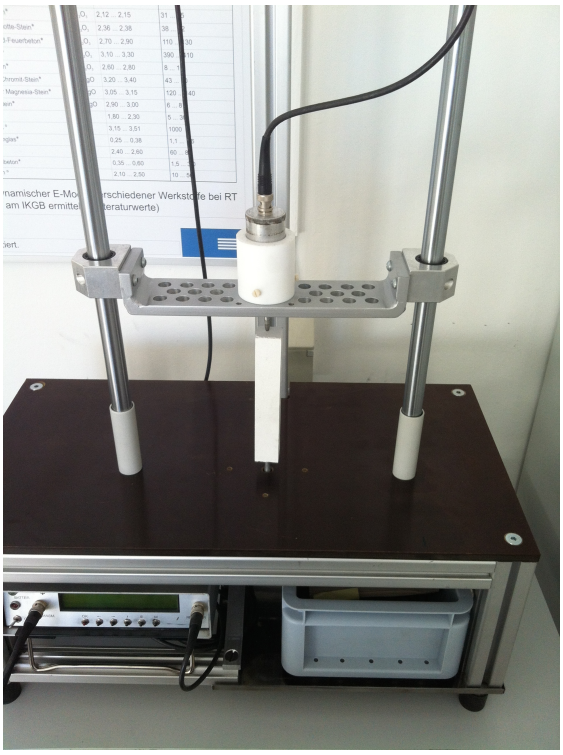

Fig. 2.5.: Ultrasonic testing device with plugged sample, transducer and receiver are above and below the sample

can calculate the elastic moduli according to equations 2.12 and 2.13. In Figure 2.5 the setup for the longitudinal wave introduction is shown. The transducer is situated above the sample whereas the receiver can be found below. As the method was developed throughout the world war two, the tremendous development of acoustical physics during that time contributed to its broad application in the following years. This has been summarized and discussed in the late 1950s by McSkimin [1959]. Its applicability for high temperature measurement was also proven. Nowadays, ultrasonic velocity measurements are used as a standard method for high temperature elastic moduli determination as well as for room temperature investigations [Auvray et al., 2001; Chotard et al., 2008; Patapy et al., 2010]. For concrete it is used to asses the structure and its properties (e.g. strength) [Jain et al., 2013]. Furthermore, Carreon et al. [2009] found a correlation between the ultrasonic velocity and the hardness of the investigated alumina-zirconia material, which showcase the versatile application possibilities of this measurement method.

ASTM E494 - 10 and EN 12504-4:2004 are standards describing the actual measurement

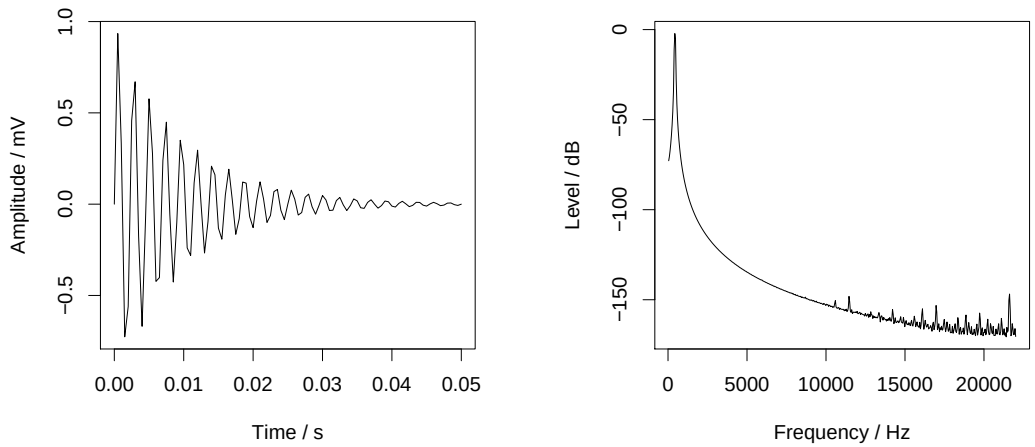

(a) Damped 440 Hz sound signal input **(b)** FFT computed frequency spectrum

Fig. 2.6.: The signal converting way of the impulse excitation technique; a 440 Hz sound signal input is transformated into a frequency spectrum by a fast Fourier transformation (FFT) algorithm

setup and providing equations for the calculation of elastic constants.

Resonance frequency method

The resonance frequency method was firstly introduced by Förster [1937]. This method is based on the fact that every material has its own resonance frequency. Pickett [1945a,b] proposed equations for the computation of the elastic constants from the resonance frequency for several specimen shapes. A first detailed description of the application of this method and the computation of the elastic constants was given by Spinner and Tefft [1961]. Nowadays ASTM E1875 - 08 and ASTM E1876 - 09 are standards describing extensively the measurement setup and the calculation of elastic moduli for several specimen shapes. A sample can either be excited constantly by a piezoelectric transducer or by a mechanical impulse. The signal input is obtained by a piezoelectric receiver or laser vibro meter; for the mechanical impulse method (also known as impulse excitation technique) a microphone is used. The transducer method can be regarded as a frequency scan. Once the resonance frequency of the specimen is introduced, the receiver signal will increase immediately (resonance).

Only the impulse excitation technique (IET) was used in this study. Therefore, it will be introduced more detailed here. IET provides an audio signal as output (shown in Figure

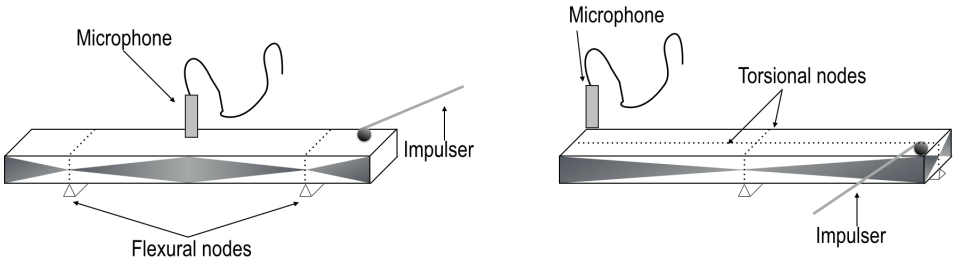

(a) Flexural mode **(b)** Torsinal mode

Fig. 2.7.: Schematic view of impulse excitation setup for a rectangular bar according to ASTM E1876

2.6). This signal is subsequently divided into single sine and cosine waves using the fast Fourier transformation algorithm to obtain a frequency spectrum. Nowadays, this is done automatically in most software assembled to the measurement devices. From the spectrum of this input signal one can obtain the flexural or torsional frequency (f_f or f_t respectively). There are specific vibration modes for bars, rods and discs corresponding to the flexural and torsional frequency (see Figure 2.7 for a rectangular bar). As can be seen in these figures the vibration is characterized by minimum and maximum amplitude ranges. To avoid a suppression of the vibration it is important to mount the specimen exactly in the minimum amplitude range, the so called nodes.

A further information to be gained from the impulse excitation measurement is the damping. Every natural oscillation exhibits a decay. A materials vibration decay, the so called damping, was attributed to the internal friction, defined as a materials capability to disperse the vibration energy [Puškár, 2001]. It is calculated using the difference of two subsequent amplitudes or a curve fit onto the decay signal. Especially for the damping determination it has to be taken care of the mentioned exact sample adjustment according to the vibration nodes.

The introduced elastic constants can be calculated in terms of impulse excitation technique according to Pickett [1945a,b] for a rectangular bar:

$$E = 0.9465 \frac{m f_f^2}{b} \frac{l^3}{h^3} T_1 \tag{2.14}$$

where m, b, l and t are the mass, width, length and thickness of the bar respectively.

f_f is the fundamental frequency in flexure and T_1 is a correction factor to be found in ASTM E1876. For the shear modulus the equation can be written:

$$G = \frac{4lmf_t^2}{bh}\frac{B}{1+A} \tag{2.15}$$

where f_t is the fundamental frequency in torsion, A and B are correction factors which can be calculated according to ASTM E1876. The calculation of damping is not described in a standard. Förster [1937] first defined damping as the logarithmic decrement δ of the vibration:

$$\delta = ln\frac{z_n}{z_{n+1}} \tag{2.16}$$

Where z_n and z_{n+1} are the n-th and $n+1$ amplitude of the damped vibration. Puškár [2001] linked δ with the damping Q^{-1} to:

$$Q^{-1} = \frac{\delta}{\pi} \tag{2.17}$$

This equation can be found in most literature about damping nowadays. Due to the development in computer technology it is common to fit an exponential function onto the obtained damped frequencies. The estimates of this function are then used to determine the damping, which is attracting more attention in the refractories research community in recent years. An interesting analytic study related the thermodynamic definition of damping to the actual measured damping and showed a relation between damping and crack appearance [Panteliou et al., 2001]. More recent studies related the damping to the thermal shock resistance of refractories. However, there is a great scattering in that data especially for the damping, indicating problems with the sample adjustment and the complicated nature of a thermal shock which can not be described by only one material parameter [Pereira et al., 2011; Traon et al., 2011].

In conclusion the resonance method is an appropriate way of elastic moduli determination. Its setup is well documented and its analysis well understood. Therefore, it can be found in many recent studies for high temperature and room temperature studies on elastic moduli of refractories [Werner and Aneziris, 2012, 2013; Werner et al., 2013, 2014; Böhm et al., 2013; Quadling et al., 2013; Traon et al., 2013; Luz et al., 2013; Souza et al., 2014]

2.2.3. Comparison of static and dynamic methods

From a theoretical point of view static and dynamic values should give the same results since Young's modulus is a constant (see section 2.1). The static modulus determination can be regarded as isothermal due to the very slow stress introduction. The dynamic method delivers adiabatic values, meaning that there is no heat compensation during the measurement. However, there is a difference between adiabatic and isothermal moduli. Landau and Lifshitz [1970] proposed a model to describe the relationship between adiabatic (E_{ad} constant entropy) and isothermal Young's modulus (E_T temperature constant):

$$E_{ad} = E_T + \frac{E_T^2 \beta^2 T}{9 c_p} \tag{2.18}$$

where β represents the volume expansion coefficient and c_p the heat capacity per volume unit at constant pressure. Considering this equation there is no reason for great discrepancies of dynamic and static values at room temperatures. The difference between both values at room temperature for alumina is as small as 0.02 % (data for the calculation was taken from Munro [1997]). This is certainly smaller as the uncertainty from the measurement itself. However, there were found remarkable differences of both values for several materials, confusing engineers to choose a "correct" value for calculations. This subsection should give a brief overview of differences between both values for several materials and some explanation for these discrepancies.

The comparison of statically and dynamically determined Young's modulus is a topic addressed very early by geophysicists. Ide [1936] firstly reviewed the difference between both values in rocks. A significant variation in static Young's modulus of rocks can be attributed to differences in the stress applied for the load-deflection measurement. Mostly due to cracks and cavities, which are closed by the applied load, leading to higher yields of the material, the Young's modulus values are scattered. This great variance in statically determined values was the motivation to do a comparison with dynamic values. He found differences of 5 to 40 % between statically and dynamically determined Young's moduli. In conclusion, he attributed the differences between static and dynamic values to the discussed cavities and cracks in the material, which are been closed due to the applied stress during the static measurement. This results in larger deflection values which reduces Young's modulus. Furthermore, Savich [1984] found a relationship for static and dynamic E values of rocks of the form:

$$log(E_{St}) = a\, log(E_D) - b \tag{2.19}$$

a and b are dependent on the stress applied to the material. van Heerden [1987] approved this relationship and suggested to expand it to large volume rock samples since static measurements are of high costs.

For composite resin based materials dynamically determined E values where found to be significantly larger than static values [Sabbagh et al., 2002]. This is particularly interesting considering resin bonded alumina carbon material as the central study material. While those composites investigated by Sabbagh et al. [2002] were only cured, carbon-bonded materials rather provide a residual carbon structure than a polymer bond due to the release of volatile products of the resin. Combining the results from the rock investigations with those described above leads to the assumption of great discording between static and dynamic elastic moduli for carbon-bonded alumina due to microcracks and cavities mainly introduced during the release of volatile resin constituents.

Schulle et al. [2000] found a similar relation between statically and dynamically determined Young's modulus for refractory materials of different bonding type. They investigated the Young's modulus in a temperature range from 25 to 1500 °C. They did not found a significant difference of E_{St} and E_D at room temperature. However, the difference at elevated temperatures was remarkable. Above 1000 °C the static modulus decreased very strong whereas the dynamic modulus only slightly decreased. They attributed this effect to an-elastic effects depending on the loading rate. They suggested the use of dynamically obtained E values for thermal shock prediction and production control due to the short time of stress application and release in the thermal shock process. For the computation of thermal stresses arising in heating and cooling of linings they suggested the use of static Young's modulus values. This suggestion is satisfying since during heating and cooling the stress rate is low compared to thermal shocks. Furthermore, the model by Landau and Lifshitz [1970] confirms this suggestion.

In conclusion there are significant differences for statically and dynamically determined Young's modulus values for many materials. It was shown that these differences mainly can be attributed to problems in static load-deflection tests, for example the closing of cracks or cavities contributing to the deflection. Furthermore, the applied strain rate contributes to the discrepancy between E_{St} and E_D. These strain rates are very low for static measurements, whereas they are very high for dynamic measurements. Just this difference in the strain rates in combination with the highly heterogeneous system "refractory" leads to big discrepancies between both values E_{St} and E_D. Therefore, it is advisable for engineering purpose to question the application and afterwards to choose the appropriate measurement method. For example, in case of thermal shock prediction

dynamic values could be used since the apparent strain rate in this process might be more comparable than for static values. However, the more accurate values can be obtained by the dynamic measurement.

2.3. Thermal shock resistance assessement for refractories

Thermal shock resistance is one of the most investigated and important properties or behavior of refractory products. There is a tremendous amount of literature describing the resistance to thermal shock of refractories. Brochen [2011] gave a detailed review of the estimation and experimental determination of thermal shock resistance parameters. This subsection should give a brief overview of the recently used parameters and experimental setups to assess and evaluate the thermal shock resistance of refractories.

As early as 1955 Kingery already addressed the problem of thermal shock resistance. He gave a detailed review of factors influencing the rise of thermal stress in a material as the Young's or shear modulus (E, G), the thermal expansion (α), Poisson's ratio (ν) and the capability of the material or structure to conduct heat Kingery [1955] . Assuming completely linear elastic behavior he proposed several so called R-factors, which basically provide the temperature gradient a material or structure will resist without failing. Throughout the refractory community two of these factors are extensively used for the quick assessment of thermal shock resistance of refractories. For a very rough thermal shock (infinite heat transfer coefficient), the maximum temperature difference a material can resist without failure is defined as

$$\Delta T = R = \frac{\sigma(1-\nu)}{E\alpha} \tag{2.20}$$

In the case of a constant heat transfer coefficient (mild thermal shock) Kingery introduced the thermal conductivity λ to take the heat transfer into account:

$$R' = \frac{\sigma(1-\nu)\lambda}{E\alpha} \tag{2.21}$$

Besides these two thermal shock parameters regarding the failure of the material, Kingery proposed more factors for example for the calculation of a maximum heating or cooling rate. However, the boarder conditions of these factors limit their application strictly to "homogeneous isotropic bodies whose physical properties are substantially independent of temperature" [Kingery, 1955]. This is far away from refractory products properties'.

In addition to Kingery's thermal shock **resistance** parameters describing the crack initiation, Hasselman [1969] considered not only the maximum stress a material can resist but also the possibility of crack introduction and propagation in the material for his so called thermal shock **damage** parameters considering the crack propagation. He proposed the distinction between thermal shock fracture resistance and thermal shock damage resistance. He introduced small Griffith flaws into his model. Thus, his approximation is closer to real refractory products than Kingery's. However, he also proposed boarder conditions such as the temperature difference should not exceed the minimum difference needed for thermal stress fracture. Otherwise additional thermal strains have to be considered. Nevertheless, two of the thermal shock damage parameters proposed by Hasselman are very popular in the refractory community [Hasselman, 1969, 1963].

$$R'''' = \frac{EG_f}{\sigma^2(1-\nu)} \tag{2.22}$$

where G_f represents the specific fracture energy. This parameter provides information regarding the arresting and propagation of cracks related to thermal shocks. It can be predicted whether the material failure might be catastrophic or cracks may be arrested. A second thermal shock damage parameter proposed by Hasselman is the so called "thermal stress crack stability" parameter:

$$R_{st} = \sqrt{\frac{G_f}{\alpha^2 E_0}} \tag{2.23}$$

where E_0 presents the Young's modulus of the material without cracks.

Comparing the concepts of Kingery and Hasselman it is obvious that there is a paradox design situation. For maximization of R, R' and R_{st} low values of E and α are of advantage. Considering the crack propagation R'''' parameter it is obvious that high E values will increase the probability of crack trapping. Besides this problem for the material scientist there is a second drawback which is described by the temperature dependence of the properties. They are assumed by Kingery and Hasselman as temperature independent. However, as shown above for the Young's modulus, they can not be considered as independent. Therefore, high temperature values should be considered for the thermal shock parameters proposed above. Thus, an intensive characterization of the Young's modulus of carbon-bonded alumina, as conducted in this study, should contribute to a better understanding of thermal shock behavior of this material.

Brochen [2011] improved Hasselman's and Kingery's parameters by solving the heat

transfer problem numerically. He showed that his modified R parameters are more accurate than the classical ones. However, a more accurate model of the wear mechanism is nothing worth without adequate material parameter input. Still temperature dependent values of the strength, Young's modulus and thermal expansion need to be considered. Salvini et al. [2012] furthermore adjusted Hasselman's theory by introducing more recent fracture mechanic concepts. They introduced the crack propagation energy γ_{WOF} (the total work of fracture measured by the chevron notched beam test) and the crack initiation energy γ_{NBT} (measured by the notched beam test). By doing so, they assumed to consider the different crack interactions with the microstructure more accurate. They could prove their equation to be more precise in forecasting the residual strength of a material than Hasselman's approach.

Besides these parameters, there are some experiments to asses and predict the thermal shock behavior. There is the standard EN-993-11 for the prediction of thermal shock behavior in Europe. The material (rectangular bars) is supposed to be heated up to 950 °C. After a holding time it should be cooled down to room temperature by an air flow. To evaluate the thermal shock resistance two possible parameters are used. The number of cycles a material could resist without failure at a load of 0.3 MPa is one criteria. As a second the relative Young's modulus or strength after five shock cycles related to the unshocked values are used. A second method is the quenching in water which is widely used in laboratory thermal shock assessment. However, besides a problem with the vaporization of the water during quenching, this procedure is not applicable for hydrate-able materials. Furthermore, it could be problematic quenching a batch of samples because the water is heated and therefore does not provide the same quenching effect to all samples.
In the US the standard nowadays is ASTM C1171. It is comparable to the EN 993-11 since air is used to quench the material and the residual strength or Young's modulus are used for the thermal shock assessment. However, the temperature difference is supposed to be 1200 °C.
There are more practical approaches which are nevertheless expensive and time consuming like the Ribbon and Panel-Spalling tests [Tomšu and Ulbricht, 2009].

In conclusion it can be said, that the assessment of thermal shock behavior still is a tough task to be solved by using temperature dependent material properties for the computation of the thermal shock parameters in the specific temperature range needed.

2.4. Carbon-bonded alumina

Carbon-bonded alumina is the material investigated within this study. Therefore, the following section will give a brief overview of its application in the refractory industry and of its microstructure.

The range of application for this material is concentrated on so called functional refractories. Typical examples are slide gate plates, stoppers and sub-merged entry nozzles. All of them are applied in continuous steel casting. Carbon-bonded alumina is used due to its high reliability. An interruption of the casting process would involve many problems. Besides the costs there could be for example health issues and frozen steel in the tundish [Shultz et al., 1986].

There are two different applications for plates. In ladles the plate has to resist very big temperature changes because they are cleaned by oxygen after the slag removal. Therefore, a high thermal shock resistance is essential for these type of plates. On the other hand plates in a tundish are not subjected such extreme temperature changes. However, they have to resist high temperatures for a longer time and need therefore a higher corrosion resistance [Itoh, 1998].

The second main application for carbon-bonded alumina are ladle shrouds and submerged entry nozzles. The first one is used to transfer the molten steel from the ladle to the tundish without oxidation and the entry nozzles are used for the transport of the molten steel from the tundish to the water cooled mold. During service they will be subjected enormous thermal shocks (sudden contact with molten steel). Therefore, their thermal shock resistance has to be very high, otherwise the whole casting process would have to be stopped [Itoh, 1998]. A serious problem of these materials is the oxidation starting at 450 °C. The addition of so called anti oxidants (metallic powder) presents a solution therefore and leads us to the microstructural characterization of these materials.

2.4.1. Microstructure

Carbon-bonded alumina refractory materials are basically composed of three components. The alumina as an oxide component, a carbon constituent and an organic binder comprising the so called carbon bond. Other oxides can be added to the alumina in order to modify the resulting properties (like zirconia for higher thermal shock resistance). As

Tab. 2.3.: Typical properties of glassy carbon derived from polymer precursors; Table taken from McKee [1973]

Bulk density	$1.3 - 1.5\,\mathrm{g\,cm^{-3}}$
Apparent porosity	$0 - 12\,\%$
Flexural strength	$5 - 80\,\mathrm{MPa}$
Young's modulus	$14 - 33\,\mathrm{GPa}$
Thermal expansion coefficient	$2 - 3.5 \times 10^{-6}\,\mathrm{K^{-1}}$

carbon constituents are used mainly natural graphite or carbon black. These components should improve the thermal shock resistance by increasing the thermal conductivity of the material, reducing the overall thermal expansion and introducing microcracks into the material. The binder phase is basically also a carbon constituent [Itoh, 1998].

Nowadays, phenolic resins are state of the art binders for Al_2O_3-C products. Despite their wide application in magnesia-carbon refractories, tar pitches are not the preferred binders anymore, due to their noxious effects. Furthermore, the resin can be processed (mixed) at room temperature in contrast to the pitch products. The resins transform in two steps from a polymer compound into a residual carbon net or lattice. In a first step the resin is cured at temperatures up to 200 °C. Depending on the kind of resin (resol or novolac) a hardener, mostly in the form of hexamethylenetetramine, has to be applied for the curing process. The second step is the actual transformation into a carbonaceous product. The so called carbonization occurs mainly in the temperature range of $200 - 1000\,^{\circ}\mathrm{C}$ and in inert gas atmosphere. In this temperature range volatile products (H_2O, CO, CO_2, CH_4 and H_2) of the resin are released accompanied by a densification of the material. Thereby, a density minimum occurs in the temperature range of $200 - 550\,^{\circ}\mathrm{C}$. However, the resulting product can not be regarded as a pure crystalline carbon like graphite [Fitzer et al., 1969; Gardziella and Suren, 1992].

Natural graphite in the form of flake graphite is the most common type of carbon filler used for Al_2O_3-C products. It is relatively cheap and comprises a good thermal conductivity, low thermal expansion and chemical stability. Therefore it is added to Al_2O_3-C products in amounts up to 30 wt % and more. However, natural flake graphite can be regarded anisotropic as a single graphite crystal. Therefore, Al_2O_3-C products turn more anisotropic by adding more graphite [Pierson, 1993a].

As mentioned above metal additives are more frequently used for the prevention of carbon oxidation. Most commonly used are aluminum and silicon metal powders. During firing they react with the carbon or atmospheric nitrogen to carbides and nitrides accompanied

with a volume expansion. Thus, by filling the voids of the microstructure the porosity is reduced leading to a reduction of oxidation. Moreover, the metals react with the CO and reduce it to C which contributes to the oxidation protection,too. A third effect is the increase of strength of the material due to an increase in the bonding [Itoh, 1998]. Furthermore, in case of Si addition SiO(g) could be formed which can be transformed into SiO_2 by a further reduction of CO. Thus, a thin layer of SiO_2 could be deposed on the graphite and prevent its oxidation [Zhang, 2006].
Besides the addition of metals also carbides and boron containing oxides are used for the oxidation prevention of carbon-bonded alumina [Yamaguchi, 2007].

More recently the addition of nanoscaled material to Al_2O_3-C refractories has been investigated. Roungos and Aneziris [2012] showed improvements of the thermal shock resistance due to the addition of magnesium aluminate spinel, alumina sheets and carbon nanotubes. However, the alumina increased the overall strength which caused a decrease of thermal shock resistance in terms of the earlier discussed parameters. Furthermore, Roungos and Aneziris noted the importance of the mixing process regarding the reproducibility.

Yet, most of these investigations have a strong application oriented focus. Therefore, many process parameters are varied to obtain the best results for a certain application. A systematic approach to understand the microstructural processes resulting in a remarkable high thermal shock resistance has not been carried out yet. Therefore, fundamental studies of the microstructure of carbon-bonded alumina could contribute to a better understanding of the material and to a more accurate design of the refractory products [Dupuy et al., 2013].

This study should be a contribution to such a fundamental understanding of the microstructure of pure alumina carbon materials. The Young's modulus of elasticity is a proper parameter to asses the microstructure of a material as described in this chapter (see section 2.1). The relation of microstructure described by scanning electron microscopy is a state of the art procedure. The indirect approach of microstructure assessment using Young's modulus of elasticity is used within this investigation, passing the time consuming and only ex-situ applicable SEM investigations. Several composition parameters (e.g binder content, bonding system, graphite content) were changed and the influence on the elasticity of the material at room and high temperature was investigated. Furthermore, empirical models for the description of these influences will be proposed. For a better understanding of these experiments, the following chapter

will give a detailed overview on the compositions investigated and the applied testing methods.

3. Materials and methods

The purpose of this study was the investigation of elastic properties of carbon-bonded alumina depending on its composition and the temperature. Therefore, three blocks of experiments were carried out,

- Industry related compositions
- Reference compositions
- Filter coating bulk material and filter structures

These blocks are composed of experiments with different compositions and processing parameters. The exact compositions and experimental procedures will be introduced in the following sections.

3.1. Industry related compositions

Industry related compositions were used within the first experimental block. They were derived from a mono-bloc stopper composition according to Roungos and Aneziris [2012] and are shown in Table 3.1. They were chosen to obtain results for industry applications. However, all additives were removed to start investigating a reference system. For this block of experiments the variation of the bonding system (type of binder and amount of binder) was chosen as composition factor influencing Young's modulus. Furthermore, the pyrolysis temperature and the molding pressure were chosen as technological factors. Thus, this block consists of four independent experiments.

3.1.1. Variation of the binder content, bonding system and maximum particle size

The raw materials used for this experiment were tabular alumina (T60/64, 99.5 % Al_2O_3, Almatis GmbH, Ludwigshafen, Germany), natural graphite (AF, carbon content 96 -

Tab. 3.1.: Industry related compositions

Raw material		T20	T20-B10	T20-C	T20-3
		wt %			
	1.0 - 3.0 mm	0.0	0.0	0.0	35.6
	0.5 - 1.0 mm	0.0	0.0	0.0	24.0
	0.2 - 0.6 mm	43.0	39.4	43	0.0
Tabular Alumina	0.0 - 0.5 mm	0.0	0.0	0	14.4
	0.0 - 0.2 mm	32.0	29.6	32.0	0.0
Graphite	d_{50}=18 μm	10.0	10.0	10.0	10.0
Graphite	d_{50}=160 μm	10.0	10.0	10.0	10.0
Novolac resin	liquid	2.0	2.0	0.0	2.0
Novolac resin	powder	4.0	8.0	0.0	4.0
Carbores® T10	liquid	0.0	0.0	2.0	0.0
Carbores® P	powder	0.0	0.0	4.0	0.0
Hexamethylene-tetramine[1]		10.0	10.0	10.0	10.0

[1] related to the resin content

98 %, and NFL, carbon content 92 - 94 %, Graphite Kropfmuehl AG), liquid as well as powder novolac resin, hexamethylenetetramine as hardener for the novolac resins (Momentive, Duisburg, Germany) and a liquid as well as modified coal tar pitch (Carbores® P and Carbores® T10, Rütgers GmbH, Germany).

All samples were produced by mixing the components in a compulsory mixer (Maschinenfabrik Gustav Eirich GmbH & Co. KG, Hardheim, Germany). In a second step, bars ($150 \times 25 \times 25\,\mathrm{mm}^3$) and cylinders ($d = 50\,\mathrm{mm}$, $h = 50\,\mathrm{mm}$) were uniaxially pressed with a pressure of 100 MPa. Afterwards, the samples were cured up to 180 °C for the resin and 300 °C for the Carbores® containing samples. Then they were fired at 1000 °C in retorts filled with calcined pet coke (Mueco GmbH & Co. KG, Germany), having a particle size between 0.2 and 2 mm, at a heating rate of 100 K/h with a dwell time of 5 h at the maximum temperature.

In industry applications the binder content and type are varied widely in dependence on the materials processing (e.g. uniaxial or isostatic pressing). Therefore, the binder content was varied for the resin compositions from 6 to 10 wt %. The bonding system was changed from resin to Carbores® at a fixed content of 6 wt %. Finally, the maximum particle size was altered from 0.6 to 3.0 mm by introducing a new composition. However, the particle size distribution was not taken into account by the composition design. The influence of these variations on the elastic properties were then investigated at room temperature as well as up to 1450 °C.

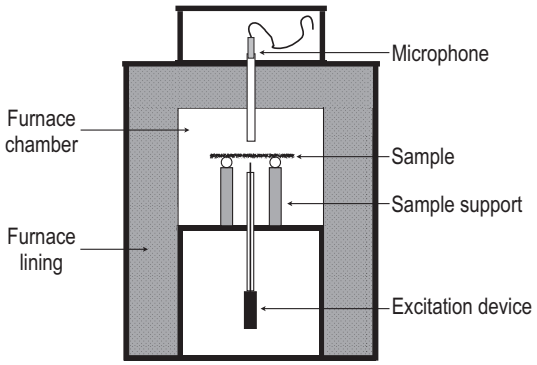

Fig. 3.1.: Schematic view of the IET-HT setup (Figure originally published in [Werner et al., 2013])

In preliminary experiments it was found that the particle size packing had a significant influence on the retained bulk density and porosity of the material. Therefore, the results of the grain size dependence of Young's modulus in this experiment were refused and a more accurate experiment was carried out described in section 3.2.
Young's modulus, shear modulus and Poisson's ratio were obtained by the impulse excitation technique (IET) according to ASTM-E1876.
The apparent porosity of the material was determined by the water immersion method according to EN 993-1. Due to the absence of hydratable phases water was used.

For the high temperature measurement a furnace with an impulse excitation setup inside was used (HTVP1600, IMCE, Belgium) [Roebben et al., 1997]. Only the flexural frequency was measured at elevated temperatures (schematic setting shown in Figure 3.1). Three samples of each composition were heated up to 1450 °C at a heating rate of 5 K/min in an argon atmosphere with a dwell time of 2 h at maximum temperature and flexural frequency was measured every 10 K. For heating as well as for cooling the same conditions were applied. The mass loss of the material was carefully registered (ex-situ) because a slight oxidation of the samples by residual oxygen within the furnace was observed.
Furthermore, an additional oxidation measurement was carried out for the composition T20 up to 1000 °C in air with a holding time of 60 min. A cycling experiment was applied to the same composition. Therefore, thermal cycles in steps of 200 K from 200 °C to 1400 °C were applied to one sample. The last cycle up to 1400 °C was repeated. A holding time of 60 min was applied at each maximum temperature. The heating rate was the same as for the above described measurement.
For the evaluation of microstructural changes during the high temperature measurement

a Philips XL 30 (Philips, Germany) scanning electron microscope (SEM) was used by comparing SEM pictures prior to and after the measurement.
X ray diffraction (XRD) analysis was carried out using a PHILIPS diffractometer with Cu-$\kappa\alpha$ radiation to obtain phase transitions due to the high temperature measurement. The thermal expansion of the compositions was determined to be compared with the results of the high temperature Young's modulus. The measurements were carried out using a Netzsch RUL/CIC 421 apparatus for determining refractoriness under load. A pressure of 0.01 MPa was applied to the samples according to DIN-EN 993-19. The same thermal cycle was applied as for the Young's modulus of elasticity measurement. However, the holding time was only 30 min. For this measurement only one sample per composition was investigated. The thermal expansion of the filter bulk material was obtained using a Netzsch DIL 402 C.
For the data analysis the software package "R" was used [R Core Team, 2013].

3.1.2. Variation of the pyrolysis temperature

Due to the binder evolution during the pyrolysis of carbon-bonded alumina the influence of different pyrolysis temperatures was studied.
The composition chosen for this experiment was T20-B10, a 0.6 mm and 10 wt % resin composition (see Table 3.1). The forming and curing parameters were equal to those explained above (subsection 3.1.1). Only, the maximum pyrolysis temperature was varied in 3 steps (700 °C, 1000 °C and 1400 °C).
The one cycle high temperature measurement of Young's modulus up to 1450 °C as well as the thermal expansion measurement were carried out according to the description in subsection 3.1.1.

3.1.3. Variation of the molding pressure for porosity variation

As shown in the fundamentals chapter the Young's modulus is dependent on the porosity. Since also the corrosion resistance of carbon-bonded alumina is determined by the porosity, the investigation of the porosity influence on E is essential. Thus, the influence of porosity on the Young's modulus was studied in this experiment. Therefore, T20-3 a 3.0 mm and 6 wt % resin composition was chosen (see Table 3.1). Apart from the molding pressure the sample preparation was completely the same as for the experiment in subsection 3.1.1.

The molding pressure was varied in 5 steps (20, 40, 70, 100 and 130 MPa) to obtain different porosity levels. Preliminary experiments revealed the molding pressure as the factor with the largest influence on porosity and Young's modulus [Werner et al., 2014]. The one cycle high temperature measurement of Young's modulus up to 1450 °C was carried out according to the described procedure in subsection 3.1.1.
The elastic properties at the pressure levels were compared by using the Tukey range test with a p-value of 0.05 (also known as Tukey's HSD [honest significant difference] test). This is a single step multiple comparison test.
The high temperature experiments were interpreted with repeated measures ANOVA between-subjects in the temperature range from 25 °C to 1025 °C (former pyrolysis temperature). Thereby the temperature was defined as the within-subjects and the porosity level as the between-subjects factor [Scheiner and Gurevitch, 1993]. Furthermore the Young's moduli at the different porosity levels were compared by a pairwise t-test with a p-value of 0.05, which was adjusted according to the Bonferroni-Holm method [Holm, 1979; Werner et al., 2014].

3.2. Reference compositions

The results of the industry related compositions revealed an influence of the maximum alumina particle size on the Young's modulus. However, a possible influence of the particle size distribution of the compositions on the elastic properties could not be eliminated and furthermore the difference between the maximum alumina particle sizes seemed to be too small. Furthermore, the influence of the carbon containing phase has not been studied in the experiment above.

Therefore three factors influencing the microstructure of carbon-bonded alumina were chosen. The graphite content was varied in four steps (0, 10, 20 and 30 wt %). The maximum particle size was altered in three steps (0.045, 1 and 3 mm). Finally, at a carbon filler content of 10 wt % the type of filler was varied (carbon black, fine graphite (AF), a mixture of fine and coarse graphite and coarse graphite (NFL)). It was used the following carbon black powder as raw material (Luvomaxx N-991, Lehmann & Voss & Co. KG, Germany, 99.0 wt % carbon, $\geq$0.01 wt % ash content, primary particle size of 200 - 500 nm). The particle size distribution for the 1 and 3 mm composition was set to n=0.65. Preliminary experiments showed the highest bulk density for this coefficient. The compositions for the different graphite contents are shown in Table 3.2. For the

carbon filler variation the particle size distribution of the 10 wt % graphite content composition was arbitrarily chosen and only the carbon filler was varied (see Table 3.2).
The elastic properties (Young's modulus, shear modulus and Poisson's ratio), apparent porosity and bulk density were investigated at room temperature. Furthermore, the Young's modulus was measured from room temperature up to 1450 °C for all compositions. The thermal expansion was also investigated.

3.3. Carbon-bonded open cell foam structures

Thermal shock resistance is the most essential property of these filter structures. Providing the elastic properties for these structures could reduce experimental affords to a minimum and therefore could reduce research and development costs, too.
Therefore in this section the coating slurry of a metal melt filter was investigated regarding its elastic properties at room and high temperature to provide information regarding the strut material. Afterwards the actual filter structure was investigated under the same conditions. The composition of the filter coating slurry was prepared according to Emmel and Aneziris [2012]. The results will be discussed regarding a relationship between the elastic properties of the bulk material and the filter structures according to Gibson and Ashby [1997].

3.3.1. Filter coating bulk material

Within this experiment the influence of the binder content and the porosity on the elastic properties were investigated. Therefore, two different compositions were used (shown in Table 3.3 and 3.4).
Additional raw materials, except those already introduced above (subsection 3.1.1 and section 3.2), were tabular alumina (Martoxid MR70, 99.8 % Al_2O_3 Martinswerk GmbH, Germany), a dispersing agent (Castament VP 95 L, BASF AG, Ludwigshafen, Germany), an anti foam agent (Contraspum K 1012, Zschimmer & Schwarz Mohsdorf GmbH & Co. KG, Germany), a ligninsulfonate (T11B, Otto-Dille®, Baeck GmbH and Co. KG, Germany) as temporary binder and a polymethyl methacrylate (Porlat K85, Zschimmer & Schwarz Mohsdorf GmbH & Co. KG, Germany) as a pore forming agent.

The bulk material was prepared as follows. Prior to shaping, a slurry was obtained by homogenizing in a ball mill for 24 h. For the pressed samples the slurry had to be dried prior to pressing at 110 °C. Bars of $70 \times 7 \times 7\,mm^3$ were slip casted as well as pressed

Tab. 3.2.: Reference compositions; the composition name can be read as follows: **T***(abular alumina of the maximum particle size)* **- Y -** *(mm and of a graphite content of)***X***(wt %)*

Raw material		T-0.045-X $d_{max} = 0.045\,\text{mm}$				T-1-X $d_{max} = 1.0\,\text{mm}$				T-3-X $d_{max} = 3.0\,\text{mm}$			
		wt %											
Graphite	AF/NFL	0.0	10.0	20.0	30.0	0.0	10.0	20.0	30.0	0.0	10.0	20.0	30.0
	0 - 0.045	100.0	90.0	80.0	70.0	0.0	0.0	0.0	0.0	0.0	0.0	0.0	0.0
	0 - 0.2 mm	0.0	0.0	0.0	0.0	9.8	3.5	0.0	0.0	15.7	7.0	0.0	0.0
	0 - 0.5 mm	0.0	0.0	0.0	0.0	49.7	44.8	36.9	25.3	22.4	16.0	10.6	3.0
Tabular Alumina	0.5 - 1.0 mm	0.0	0.0	0.0	0.0	40.5	41.7	43.1	44.7	13.2	12.9	12.6	12.4
	1.0 - 2.0 mm	0.0	0.0	0.0	0.0	0.0	0.0	0.0	0.0	9.9	8.3	8.6	12.9
	1.0 - 3.0 mm	0.0	0.0	0.0	0.0	0.0	0.0	0.0	0.0	38.8	45.8	48.3	41.6
Novolac resin[1]	liquid	2.0	2.0	2.0	2.0	2.0	2.0	2.0	2.0	2.0	2.0	2.0	2.0
Novolac resin[1]	powder	4.0	4.0	4.0	4.0	4.0	4.0	4.0	4.0	4.0	4.0	4.0	4.0
Hexamethylenetetramine[2]		10.0	10.0	10.0	10.0	10.0	10.0	10.0	10.0	10.0	10.0	10.0	10.0

[1] related to the alumina and graphite content
[2] related to the resin content

Tab. 3.3.: Filter coating bulk material composition according to Emmel and Aneziris [2012]; Three different levels of porosity were obtained by introducing a pore forming agent

Raw material		AC4
		wt %
Alumina Martoxid MR 70	d_{50}=0.5-0.8 μm	64.8
Carbores® P	powder	19.6
Carbon black	d_{50}=200-500 nm	6.2
Graphite	d_{50}=18 μm	7.6
Castament VP 95 L		0.3
Contraspum K 1012		0.1
Ligninsulfonate T11B		1.5
Porlat K85[1,2]	0-150 μm	0.0
Water content[1]		75.0

[1] related to the solid content
[2] was varied in 3 steps of 20 wt % each (20, 40, 60)

Tab. 3.4.: Filter coating bulk material composition with Carbores® P variation to study its influence on the elastic properties

Raw material		AC5	AC10	AC20	AC30
			wt %		
Alumina Martoxid MR 70	d_{50}=0.5-0.8 μm	95.0	90.0	80.0	70.0
Carbores® P	powder	5.0	10.0	20.0	30.0
Castament VP 95 L		0.3	0.3	0.3	0.3
Contraspum K 1012		0.1	0.1	0.1	0.1
Ligninsulfonate T11B		1.5	1.5	1.5	1.5
Water content[1]		81	79	75	71.0

[1] related to the solid content

at 150 MPa to obtain different porosity levels. A pore forming agent was introduced for obtaining higher porosity levels. Its amount was varied in three steps of 20 wt % each, from 20 to 60 wt %. The samples containing pore forming agent were only pressed. Afterwards, the samples were heat treated at 800 °C for 3 h in a pet coke filled retort according to Emmel and Aneziris [2012].

For the high temperature measurement of Young's modulus three samples of AC4 were heated up to 1000 °C and 1450 °C at a heating rate of 5 K/min in an argon atmosphere with a dwell time of 2 h at maximum temperature and flexural frequency was measured every 10 K. For heating as well as for cooling the same conditions were applied. The mass loss of the material was carefully registered (ex-situ) because a slight oxidation of the samples by residual oxygen within the furnace was observed.

In a second experiment the carbon fillers (graphite and carbon black) were removed to retain only alumina and Carbores® P, to study the influence of the binder phase on the elastic properties of the composite. Therefore, the Carbores® P content was varied from 5 to 30 wt % (see Table 3.4). All samples were mixed and pressed according to the above introduced procedure. The heat treatment was also the same.

3.3.2. Filter structures

Metal melt filters for steel melt filtration were prepared according to Schwartzwalder [1963]. The slurry was prepared exactly according to Emmel and Aneziris [2012] in a two step process. At first an impregnation slurry was produced by dry mixing and adding subsequently deionized water. This slurry was then used to impregnate PU-foams ($150 \times 50 \times 25\,\mathrm{mm}^3$). Afterwards, the foams were dried for 12 h at 25 to 40 °C. The second step was the addition of a second layer of the same material by spraying.
The heat treatment as well as the high temperature measurement up to 1000 °C of E was the same as for the bulk material.

4. Results and discussion

Within this chapter the results of the three previously introduced experimental blocks will be presented and discussed. In addition, at the end of each section a concluding discussion subsection can be found.

4.1. Industry related compositions - Processing and composition influence on Young's modulus

In this section the influence of changing either the composition or the processing of the material was investigated. Therefore, a reference composition was chosen (T20, 0.6 mm alumina particle with 20 wt % graphite content, 6 wt % resin) and firstly analyzed. Afterwards the binder content, type of binder and the pyrolysis temperature were varied. Furthermore, the influence of oxidation and cycling during a high temperature measurement was studied for the reference composition. The last experiment of this block investigated the influence of the porosity on the Young's modulus at room and high temperature.

4.1.1. Composition T20 an exemplary carbon-bonded alumina

Composition T20 was chosen as reference system to which all samples will be compared within this section. The reason for this decision was the graphite content which is in accordance to the used graphite amount in submerged entry nozzles and stopper systems.

The room temperature values of Young's modulus and porosity are shown in Table 4.1. The high temperature investigation of the reference material is shown in Figure 4.1a. For a better comparability, the Young's modulus at elevated temperatures was normalized to the room temperature value. A measurement in argon atmosphere was carried out up to 1450 °C. A second measurement in air was done up to 1000 °C. Furthermore, the

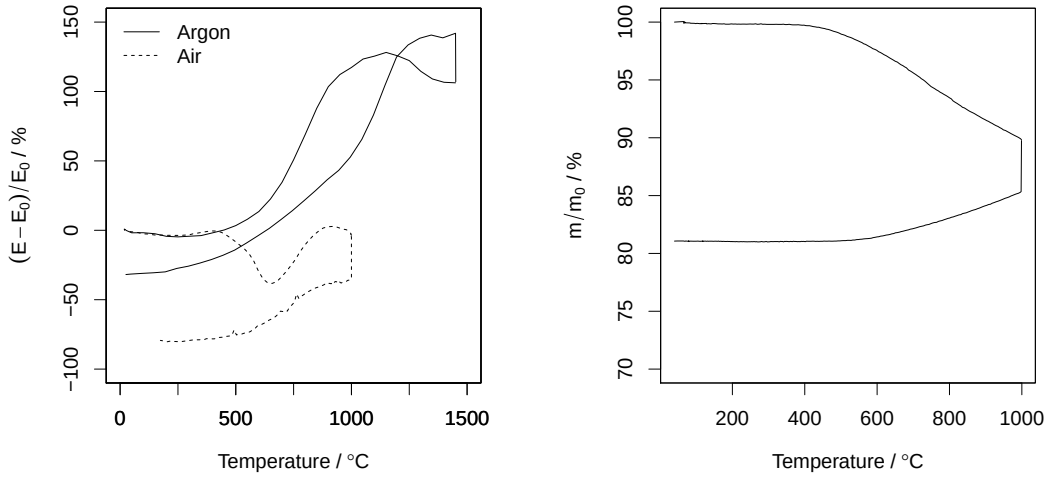

(a) Air and Argon atmosphere **(b)** Mass change

Fig. 4.1.: Young's modulus of elasticity variation versus temperature normalized to room temperature value E_0 for T20 and the oxidation experiment; on the right the mass change during the oxidation cycle is shown

mass change during the oxidation experiment was triggered and can be seen in Figure 4.1b.

For the argon measurement there was a clear hysteresis between heating and cooling, which resulted in lower E values compared to the initial ones. The evolution of Young's modulus of elasticity for the reference composition T20 could be classified into three significant stages. **Stage 1: $25 - 400\,°C$**
In this range E decreased almost linearly as for the pure alumina.
Stage 2: $400 - 1200\,°C$
E increased significantly within this temperature range. Approximately $100 - 200\,°C$ above the former pyrolysis temperature the peak of the curve was reached.
Stage 3: $1200 - 1450\,°C$
Above the former pyrolysis temperature, in the third stage, there was a slight decrease of E compared to the maximum value at about $1200\,°C$. At the holding time an increase of E was observed, which was found to be time dependent (see Figure 4.3). First sintering stages could contribute to this increase.

The cooling behavior might also be divided into these stages but vice versa. However, the temperature ranges were slightly switched. In stage 3 after the soak time E remained almost constant. The decrease of E in stage two (similar to the remarkable increase

Tab. 4.1.: Apparent porosity π_a and E of the investigated compositions at room temperature; mean values and the confidence interval for $\alpha = 0.05$ are shown

Composition	π_a / %	E/ GPA
T20	18.16 ± 0.21	7.94 ± 0.25
T20-B10	23.00 ± 0.39	8.83 ± 0.26
T20-C	16.69 ± 0.33	7.36 ± 0.16

during heating), occurred at 1150 °C. This decrease was significantly steeper than the increase during heating. The transition from stage 2 to stage 1 was very smooth and to be found around 900 °C. E decreased slightly down to room temperature. The residual Young's modulus was significantly lower than the initial value.

The results of the oxidation experiment are shown in Figure 4.1b. Up to 400 °C the evolution of E for the cycle in air was the same as in argon atmosphere. Above this temperature the difference was very obvious. From $400 - 650$ °C there was a remarkable decrease of E in air, while in argon E increased strongly. In the temperature range of $650 - 1000$ °C E increased in air, disproving the assumption of a constant decrease due to a continuing oxidation. The ongoing oxidation was proven by the constant mass loss (see Figure 4.1b). Thus, it was assumed that microstructural changes (e.g. gap closure between grains and matrix) compensated this oxygen attack up to 1000 °C. At the holding time there was a strong decrease of E observed, which continued at cooling due to an ongoing oxygen attack. After one measurement cycle the Young's modulus was reduced below 80 % of its initial value which basically resulted in the destruction of the material.

The pyrolysis temperature seemed to determined the temperature at which the maximum value for E was reached. For further investigation a thermal cycling experiment was carried out in steps of 200 K from 200 °C to 1400 °C. Figure 4.2b presents an overview of E loss and peak values for the cycles. After each cycle E was decreased. The maximum values of E for each cycle indicated the same behavior like for one continuous cycle up to 1450 °C (see Figure 4.1a). The highest peak was found at 1000 °C. All the cycles showed the three characteristic stages, defined above (see Figure 4.2a). However, the beginning of the increase and also of the decrease in stage two changed as a function of the maximum temperature of the cycle. There was a lowering of Young's modulus of elasticity after each cycle. The earlier mentioned oxygen attack certainly contributed to the increase of the porosity, resulting in lower E values. At the end of the whole cycling experiment the apparent porosity reached a value of 24 % which is an increase of approximately 6 %.

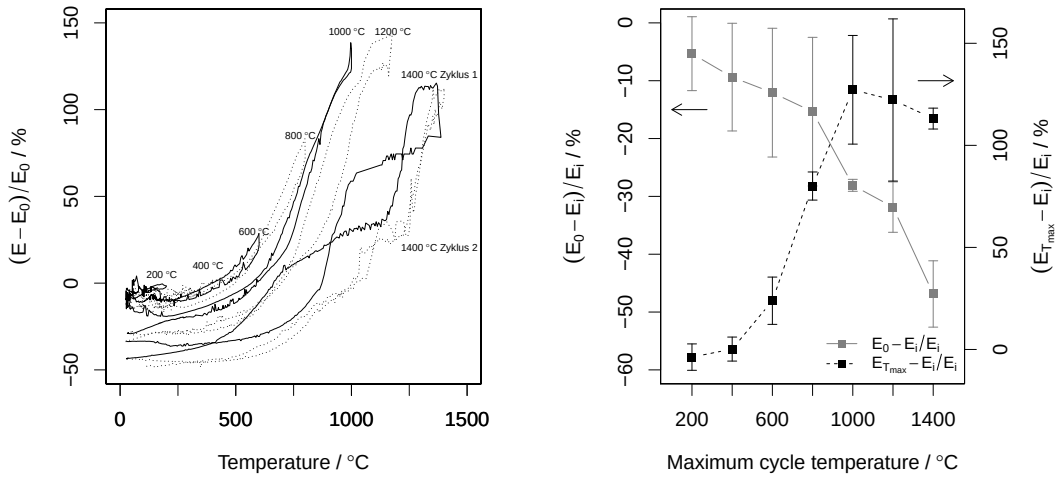

(a) **(b)**

Fig. 4.2.: Young's modulus of elasticity evolution within the cycling experiment for T20; E_i is the initial E value before the experiment started, E_0 presents the E value at room temperature after each cycle while $E_{T\,max}$ is the maximum E value after the holding time

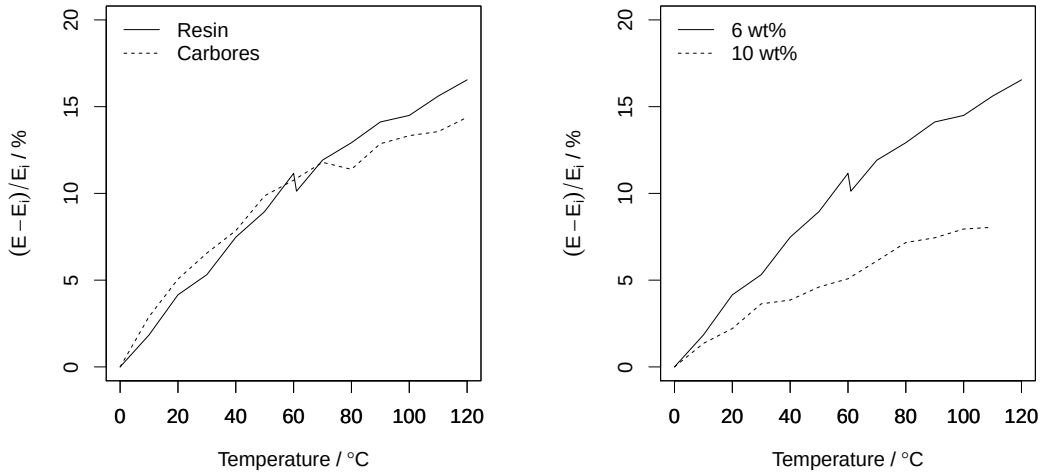

(a) Change in type of binder **(b)** Change in amount of resin

Fig. 4.3.: Change of Young's modulus during the soak time of the resin (T20 and T20-B10) and Carbores® bonded (T20-C) materials, E_i represents the initial value of E at 1450 °C

4.1.2. Influence of different binder systems

In Table 4.1 the Young's modulus and porosity of the reference composition (T20) at room temperature can be found. The apparent porosity of approximately 18 % was in good agreement with other studies of this material [Roungos and Aneziris, 2012]. The Young's modulus was as low as assumed due to the graphite and resin addition to the alumina. Obviously, the minor phase or phases (graphite and resin) determine the macroscopic elastic behavior of the material.

The increase of the resin content (6 $\Rightarrow$ 10 wt %, T20-B10) resulted in a higher E value and porosity at room temperature. This seems paradox since the Young's modulus is reduced by increasing porosity. However, the increase of resin resulted in a stronger release of volatile products during pyrolysis which increased the porosity. On the other hand there was more residual carbon left, compared to the lower resin content material, contributing to an increase in the stiffness of the material.

The change from resin to Carbores® (T20-C) as a binder resulted in a decrease of porosity but also in a slight decrease of E at room temperature. However, T20 and T20-C can be regarded as approximately equal stiff. The reduction in porosity of T20-C can be explained with the melting of Carbores® at around 300 °C resulting in a closing of voids and cavities remained from the pressing.

The influence of different amounts of resin on the Young's modulus evolution at high temperatures is shown in Figure 4.4a. The maximum increase of E at heating increased with decreasing resin content. Also the increase of E during the holding time was stronger, the less resin there was within a composition (see Figure 4.3b). This was clearly due to the resin, which inhibited the alumina grains from sintering since it could be found between them. For the 10 wt % resin composition the decrease of E after one cycle was slightly higher (−50 %) than for the 6 wt % composition (−35 %). This might also be related to a lower sintering during holding time, due to the higher binder amount which inhibited the sintering of the alumina grains. Furthermore, the decrease during cooling started at a higher temperature (1300 °C) for the higher resin containing composition.

Comparing the dilatometer measurements in Figure 4.4b reveals a hysteresis behavior for both compositions (T20 as well as T20-B10). The expansion during heating was almost linear up to 1000 °C. However, the slope of the expansion was significantly lower for the 10 wt % composition. The expansion during heating was linear for T20-B10 up to

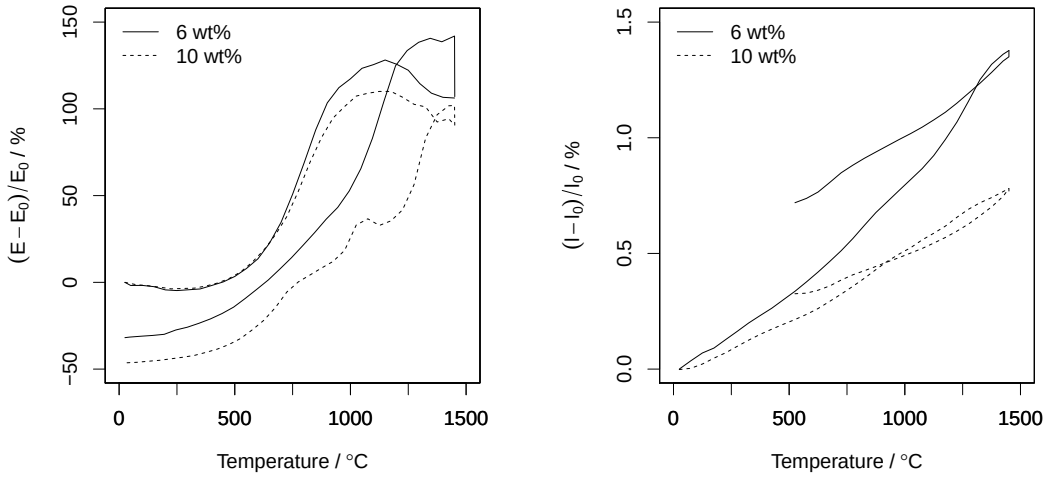

(a) Young's modulus measurement **(b)** Dilatometer measurement

Fig. 4.4.: Young's modulus of elasticity variation versus temperature normalized to room temperature value E_0 for 6 and 10 wt % resin bonded material; on the right the thermal expansion is shown

1450 °C whereas for T20 a steeper increase above 1000 °C was observed. During holding time a small shrinkage could be observed for T20 whereas there was almost no shrinkage for T20-B10. The decrease of expansion during cooling was somehow linear for both materials, however the overall expansion after one cycle was higher for T20 than for T20-B10.

The comparison between the resin and Carbores® bond is presented in Figure 4.5. The Young's modulus evolution of both compositions was almost similar as can be seen in Figure 4.5a. The maximum increase at heating was about 10 % higher for the Carbores® containing composition. Mainly there were two significant differences in the curve charts observed. Above 1150 °C there was a decrease of E for the resin containing composition which was less for the Carbores® containing composition. Furthermore, the strong decrease of E at cooling was more rapid than for the resin composition. The overall lowering of E after one cycle was found to be almost equal between 35 and 40 % for both compositions. Also, the behavior during soak time was the same (see Figure 4.3a).
Clearly the Carbores® bond provided a lower overall expansion than the resin as can be seen in Figure 4.5b. Qualitatively, there was almost no difference for both compositions. The expansion at heating was followed by a small shrinkage during holding. The contraction during cooling was linear till 1100 °C, and below it tended to get lower resulting in a residual expansion of the material. This hysteresis within the contraction

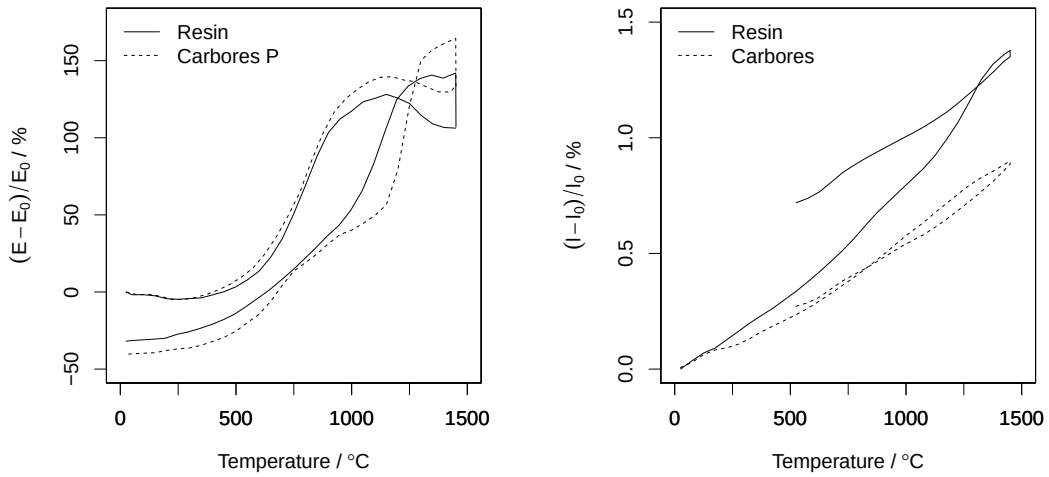

(a) Young's modulus measurement **(b)** Dilatometer measurement

Fig. 4.5.: Young's modulus of elasticity variation versus temperature normalized to room temperature value E_0 for resin and Carbores® bonded materials; on the right the thermal expansion is shown

Tab. 4.2.: Mass loss, change of apparent porosity (difference of initial and end value; $\pi_a^i - \pi_a^e$) apparent porosity and Young's modulus at room temperature after the measurement cycles

Composition	$(m\text{-}m_0)/m_0$ / %	$\pi_a^i - \pi_a^e$	π_a / %	E / GPA
T20	-1.58 ± 0.34	4.00 ± 0.52	22.16 ± 0.31	5.45 ± 0.40
T20-B10	-2.38 ± 0.21	2.47 ± 0.68	25.47 ± 0.29	4.72 ± 0.11
T20-C	-1.94 ± 0.22	4.54 ± 1.03	21.23 ± 0.71	4.09 ± 0.40

path can be found also in the Young's modulus of elasticity curves. The differences in the overall expansion might be attributed to the differences in the carbonization process of the binders.

In Table 4.2 the change in porosity, sample mass and Young's modulus after one cycle are shown. Although an argon atmosphere was applied during the measurement, a mass loss could still be observed. This could be attributed either to residual oxygen left in the furnace lining, or to the release of volatile parts of the resin which have not been released during the pyrolysis. The mass loss was to be found lowest for the reference composition T20 followed by the Carbores® composition and the 10 wt % resin T20-B10. This composition had the highest initial porosity which could contribute to a stronger oxidation due to a bigger surface to be attacked. However, the increase in porosity did not correlate to the mass loss.

Tab. 4.3.: Results of the pairwise Student's t-test (adjusted p-value according to the Holm-Bonferroni method [Holm, 1979]) for the binder influence on the high temperature measurement of E up to 1450 °C; for each pair a p-value is shown, $p < 0.05$ indicates a significant difference

	T20	T20-B10
T20-B10	$5.7e-11$	–
T20-C	$7.2e-14$	$8.9e-15$

Despite the qualitative observation of the influence of binder type and content, an ANOVA and a pairewise t-test for the different binder levels at each temperature was carried out. The ANOVA confirmed the obvious influence of the binder content and type as well as of the temperature on the Young's modulus ($p < 0.05$). The results of the t-test can be seen in Table 4.3. For all pairs of binder amount or type there was a significant difference during the high temperature measurement. However, this quantitative evaluation has to be combined with the visual observation of the results, as done above.

These results revealed a significant influence of the binder on the Young's modulus up to 1450 °C. Furthermore, it was shown that the oxidation of the material accompanied by a decrease of E was kind of superimposed by microstructural processes not described yet. Therefore, the influence of the pyrolysis temperature on the Young's modulus up to 1450 °C was investigated.

4.1.3. Influence of different pyrolysis temperatures

The composition was treated with three different pyrolysis temperatures of 700 °C, 1000 °C and 1400 °C. According to the previous results, the highest Young's modulus during heating was always observed around the former pyrolysis temperature. Therefore, this experiment was designed to confirm or deny this observation and to understand the microstructural changes during reheating of the material.

In Figure 4.6 the basic properties (E, G, ν, π_a and ρ_b) at room temperature are shown. Moreover, in Table 4.4 the results of a multiple comparison of means test to obtain significant differences between the different pyrolysis temperatures are presented. The apparent porosity and bulk density were determined on three samples, whereas for the other measurements 10 samples were investigated. There was an increase of apparent porosity with increasing pyrolysis temperature observed. Correspondingly, the bulk density was found to be decreased. However, there was no significant influence of pyrolysis temperature above 1000 °C on the apparent porosity (see Table 4.4). The Young's and

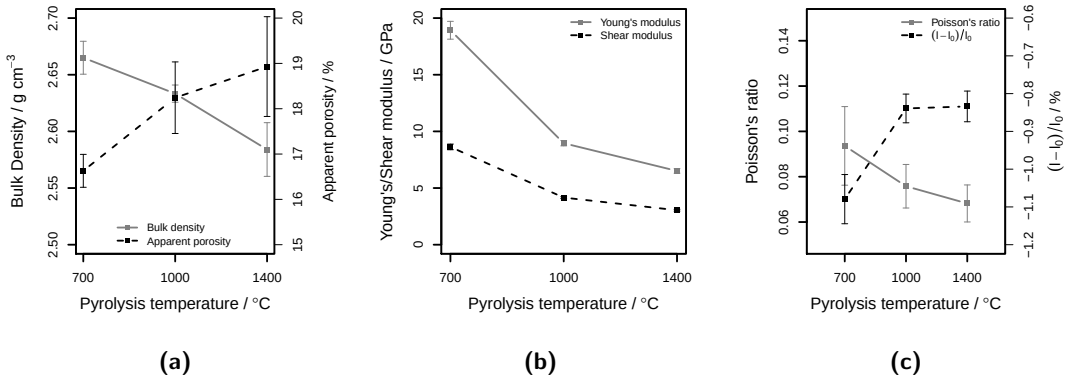

Fig. 4.6.: Elastic and physical properties of the T20-B10 samples treated at pyrolysis temperatures of 700 °C, 1000 °C and 1400 °C; measured at room temperature

Tab. 4.4.: Results of the Tukey range test with a p-value of 0.05 for the different pyrolysis temperatures and response values (E, G, ν, π_a and ρ_b); the values tested were evaluated at room temperature, $p < 0.05$ indicates significant differences between the tested pair

Temperature pair	p_E	p_G	p_ν	p_{π_a}	p_{ρ_b}	$p_{(l-l_0)/l_0}$
1000 °C − 700 °C	< 0.005	< 0.005	**0.073**	< 0.005	< 0.005	< 0.005
1400 °C − 700 °C	< 0.005	< 0.005	0.008	< 0.005	< 0.005	< 0.005
1400 °C − 1000 °C	< 0.005	< 0.005	**0.594**	**0.084**	< 0.005	**0.983**

shear modulus were significantly decreased due to the increase in pyrolysis temperature. There was no significant influence of the pyrolysis temperature on Poisson's ratio. Furthermore, the length change of the samples was found to be increased up to 1000 °C. However, from 1000 °C to 1400 °C there was no significant change in Δl. These results confirm those found by Franklin and Tucker [1995] and Yamaguchi [2007] for carbon-bonded magnesia materials.

In Figure 4.7 the Young's modulus in dependence on the temperature, the thermal expansion and the soak time behavior during Young's modulus measurement are shown. The maximum value of E was found at the former pyrolysis temperature. Furthermore, the residual Young's modulus after one cycle was found to be almost equal for all treatments at around 5 GPa. A second interesting observation was the reduction of the hysteresis behavior with an increasing pyrolysis temperature. Moreover, in Figure 4.7b it can be seen that there were no differences regarding the increase of E during the soak time. Above the former pyrolysis temperature a slight decrease of E was observed, confirming the previous results.

The expansion measurement revealed a significant correlation between the pyrolysis tem-

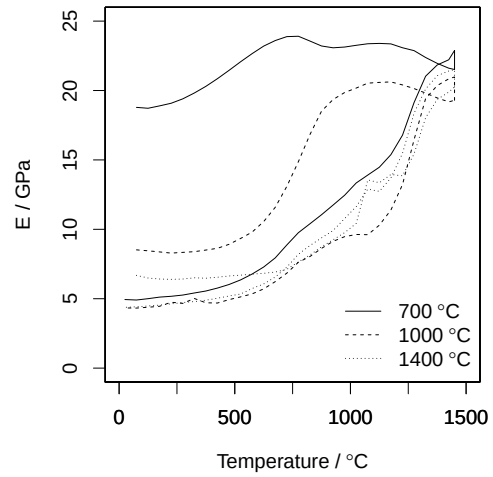

(a) Young's modulus measurement

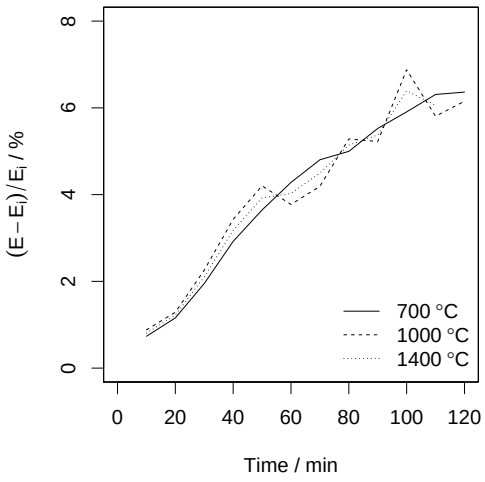

(b) Soak time behavior

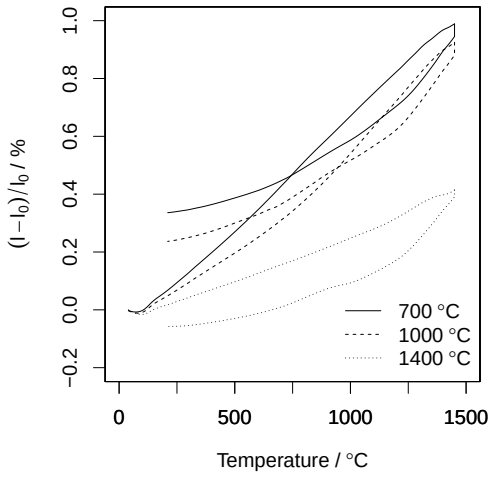

(c) Dilatometer measurement

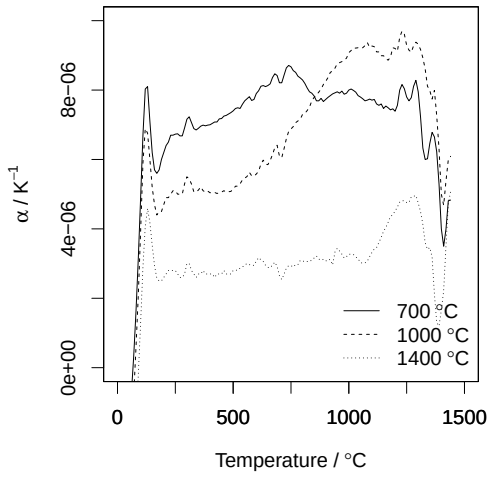

(d) $\alpha(T)$

Fig. 4.7.: Young's modulus and thermal expansion measurements up to 1450 °C for the composition T20-B10 at different pyrolysis temperatures

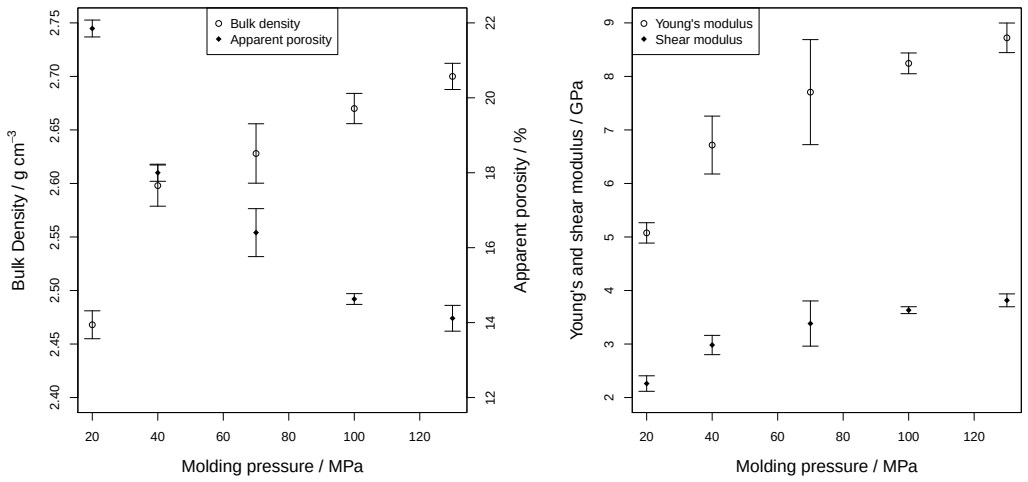

(a) Apparent porosity and bulk density versus molding pressure

(b) E and G versus molding pressure

Fig. 4.8.: Effect of molding pressure on the apparent porosity, bulk density, Young's modulus and shear modulus at room temperature

perature and the thermal expansion (linear CTE). The higher the pyrolysis temperature was, the lower was the overall thermal expansion and therefore the expansion coefficient. In Figure 4.7d the coefficient of thermal expansion α is shown in dependence on the temperature. The 700 °C composition showed an increasing α up to its pyrolysis temperature. Above it remained constant and decreased significantly at around 1250 °C. The higher the former pyrolysis temperature was the later (at higher temperatures) an increase of α was registered. This correlation is similar to the observed behavior for the Young's modulus measurement. It seems that the macroscopic expansion behavior was somehow linked to the elasticity of the carbon-bonded alumina.

4.1.4. Influence of porosity

For the porosity experiment composition T20-3 was used. To change the porosity of the samples the molding pressure was changed within 5 steps (20, 40, 70, 100 and 130 MPa). As anticipated, there was a remarkable effect of this modification on the apparent porosity and bulk density at room temperature as shown in Figure 4.8a. The higher the molding pressure was, the lower was the apparent porosity and correspondingly the higher was the bulk density of the samples. Furthermore, there was a significant increase of the Young's modulus and shear modulus due to the increasing molding pressure as can

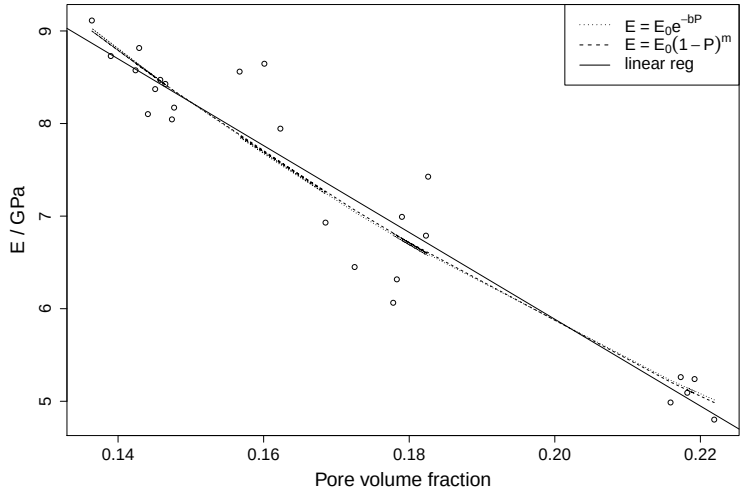

Fig. 4.9.: Young's modulus E plotted versus pore volume fraction P including the linear regression model (solid line), the Spriggs approach Spriggs [1961] (dotted line) and the Phani model [Phani and Niyogi, 1986] (dashed line) fitted to the data

be seen in Figure 4.8b. Nevertheless, the influence of the molding pressure was decreasing with higher pressures, due to a very high rate of densification at lower pressures, decreasing rapidly at higher pressures [Reed, 1995].

All pairs of molding pressure were tested by applying the Tukey range test (multiple comparison of means, single step method) and significance for almost all of them was detected. Nevertheless, there was no significant effect increasing the molding pressure from 100 to 130 MPa ($p > 0.10$). Furthermore, the significance of the effect of increasing molding pressure from 40 to 70 MPa was hardly significant ($0.05 < p < 0.10$). Despite significant effects on the apparent porosity and bulk density, there was no significant effect on Young's modulus and shear modulus observed by increasing the molding pressure from 70 to 100 MPa ($p > 0.10$). This could be due to the strong standard deviation of the Young's modulus and shear modulus values of the 70 MPa batch as indicated in Figures 4.8a and 4.8b. A contribution to this deviation could be the oxygen partial pressure inside the pet coke filled retort, which can be considered as a function of the sample position during coking. Thus, differences in oxidation of the samples could contribute to a deviation in the microstructure of the sample and could affect the Young's modulus and shear modulus.

In Figure 4.9 and Table 4.6 the experimental values of Young's modulus were plotted against the pore volume fraction, followed by fitting them to a linear regression model and

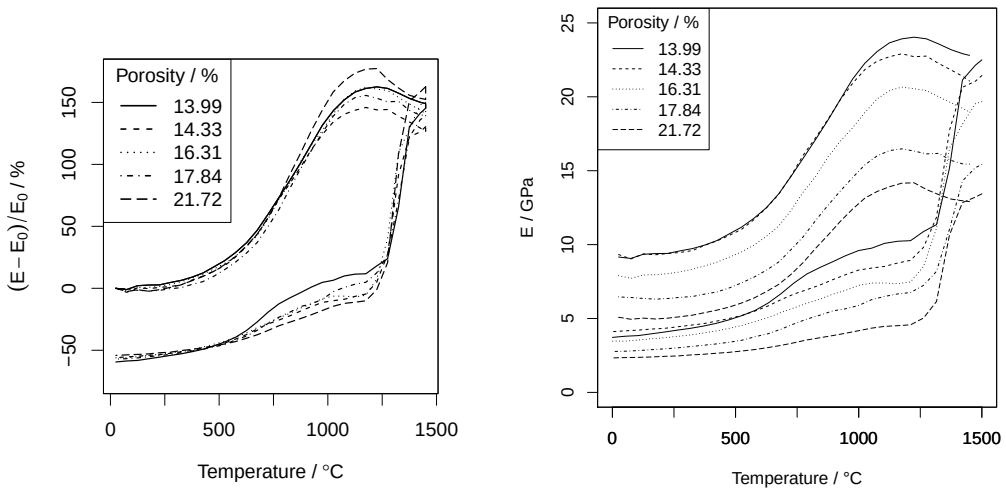

(a) Normalized Young's modulus variation **(b)** Young's modulus variation

Fig. 4.10.: Young's modulus variation versus temperature and normalized to room temperature value E_0 for the tested porosity levels

to two well known and widely used models from the literature [Spriggs, 1961; Phani and Niyogi, 1986]. With increasing porosity the Young's modulus was significantly decreased. Within the observed porosity range this correlation can be described as linear according to the observed adjusted-R^2 values.

The results of the high temperature measurement of Young's modulus (E) can be regarded qualitatively similar for all porosity levels (Figure 4.10a) considering the normalized values ($\Delta E/E_0$). There was a major increase for E between 400 and 1000 °C. Above this temperature a slight decrease in E was observed. After the holding time a steep decrease of E down to 1200 °C was detected. From 1200 °C down to room temperature E was slightly decreasing. This behavior was similar to that observed for the compositions tested above and comprised the same three stages. Besides this somewhat similar behavior, there were quantitative differences between the high temperature Young's modulus values at different porosity levels. As shown in the previous results, Young's modulus decreased due to the porosity increase at room temperature. Hence, for higher porosity the high temperature values of Young's modulus were correspondingly lower (see Figure 4.10b).

A statistical analysis was carried out for the normalized Young's modulus ($E - E_0/E_0$) results for temperatures up to 1025 °C (shown in Table 4.5). The temperature limit was chosen due to assumed microstructure changes above this temperature (former pyrolysis

Tab. 4.5.: Results of the pairwise Student's t-test (adjusted p-value according to the Holm-Bonferroni method [Holm, 1979]) for the porosity influence on the high temperature measurement of E up to 1025 °C; for each pair a p-value is shown, $p < 0.05$ indicates a significant difference

Porosity level / %	13.99	14.33	16.31	17.84	21.72
14.33	3.4e-05	-	-	-	-
16.31	0.0255	**0.1164**	-	-	-
17.84	3.6e-08	0.0108	6.1e-05	-	-
21.72	**0.1164**	0.0025	0.0220	3.4e-06	-
31.60	5.2e-16	1.6e-14	1.1e-13	1.9e-08	9.9e-11

temperature) [Franklin and Tucker, 1995]. This analysis supports the visual evaluation of the results seen in Figure 4.10a. There were clearly significant differences between most pairs of porosity. However, there were no significant differences within the pairs of porosity level 13.99 % − 21.72 % and 14.33 % − 16.31 %.

4.1.5. Discussion

The presented results clearly showed a characteristic behavior of Young's modulus in dependence on the temperature. There was a standard linear decrease in stage one, which can be found for most oxide ceramics [Wachtman et al., 1961]. However, the most interesting observation was the strong increase of E within stage two at heating. This somewhat exponential behavior was characterized by ending slightly above the former pyrolysis temperature. XRD measurement of the material prior and after the high temperature Young's modulus measurement did not reveal any changes in the phase composition. Therefore, no phase transformation occurred and could contribute to that increase of E.

A second possible mechanism which could contribute to an increase of E could be sintering. However, all tested compositions were already subjected to their former pyrolysis temperature, which was always higher as the exponential E increase. Furthermore, temperatures below 1000 °C are not sufficient for the sintering of alumina with a maximum particle size up to 0.6 mm. Thus, sintering also can be excluded in this consideration.

Since the described mechanisms could be excluded, there were other possible microstructural changes within the material. For example a microcrack healing of the composites' structure as well as of the single alumina and graphite constituents, within this stage could be a contribution to the observed effect of E increase [Eto et al., 1991; Case et al., 1981]. All the single materials expand in a different amount while heated up. The thermal expansion coefficient (CTE) of graphite depends on the orientation of its crystal

layers. In layer direction it is negative below 400 °C and increases slightly up to 1450 °C, while in perpendicular direction a CTE of 25×10^{-6} to $42 \times 10^{-6}\,K^{-1}$ can be found for the same temperature range [Pierson, 1993b]. The CTE of the used tabular alumina is approximately 7×10^{-6} to $9 \times 10^{-6}\,K^{-1}$ (own measurement). For the carbonized resin a CTE from 3.2×10^{-6} to $6.9 \times 10^{-6}\,K^{-1}$ depending on the resin and the preparation route was obtained by Iacono et al. [2007]. For alumina and graphite the values of the CTE are valid in a temperature range between 25 °C to 1450 °C. The glassy carbon values were investigated up to 1000 °C. Regarding these big differences in the thermal expansion behavior, the assumption of a contribution of this CTE mismatch to the high temperature Young's modulus behavior is self-evident.

Stage three (above the former pyrolysis temperature and the soak time) showed a slight decrease of E and during the soak time a significant increase. This decrease can be attributed to the beginning of a grain boundary sliding of the alumina, observed already by Wachtman and Lam [1959] and described by Chang [1959]. It could be assumed that first sintering stages contributed to the increase of E, observed for all compositions at the soak time. The small shrinkage found in the expansion measurement supports this assumption. A similar phenomena was mentioned by Baudson et al. [1999] for carbon-bonded magnesia. The differences found for the soak time (lower E increase for higher binder amount) could be due to the binder inhibiting the bridging of the alumina.

The hysteresis found between heating and cooling behavior supports the theory of microstructural changes in the material due to the thermal expansion mismatch. Apparently, the microstructure was remarkably disturbed, since the Young's modulus was decreased irreversibly at the end of a measurement.

Figure 4.11 presents a schematic principle of the imagined microstructural changes within one measurement cycle. Several authors already observed related phenomena and the model to be presented here can be regarded as a summary of those preexisting literature models [Li and Rigaud, 1993; Franklin and Tucker, 1995; Buchebner et al., 2008; Hampel, 2010].
The material is composed of coarse alumina and graphite particles and a matrix (containing graphite, glassy carbon and fine alumina particles). During cooling, after the pyrolysis (shown in Figure 4.11a) the coarse alumina particles and graphite flakes detach from the surrounding matrix, due to the significant lower CTE of glassy carbon compared to alumina and natural graphite. Furthermore, the anisotropic expansion of graphite flakes could contribute to this effect. This process leads to a very heterogeneous microstructure comprised of many microcracks.

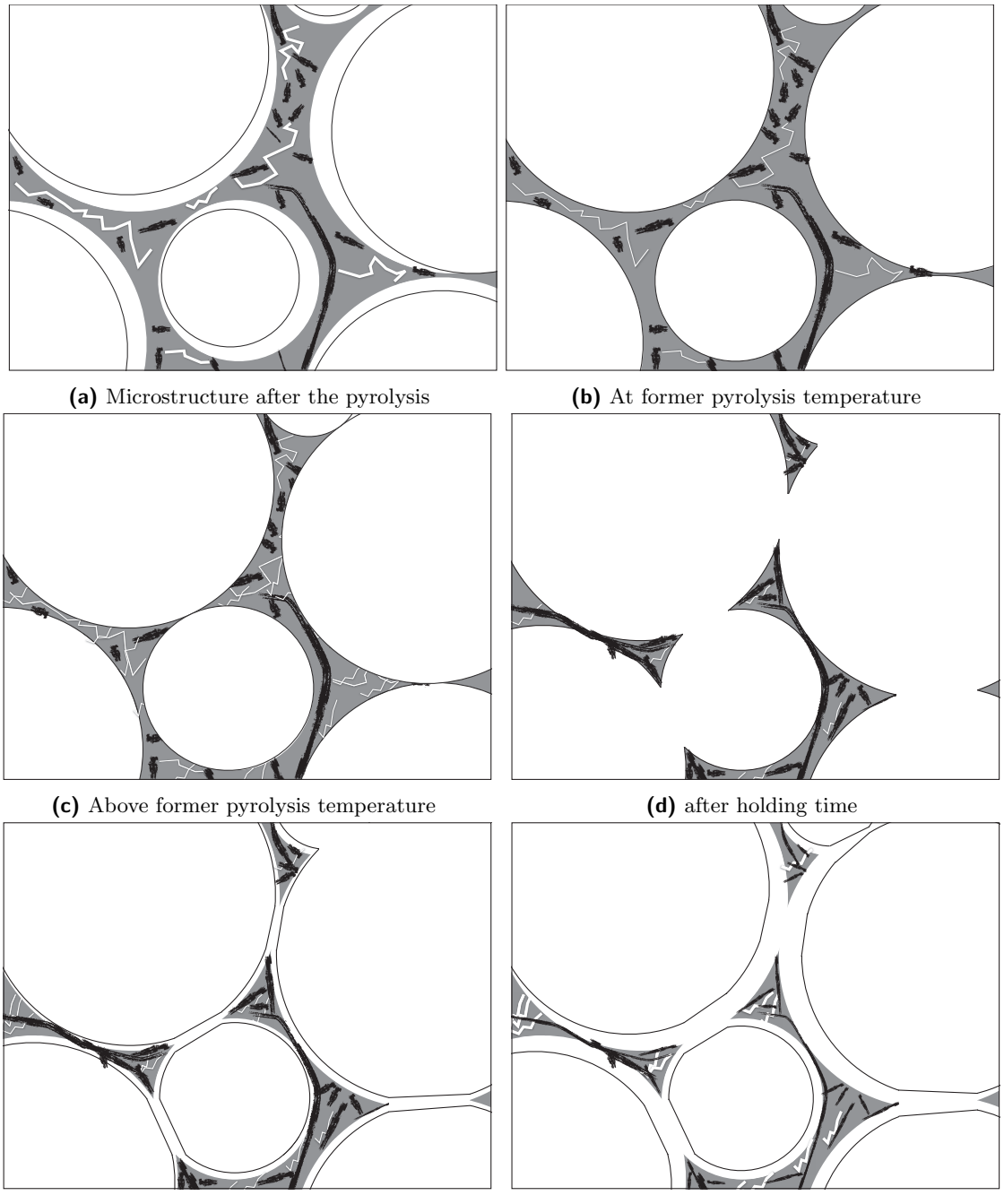

(a) Microstructure after the pyrolysis

(b) At former pyrolysis temperature

(c) Above former pyrolysis temperature

(d) after holding time

(e) At the stage of particle detachment

(f) Room temperature after the measurement

Fig. 4.11.: A summarizing model of the assumed microstructural changes within the carbon-bonded alumina during a measurement of $E(T)$ based on theories proposed earlier by several authors [Buchebner et al., 2008; Li and Rigaud, 1993; Franklin and Tucker, 1995; Hampel, 2010]

While heated again within the measurement the alumina particles expand faster than the surrounding matrix, resulting in a closure of the preexisting crack or gap. Thus, Young's modulus of elasticity increase significantly up to the state of pyrolysis (Figure 4.11b).
Increasing the temperature above the former pyrolysis temperature, results in a further cracking of the microstructure. This is due to an extensive expansion of alumina as well as graphite and leads to lower E values (Figure 4.11c). The significant increase of E at the holding time is related to first sintering stages.
The decrease of E during cooling is attributed to the detachment of the grains from the surrounding matrix (Figure 4.11e). This occurs suddenly.
At room temperature the gap between the grains and the surrounding matrix is bigger than before, due to the ongoing expansion above the former pyrolysis temperature. This leads to lower E values compared to the initial ones for all carbon-bonded compositions.
The results of the cycling experiment support the theory of matrix expansion due to the thermal expansion of the single components. Once the pyrolysis temperature was exceeded, the matrix was expanded, leading to greater gaps between the alumina grains and the matrix. The delayed increase of E within each new cycle also supports the theory of gap closing or healing, due to this further expansion of the matrix.
The results of the oxidation experiment emphasize the influence of this gap closure described above. Despite the oxygen attack beginning at 400 °C, Young's modulus was increased again after a short period of decreasing due to oxidation. This recurring increase clearly could be attributed to the gap closure between the matrix and alumina. At the former pyrolysis temperature Young's modulus was found to be at the same level as initially. Afterwards, the oxygen attack became apparent and further contributed to a decrease of Young's modulus down to 80 % of its original value.

Besides the described similar behavior, there was a clear influence of the binder content, binder amount, the pyrolysis temperature and the porosity on the high temperature Young's modulus. An increase of the binder content resulted in a reduced maximum of E and a lower increase during the soak time as well as a decrease of the residual E. In terms of the model described above, the amount of matrix was increased and less coarse particles were present. Thus, the detachment of these particles from the matrix was less after the pyrolysis, resulting in a smaller increase of E during reheating. Furthermore, the bigger amount of binder phase reduced the contact possibilities of the alumina particles, leading to a smaller increase of E during the soak time.
Apparently this sintering related increase of E also contributes to the cooling behavior. The particle detachment related decrease of E at cooling started at higher temperatures

for the high binder amount composition. Therefore, it is likely that the preliminary sintering effects determined the temperature at which the coarse alumina particles detach from the matrix or possibly even from each other. The residual E-value after one cycle also correlated with this soak time increase of E. The higher this observed increase was, the higher was the residual E. Thus, these sintering effects contributed to a stiffening of the microstructure. Taking the thermal expansion measurements into account, a significant lower expansion behavior of the high binder amount composition was found. This showed the influence of the binder phase and a reduced contribution of the alumina to the overall composite expansion. Furthermore, above the former pyrolysis temperature the lower binder amount composition showed an increased CTE which was not observed for the high binder content material. This supports the model described above and shows the significant influence of the binder.
The influence of the binder type was not as remarkable as for the binder amount. The overall high temperature Young's modulus behavior was similar for both compositions. However, for the Carbores® bonded material the maximum E values were found to be higher than for the resin bonded material. The behavior during the soak time was equal, which is supporting the results regarding the binder content since the amount of binder was equal and only the type was changed. Therefore, it can be concluded that the change from the resin to the Carbores® binder only contributed to an increase of E above the former pyrolysis temperature.

The thermal expansion measurements were in accordance with this model. In Figure 4.12 the thermal expansion of composition T20 is shown as an example of a thermal expansion coefficient change below and above the former pyrolysis temperature. It can be seen that all compositions showed a higher CTE above the former pyrolysis temperature than below (see CTE values in the table of Figure 4.12). This confirms the Young's modulus measurement and the explanatory model. Above the former pyrolysis temperature the material expands faster since all gaps were closed. Below the expansion of the constituents was kind of absorbed due to gaps and microcracks.

The results of the pyrolysis temperature experiment strongly support the described model. The higher the temperature of the preliminary pyrolysis was, the later (at higher temperatures) the strong increase of E during heating was observed. The absolute Young's modulus at the maximum temperature was found to be almost similarly independent of the pyrolysis temperature. Furthermore, the amount and slope of the increase of E was higher, the higher the pyrolysis temperature was. Thus, the gaps between coarse particles and the matrix increased with increasing pyrolysis temperature and were correspondingly closed at the former temperature. Also the residual E was

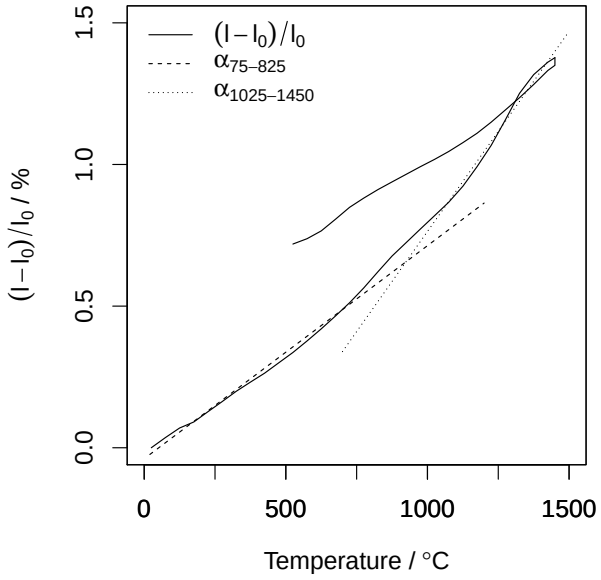

Composition	α_{25-825}	$\alpha_{1025-1450}$
	$\times 10^{-6}\,\mathrm{K}$	
T20	7.52	14.1
T20-C	5.16	7.19
T20-B10	4.93	6.08
T20-3	4.90	10.9

Fig. 4.12.: Thermal expansion of T20 (6 wt % resin, 0.6 mm alumina particle size and 20 wt % graphite) is shown, the dotted lines are approximations of the coefficient of thermal expansion below and above the former pyrolysis temperature; In the table on the right the expansion coefficients above and below the former pyrolysis temperature of the investigated compositions are shown

influenced by the pyrolysis temperature. According to the model theory, the highest pyrolized composition should comprise the smallest Young's modulus decrease. The reason therefore is the matrix which was expanded during the pyrolysis up to a temperature of 1400 °C, which is approximately the maximum measurement temperature of 1450 °C. This result was confirmed by the Young's modulus measurement as well as by the thermal expansion results. The overall expansion correlated directly with the pyrolysis temperature. The lower the pyrolysis temperature was, the higher was the expansion. Again, the 1400 °C treated composition did not expand as strong as the lower ones, because during the preliminary pyrolysis the matrix was already stretched. Therefore, at reheating the expansion was significant lower. Furthermore, the expansion velocity correlated directly with the Young's modulus measurement. The higher the former pyrolysis was, the later an increase of the expansion speed was investigated. This increase was attributed to the gap closing described above. The pyrolysis temperature did not affect the behavior during the soak time. This confirms the results of the binder amount comparison, because there was only a change in the pyrolysis temperature but not in the composition.

For the following considerations an equal pore structure in all samples is assumed, due to the variation of the molding pressure as the exclusive factor of porosity variation.
The observed relation between Young's modulus and porosity at room temperature can be considered as almost linear (see Figure 4.9). All three models are sufficiently representing the experimental data according to their R^2 values. (see Table 4.6). The R^2-values of the well known models by Spriggs [Spriggs, 1961] ($R^2 = 0.9195$) and Phani [Phani and Niyogi, 1986] ($R^2 = 0.9071$) indicate a good agreement of the model fit with the data. Despite the composite nature of this carbon-bonded alumina material these models might be applied for the calculation of E. However, the influence of the maximal particle size, graphite and binder phase on Young's modulus should be considered as described above. Therefore, the stated estimates E_0, b and m (see Table 4.6) may be valid just for the described material.
The linear model seems to fit the data well at room temperature ($R^2 = 0.9078$). However, in terms of the model regarding $E(T)$ described above, the porosity could be regarded as being reduced during heating. The highest observed value of E in this investigation was 24 ± 2 GPa (for the 130 MPa samples) at 1225 °C. Certainly, other effects might contribute to this result, but porosity reduction (or gap closure) could be regarded as the most important one. Therefore, the data of the high temperature measurement of E in dependence on the porosity indicated that the $E_0 = 15.26$ GPa estimate of the linear model at room temperature must be too low. Thus, the linear model fitted to the data can not be considered as valid outside the measured porosity range.

Tab. 4.6.: Model functions and the obtained model parameters for the experimental $E(P)$ data; E_0 represents the Young's modulus at zero porosity; z, m and b are empirical constants

Model	Estimate		R^2	Reference
	E_0	Factor		
$E = E_0 - zP$	15.26	46.88	0.9078	-
$E = E_0 e^{-bP}$	23.40	−6.97	0.9195	Spriggs et al.[Spriggs, 1961]
$E = E_0(1-P)^m$	20.65	0.40	0.9071	Phani et al. [Phani and Niyogi, 1986]

As stated in the results section there was an influence of the porosity as well as of the temperature on the Young's modulus. A suitable model for this relationship was proposed by Munro [Munro, 2004]. Porosity and temperature are assumed to be independent variables in this case.

$$E(T,P) = E_T(T)E_P(P) \tag{4.1}$$

Applying this approach to the data obtained in this investigation resulted in:

$$E(T,P) = E_0 e^{a_1 T + a_2 T^2} e^{a_3 P} \tag{4.2}$$

where $E_0 = 29.844\,\text{GPa}$ represents the Young's modulus at room temperature and zero porosity. a_1 to a_3 are empirical factors with $a_1 = -2.096 \times 10^{-4}\,°\text{C}$, $a_2 = 1.113 \times 10^{-6}\,°\text{C}^2$, $a_3 = -8.324$. The adjusted-R^2-value for this model was found to be $R^2 = 0.9607$. This indicates an excellent agreement with the measured data as shown in Figure 4.13. However, this model only represents the data up to 1025 °C. For higher temperatures a polynomial of higher order may be applied.

In terms of thermal shock resistance and the concepts used these days, the obtained results are very interesting. The Young's modulus at 1450 °C or more precisely at temperatures above the former pyrolysis temperature, differs significantly from the room temperature values. Also the change of binder amount, type or pyrolysis temperature has a significant influence on the Young's modulus at high temperatures. It is not possible to conclude from the room temperature elasticity to the high temperature elastic behavior. However, it was shown that at least the porosity does not influence the relative Young's modulus behavior at high temperatures which would allow to conclude from room temperature E to high temperature E values.

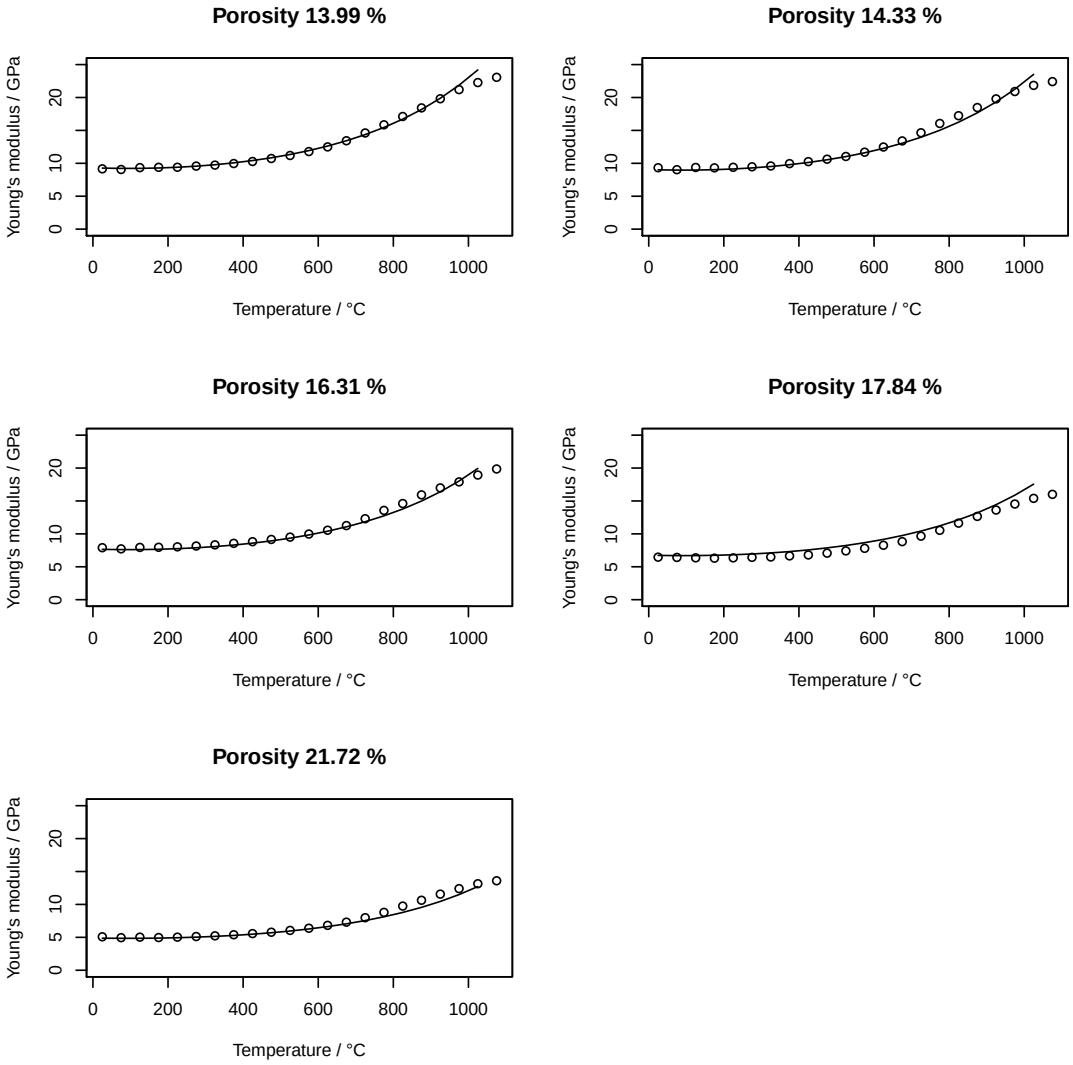

Fig. 4.13.: Measured Young's modulus E plotted versus temperature T at different porosity levels P compared to the introduced model (solid line)

Tab. 4.7.: The factorial design for the investigation of the influence of graphite content and maximum particle size on the elastic and additional properties

Factor	−	+
A - Graphite content / wt %	0	10
	10	30
B - Particle size / mm	0.045	3

4.2. Reference compositions

4.2.1. Influence of the maximum alumina particle size and the graphite content

Room temperature investigation

In this section the influence of the composition (particle size and graphite content) on the elastic properties was investigated. Therefore, the maximum alumina particle size was varied in three steps (0.045 mm, 1 mm, 3 mm). The graphite content was changed in 4 steps (0, 10, 20, 30 wt%).
In order to obtain the most important information and probable interactions between both factors, the analysis of the results were categorized by 2 factors with 2 levels each (2^2 factorial design as shown in Table 4.7). Therefore, maximum particle sizes of 0.045 mm and 3 mm were considered as factor levels, whereas the 1 mm composition was omitted in the analysis. The graphite content levels were split up into 0 to 10 wt % and 10 to 30 wt %. The 20 wt % level was omitted. However, complete confidence plots are shown in the appendix A.1.1 and A.1.2.
The effect of the factors will be illustrated by using bar charts showing the deviation of the factor mean from the overall mean of the response variable. The significance of these effects will be illustrated by dotted horizontal lines representing the confidence interval of the effect for $p < 0.05$. An effect needs to be bigger than these confidence borders in order to be regarded significant. A porosity after the pressing was calculated to obtain a possible influence of the graphite addition in the compaction behavior during pressing. The following equation was used for the calculation:

$$\pi_P = \left(1 - \frac{\rho_{bg}}{\rho_t}\right) * 100 \tag{4.3}$$

where ρ_{bg} is the bulk density after pressing (calculated by using the sample dimensions) and ρ_t is the theoretical density of the material.

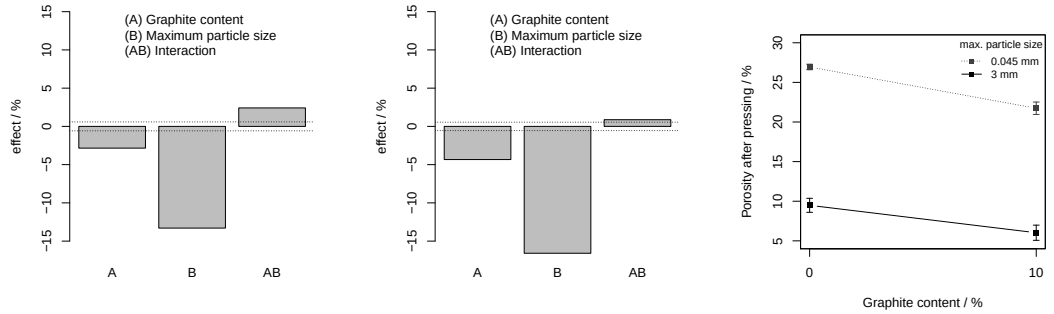

(a) $0 - 10\,\mathrm{wt\,\%}$ **(b)** $10 - 30\,\mathrm{wt\,\%}$ **(c)** Means and confidence intervalls for $0 - 10\,\mathrm{wt\,\%}$

Fig. 4.14.: Effect of the graphite content and maximum particle size (0.045 mm to 3 mm) on the apparent porosity after the pressing of the reference compositions, the dotted horizontal lines represent the confidence levels

In Figure 4.14 the effects of increasing either the graphite content ($0 - 10\,\mathrm{wt\,\%}$ or $10 - 30\,\mathrm{wt\,\%}$) or the maximum alumina particle size (from $0.045 - 3\,\mathrm{mm}$) on the porosity after pressing are shown. First of all both factors and their interaction can be considered significant because they were found to be bigger than the confidence level. However, the strongest influence on the porosity after pressing clearly was factor B the maximum particle size. Increasing the particle size resulted in a remarkably decreased porosity after pressing. The graphite addition also decreased the porosity, however considerably less. According to Oshima and McCarty [2012] "an interaction effect exists when the effect of one independent variable on the dependent variable depends on the value (level) of some other independent variable included in the study design." Regarding Figure 4.14c helps to understand this. Both main effects can be analyzed globally because the effect direction still remained the same. A small interaction effect of the graphite content on the effect of maximum particle size could be seen. Increasing the graphite content had a slightly reducing effect on the effect of increasing the maximum particle size. However, this effect was very small compared to the main effect of factor B. Thus, the conclusion that both factors had a reducing effect on the porosity after pressing is correct.

Exactly the same effects were observed for the apparent porosity after the pyrolysis (see Figure 4.15). The effect of the graphite increase from $0 - 10\,\mathrm{wt\,\%}$ was slightly increased. However, the influence of the maximum particle size was still approximately three times bigger than for the change in the graphite content (independent of the level). Furthermore, a significant interaction was found in the graphite range from $10 - 30\,\mathrm{wt\,\%}$. In Figure 4.15c it can be seen that the effect of increasing the maximum particle size

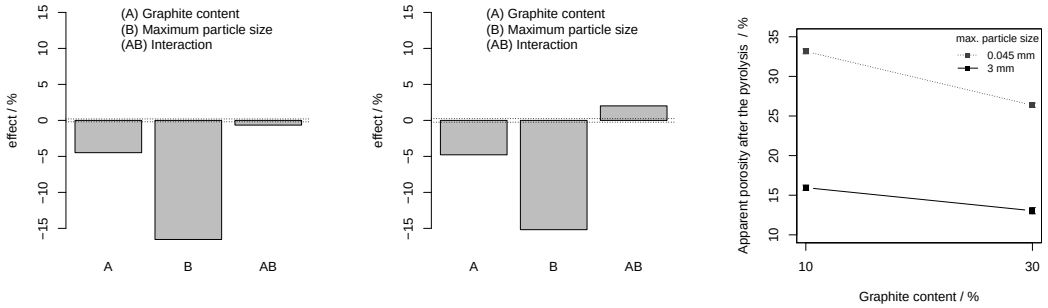

(a) $0 - 10\,\mathrm{wt\,\%}$ **(b)** $10 - 30\,\mathrm{wt\,\%}$ **(c)** Means and confidence intervalls for $10 - 30\,\mathrm{wt\,\%}$

Fig. 4.15.: Effect of the graphite content and maximum particle size (0.045 mm to 3 mm) on the apparent porosity after the pyrolysis of the reference compositions, the dotted horizontal lines represent the confidence levels

was reduced due to the increase of factor B , the graphite content. Nevertheless, the main effect conclusions still remain valid.
Therefore, the porosity of these materials was determined by the pressing process, which was remarkably influenced by the maximum alumina particle size. The graphite content had less influence on the compaction behavior. This porosity difference has to be taken into account for the discussion of the elastic properties.

Considering the bulk density in Figure 4.16, the influence of the two factors were found to be similar according to the changes in the porosity, however vice versa. Increasing the maximum particle size resulted in a strong increase of the bulk density of approximately $0.4\,\mathrm{g/cm^3}$. Of course the increase of the graphite content resulted in a decrease of the bulk density due to the lower density of graphite compared to alumina, which was substituted by the graphite. Again there was an interaction (see Figure 4.16c). The effect of increasing the maximum particle size on the bulk density was reduced at the upper level of the graphite content. Concluding, the bulk density was increased by the increase of the maximum particle size. However, this effect depended on the graphite level. Above $10\,\mathrm{wt\,\%}$ this effect might be decreased due to the graphite addition

The results of the two factorial comparisons of the Young's modulus are shown in Figure 4.17. The $0 - 10\,\mathrm{wt\,\%}$ graphite experiment in Figure 4.17a revealed clear significance of the two main effects and the interaction of both. Therefore, the confidence plot in Figure 4.17c was introduced to prevent erroneous conclusions. The two main effects showed a strong reducing effect on the Young's modulus. The biggest impact was found to be

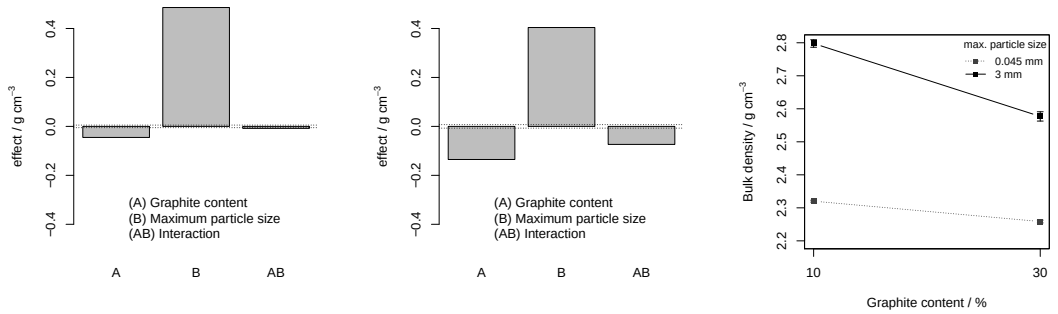

(a) $0 - 10\,\mathrm{wt\,\%}$ **(b)** $10 - 30\,\mathrm{wt\,\%}$ **(c)** Means and confidence intervalls for $10 - 30\,\mathrm{wt\,\%}$

Fig. 4.16.: Effect of the graphite content and maximum particle size (0.045 mm to 3 mm) on the bulk density of the reference compositions, the dotted horizontal lines represent the confidence levels

factor B, the maximum particle size. Regarding the confidence plot in Figure 4.17a the influence of factor B, the maximum particle size, always showed the same effect direction (reducing E). Therefore, it can be concluded that the maximum particle size increase was accompanied by a decrease of E in the graphite range of $0 - 10\,\mathrm{wt\,\%}$. Unfortunately, there was no such a global conclusion for the graphite content. Its effect on E clearly depended on the level of the maximum particle size. At the small particle size level, an increase of the graphite content significantly reduced the Young's modulus, whereas there was no significant effect found at the high particle size level.

In case of a graphite variation of $10 - 30\,\mathrm{wt\,\%}$, there was no significant interaction found. In Figure 4.17b the two main effects were significant. Thus, the increase of the graphite content at a constant particle size level resulted in a decrease of E. Furthermore, the increase of the maximum particle size showed a decrease of E, too. The absolute effects on E were remarkably smaller than for the $0 - 10\,\mathrm{wt\,\%}$ step comparison. Therefore, the effects of changing the maximum particle size or the graphite content on the Young's modulus were decreased by increasing the graphite content.

Concluding, the increase of the maximum alumina particle size was accompanied by a decrease of Young's modulus in both observed graphite ranges. The impact of this effect was greatest when changing from a zero graphite composition to a $10\,\mathrm{wt\,\%}$ composition. The addition of more graphite did not enforce this effect. The influence of the graphite content was dependent on the maximum particle size at the low graphite levels $0 - 10\,\mathrm{wt\,\%}$. At higher levels ($10 - 30\,\mathrm{wt\,\%}$) the graphite addition also caused a reduction of E, whereas no such influence was found in the low level experiment.

In Figure 4.18 the results for the shear modulus are shown. Clearly, the effects were

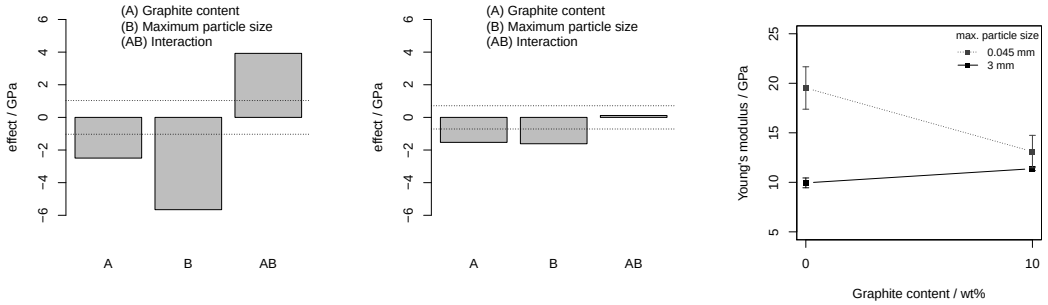

(a) $0 - 10\,\mathrm{wt\,\%}$ **(b)** $10 - 30\,\mathrm{wt\,\%}$ **(c)** Means and confidence intervalls for $0 - 10\,\mathrm{wt\,\%}$

Fig. 4.17.: Effect of the graphite content and maximum particle size (0.045 mm to 3 mm) on the Young's modulus of the reference compositions, the dotted horizontal lines represent the confidence levels, the confidence plot in (c) might support the interpretation of the interaction effect found in a)

smaller in absolute values than for the Young's modulus, but the tendency was the same as for the graphite change of $0 - 10\,\mathrm{wt\,\%}$. Again the interaction was significant, resulting in a more differentiated analysis shown in Figure 4.18c. The results are exactly the same as for the Young's modulus. No effect was found by changing the particle size at a graphite level of $10\,\mathrm{wt\,\%}$ and also by changing the graphite at a particle size of 3 mm.

However, the results of the $10 - 30\,\mathrm{wt\,\%}$ experiment were different to the Young's modulus results. Again there was no significant interaction. The increase of graphite from $10 - 30\,\mathrm{wt\,\%}$ showed the strongest effect on the shear modulus which was reduced. The increase of the maximum particle size also had a reducing effect on G, which however was significant lower than the effect of the graphite content. This might influence the results of the Poisson's ratio since it is calculated by those two variables.

The influence on Poisson's ratio of the graphite amount and the maximum particle size is shown in Figure 4.19. In case of changing the graphite content from $0 - 10\,\mathrm{wt\,\%}$ there was no significant effect observed; neither for the graphite amount nor the particle size. However, according to the differences in shear and Young's modulus described above, there was a significant influence of the graphite content on Poisson's ratio found for the graphite content range of $10 - 30\,\mathrm{wt\,\%}$. Within this border, increasing the graphite amount resulted in a significant increase of Poisson's ratio.

The damping behavior and its response to the change of graphite content and maximum particle size is shown in Figure 4.20. From $0 - 10\,\mathrm{wt\,\%}$ graphite both factors and their interaction were significant. The strongest influence on the damping showed the graphite

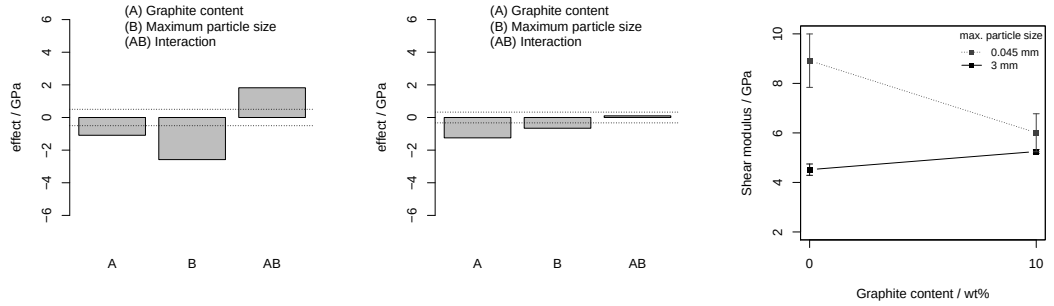

(a) $0 - 10\,\mathrm{wt\,\%}$ **(b)** $10 - 30\,\mathrm{wt\,\%}$ **(c)** Means and confidence intervalls for $0 - 10\,\mathrm{wt\,\%}$

Fig. 4.18.: Effect of the graphite content and maximum particle size (0.045 mm to 3 mm) on the shear modulus of the reference compositions, the dotted horizontal lines represent the confidence levels

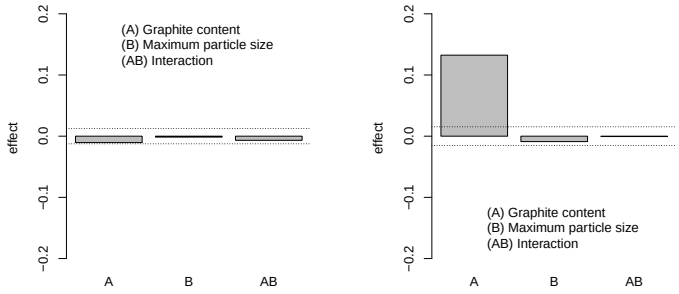

(a) $0 - 10\,\mathrm{wt\,\%}$ **(b)** $10 - 30\,\mathrm{wt\,\%}$

Fig. 4.19.: Effect of the graphite content and maximum particle size (0.045 mm to 3 mm) on the Poisson' ratio of the reference compositions, the dotted horizontal lines represent the confidence levels

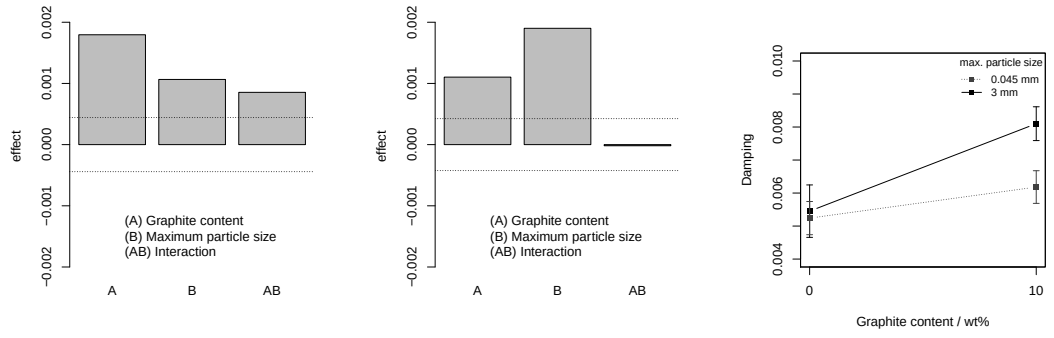

(a) $0 - 10\,\mathrm{wt\,\%}$ **(b)** $10 - 30\,\mathrm{wt\,\%}$ **(c)** Means and confidence intervalls for $0 - 10\,\mathrm{wt\,\%}$

Fig. 4.20.: Effect of the graphite content and maximum particle size (0.045 mm to 3 mm) on the Damping of the reference compositions, the dotted horizontal lines represent the confidence levels

content, followed by the maximum particle size. Regarding the confidence plot in Figure 4.20c, there was no effect of the particle size on the damping at zero graphite content. Nevertheless, the increase of the graphite content always was accompanied by higher damping values. Furthermore, at the 10 wt % graphite level the maximum particle size variation from low to high caused an increase of the damping.
The results of the $10-30$ wt % graphite comparison confirmed this observation. The two main factors showed significant effects on the damping of the material. The strongest impact was the maximum particle size change.

Discussion

The results presented above clearly showed the influence of the graphite content and maximum alumina particle size on the elastic and other physical properties of carbon-bonded alumina. First of all, the increase of the maximum particle size showed the most relevant effect on the compaction behavior. Increasing the particle size resulted in a better compaction, lower apparent porosity and higher bulk density. The reason therefore clearly was the better particle size distribution of the coarse particle composition compared to the small particle size composition (see Table 3.2). The graphite content also had a positive effect on the pressing process. Hence, it can be regarded as a lubricant. Furthermore, there was an interaction between these two factors. This means changing the levels of both factors resulted in a dependence of either the effect of graphite content change on the particle size change or vice versa.
The elastic properties (E, G, ν and damping) responded remarkably on the two factors. The Young's modulus was clearly influenced by both factors. Furthermore, there was an interaction found. The influence of the pressing process on these results has to be considered. At the small particle size level an increase of the graphite from $0-10$ wt % content resulted in a decrease of E and G. Furthermore, ν was not influenced. This result is in good agreement with the theory regarding the Young's modulus of composite materials presented in section 2 since E and G of graphite are significantly lower than those of alumina. However, at the high particle size level the effect of graphite addition was almost contrary. A reason therefore could be the different particle size distribution of both compositions. A lower apparent porosity might contribute to this effect. Therefore, the effect of graphite addition was depended on the level of the maximum particle size at low graphite contents.
At higher graphite contents of $10-30$ wt % the interaction was not significant anymore. Increasing the graphite content resulted in a decrease of E and G. The decrease of the

elastic properties due to the particle size increase is hard to explain since the apparent porosity was decreased within the same graphite content range. The decrease due to the graphite addition can be explained easily by the mixture laws introduced earlier (see section 2). Furthermore, the introduction of microcracks due to a different absolute expansion of the small and coarse alumina grains might be one explanation for the reduction of E and G with increasing particle size. Besides, Poisson's ratio responded significantly on the addition of graphite above 10 wt %. This also can be explained with the increasing amount of a second phase in this composite material.
The damping responded significantly on the graphite content change as well as on the maximum particle size. Again there was found a significant interaction for the low graphite content experiment. This was due to the lack of a maximum particle size influence on the damping at zero graphite content. At higher graphite contents both factors (graphite content and maximum particle size) were significantly influencing the damping behavior. It was assumed that only internal damping was measured (damping related to the microstructure). The introduction of either graphite or bigger particles caused an increase of grain boundaries or at least a change of the former grain boundary state. Thus, vibration energy was more dissipated due to the graphite introduction. Furthermore, the bigger particles could introduce microcracks due to their stronger absolute thermal expansion during pyrolysis. All these microstructural processes could contribute to the damping effects shown above [de Silva, 2005].

Comparing the obtained results with the composite-model of Hashin and Shtrikman [1963] could contribute to a better predictability of the elastic properties of carbon-bonded alumina. Therefore, the Hashin and Shtrikman Bounds (HS) were calculated for the reference compositions. However, these bounds provide only a two-phase model, whereas the carbon-bonded alumina is a three phase material. Therefore, at first the composite E of the two-phase material alumina-glassy carbon was calculated. Thereafter, this alumina-glassy carbon two phase composite was regarded as one phase and a second phase, graphite, was added to the model. The alumina-glassy carbon E value from the first calculation was then used as one phase E. This is the reason for the discrepancy of upper and lower HS-bounds at zero graphite content, since they actually represent the bounds for an alumina-glassy composite.

The results of this calculation are shown in Figure 4.21. The upper as well as the lower bounds were very far away from the measured results. Considering Figure 4.21b, the measured E values did not show a comparable dependence on the graphite content as the calculated values did. However, the porosity differences of the samples discussed above, contributed to this result. The porosity was directly correlated to the graphite

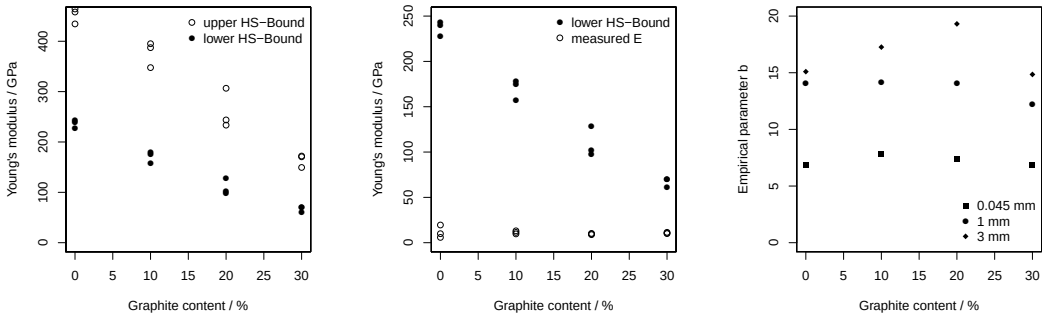

(a) HS-bounds

(b) Lower HS-bound and measured Young's modulus

(c) Calculated parameter b

Fig. 4.21.: Calculated HS-bounds compared to the measured E of the reference compositions; in (c) the calculated b parameter according to Spriggs in dependence on the maximum particle size is shown

content. The higher the graphite content was, the lower was the apparent porosity. The calculated HS-bounds did not take the porosity into account. Therefore, the porosity influence on the E values can be clearly seen here. Furthermore, the existence of microcracks within the composition, certainly contributed to the discrepancy of theoretical and measured values. It also has to be considered that the HS-bounds were established for homogeneous material, which is clearly not the case for the investigated compositions.
Applying Spriggs's model (see Table 2.2) to the measured and calculated E values, offers the opportunity to compute the b parameter in dependence on the graphite content. In Figure 4.21c this parameter is shown in dependence on the graphite content and the maximum particle size of the composition. Besides the exception of 20 wt % graphite content and 3 mm particle size, it could be said that the parameter b was almost independent on the graphite content. However, a dependence on the maximum particle size was found. As discussed in chapter "State of the art", the pore shape plays an important role in the relationship of Young's modulus and porosity. Therefore, it could be assumed that the observed particle size influence might be attributed to differences in the pore shape within the compositions. This could be caused by the differences in the particle size distribution and maximum particle sizes. In conclusion, this calculation showed clearly the contribution of the pore shape on the Young's modulus dependence on the porosity.

High temperature investigation

The results of the high temperature investigation are illustrated in the same way as in the previous section 4.1 "Industry related compositions". The Young's modulus difference of $E_T - E_0$ was normalized to its room temperature value E_0. Furthermore, the thermal expansion of the compositions and the behavior of the samples during the holding time ($E - E_i$ normalized to E_i the initial E at the holding time) are shown.

The results of the high temperature measurements for the 0.045 mm compositions are shown in Figure 4.22. The Young's modulus measurement results up to 1450 °C are shown in Figure 4.22a. E increased significantly up to the former pyrolysis temperature of 1000 °C during heating. Above this temperature E remained almost constant. The graphite content contributed significantly to this increase. The graphite containing compositions showed an almost 2 to 3 times higher increase of E than the zero graphite composition with a total increase of $\approx 30\,\%$. There was no significant relationship between the total increase and the graphite amount. The highest increase of E was found for the 20 wt % graphite composition ($E - E_0/E_0 \approx 75\,\%$), whereas there was almost no difference between the 10 and 30 wt % graphite compositions which were between the 20 wt % and zero wt % graphite compositions.

During soaking a strong increase of E was found (see Figure 4.22c). The carried out ANOVA revealed a significant influence of the time on E and no influence of the graphite content on E (see Table A.14 in the appendix).

During cooling all compositions showed a hysteresis behavior. Down to temperatures between 600 and 800 °C E remained almost constant and above the values reached during heating. Below these temperatures E decreased significantly to room temperature. Depending on the graphite content the residual Young's modulus was equal or higher than the initial value (20 and 30 wt % compositions) or lower for the zero and 10 wt % composition.

The results of the thermal expansion measurement are shown in Figure 4.22b. Unfortunately the result of the 10 wt % composition measurement got lost due to an energy shutdown during the measurement. Up to approximately 1250 °C the expansion behavior of all compositions can be regarded as equal. Above this temperature the compositions started to show a reduced expansion in dependence on the graphite content. The higher the graphite content the less was the reduction in expansion. In other words the strongest total expansion was found for the highest graphite content. The zero graphite compositions showed an unusual expansion during soaking. There could be several possible reasons for this phenomenon. The most reasonable would be related to the heat dis-

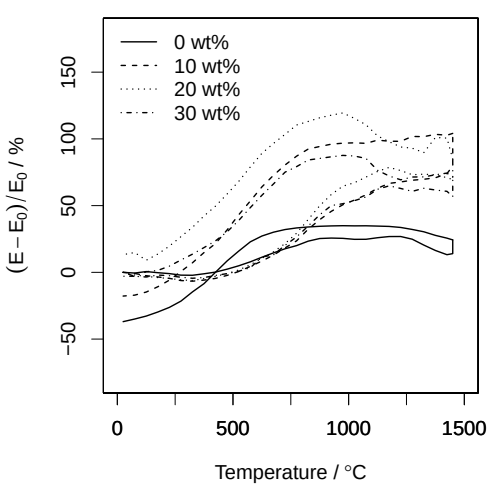

(a) Young's modulus measurement

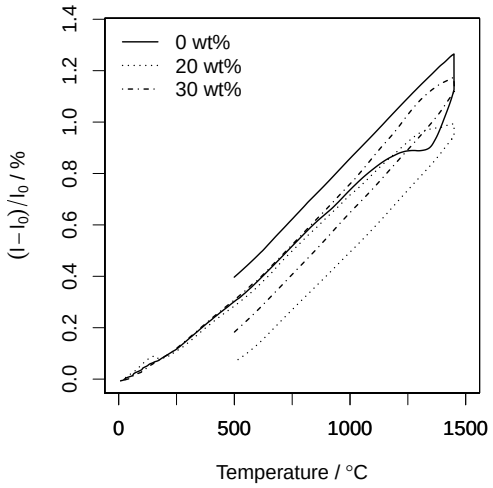

(b) Dilatometer measurement

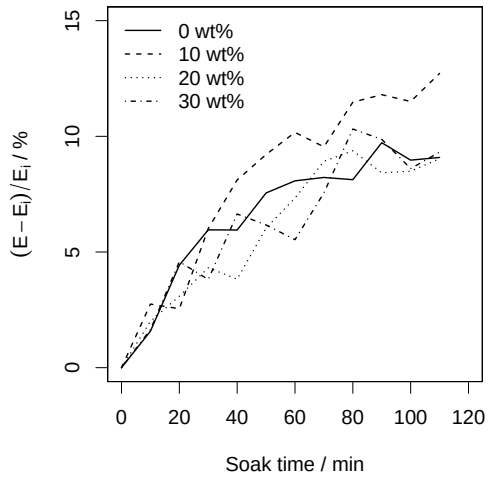

(c) Soak time behavior

Fig. 4.22.: Young's modulus and thermal expansion measurement up to 1450 °C of the 0.045 mm composition

sipation within the testing apparatus. There was an alumina ring around the sample filled with pet coke to protect the samples from oxidation. The thermocouple however was assembled outside of this circle. Furthermore, the high porosity of the zero graphite composition certainly caused a lower heat conduction in the material. Thus, the ongoing expansion during the soak time of the zero graphite composition might be related to a delay due to the reasons described. During cooling all compositions showed a linear shrinkage.

In Figure 4.23 the results of the high temperature investigation of the 1 mm composition are shown. The Young's modulus evolution in Figure 4.23a was the same as for the industry related compositions pyrolized at 1000 °C. However, there was clearly a significant influence of the graphite content on this behavior. The less graphite the composition contained the stronger was the slope of $E(T)$ in the temperature range of $500 - 1000\,°$. Additionally, E_{max} decreased with increasing graphite content. A sudden decrease of E after the holding time was observed. This decrease was steeper for the zero graphite composition than for the graphite containing ones. The overall reduction of E was around 50 % for the 20 & 30 wt % graphite compositions and around 70 % for the 0 & 10 wt % compositions.
The difference between 0 & 30 wt % graphite was around 70 % at the former pyrolysis temperature, whereas there was no difference between 10 & 20 wt % at this temperature.
The thermal expansion behavior is shown in Figure 4.23b. Considering only the heating curves, a significant influence of the graphite on $\alpha(T)$ was found. The higher the graphite content was the more nonlinear was the heating curve evolution. For the higher graphite compositions (20 & 30 wt %) the slope of the expansion increased strongly between 750 °C and 1000 °C. This might be due to the pyrolysis temperature of 1000 °C which was also clearly visible in the E measurement.
During the holding time again there was a strong expansion found for the zero graphite composition. The explanation was already given for the 0.045 mm composition.
The cooling curve behavior again was affected by the graphite content. For the non graphite composition a linear decrease was found whereas the curves appeared to be more nonlinear with increasing graphite content.
The Young's modulus was not significantly dependent on the soak time (see Figure 4.23c). Furthermore, there was a strong scattering of the measurement data contributing to this result. However, the graphite content was determined as a significant factor by the carried out ANOVA (see Table A.25). Therefore, a pairwise comparison was additionally done to determine the differences between the compositions. The results are shown in Table 4.8. There were significant differences found between 0-20 wt %, 0-

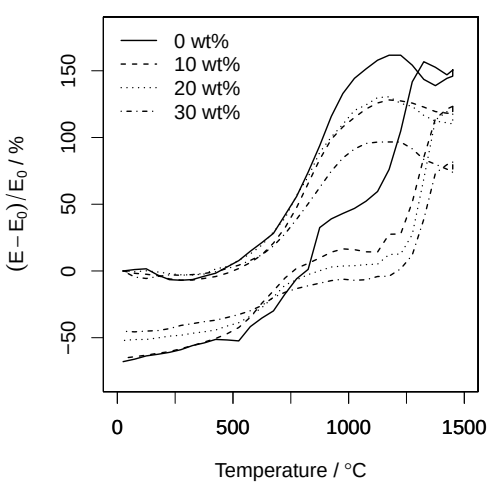

(a) Young's modulus measurement

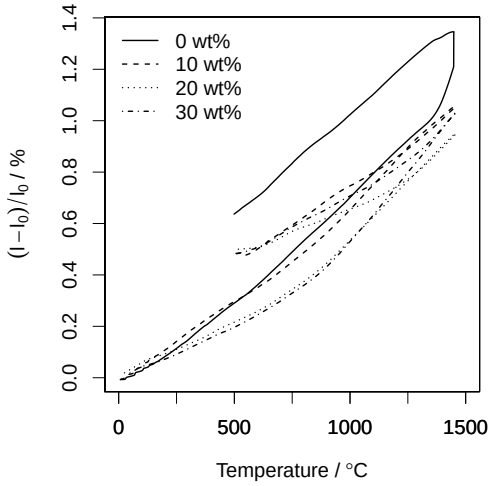

(b) Dilatometer measurement

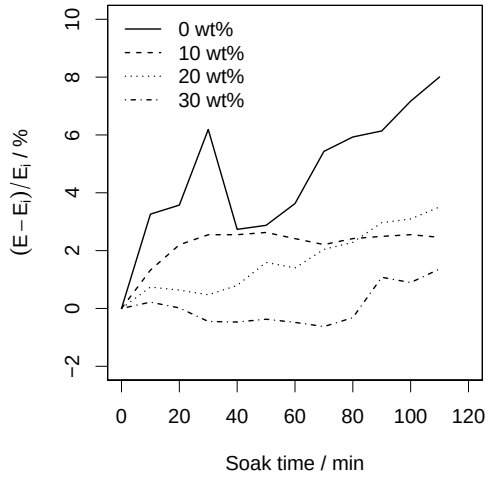

(c) Soak time behavior

Fig. 4.23.: Young's modulus and thermal expansion measurement up to 1450 °C of the 1 mm composition

Tab. 4.8.: Results of the pairwise Student's t-test (adjusted p-value according to the Holm-Bonferroni method [Holm, 1979]) for the graphite content influence on the soak time behavior of E for the 1 mm compositions; for each pair a p-value is shown, $p < 0.05$ indicates a significant difference

	0	10	20
10	0.1813	–	-
20	0.0205	0.0049	-
30	0.0205	0.1813	0.1813

30 wt % and 10-20 wt % graphite compositions. Furthermore, a tendency of increasing Young's modulus could be seen for all compositions.

The results of the high temperature Young's modulus measurement for the 3 mm compositions are shown in Figure 4.24a. The actual curve development was the same as for all carbon-bonded compositions before. However, compared to the 1 mm composition results the graphite content influence was different. The lowest increase of E during heating was found for the zero and 20 wt % graphite compositions, whereas the highest E values were found for the 30 wt % composition. The graphite content influence was not as linear as for the 1 mm composition. Furthermore, the maximum ΔE was 175 % for 30 wt % graphite and 130 % for 0 wt % graphite. This was significantly higher than for the 1 mm compositions. A decrease of E of around 65 % (0,10,30 wt % graphite) and 50 % for the 20 wt % composition was observed after a measurement.

The thermal expansion up to 1450 °C is shown in Figure 4.24b. Again, the influence of the graphite amount on the thermal expansion was quite obvious as for the 1 mm compositions, too. The higher the graphite amount was, the lower was the obtained maximum expansion at 1450 °C. Furthermore, the expansion during heating was more nonlinear for the higher graphite amount compositions. The highest expansion was found for the non graphite composition. The cooling behavior was comparable to the heating curve since it turned more nonlinear with increasing graphite content resulting in a residual expansion of the material (in case of extrapolating to room temperature). Once again, an expansion during the holding time of the zero graphite composition occurred. The reason therefore was already described for the 0.045 mm composition.

The soak time behavior can be found in Figure 4.24c. Clearly a dependence of E on the graphite content was observed. The lower the graphite content was, the more apparent was an increase of E during the holding time.

A significant mass loss and porosity increase during the high temperature E measurement was observed for samples of all compositions. Therefore, several ANOVA were carried

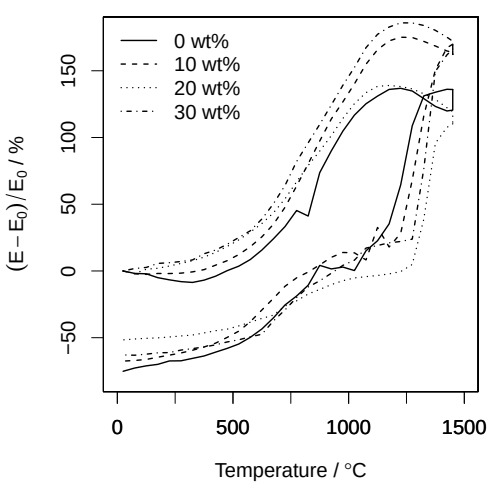

(a) Young's modulus measurement

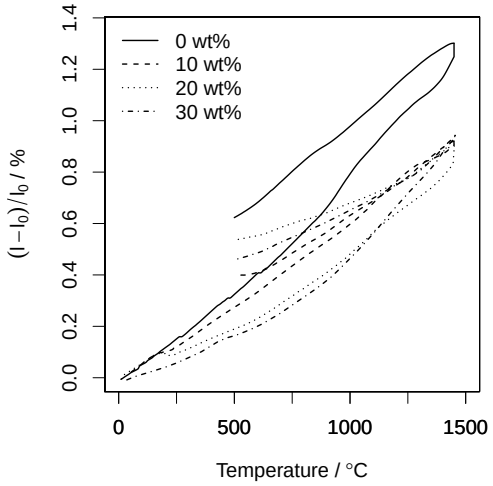

(b) Dilatometer measurement

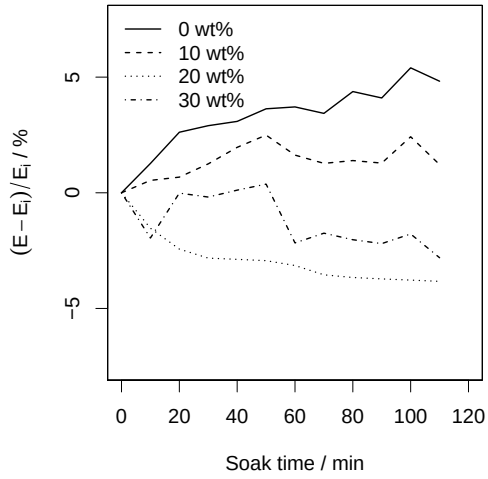

(c) Soak time behavior

Fig. 4.24.: Young's modulus and thermal expansion measurement up to 1450 °C of the 3 mm composition

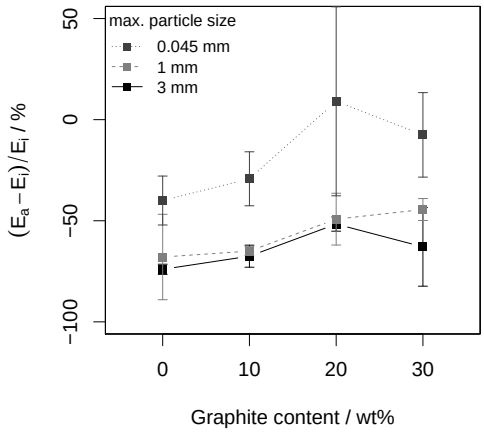

Fig. 4.25.: Young's modulus change after the high temperature measurement in dependence on the maximum particle size and graphite content; where E_a represents E after the measurement and E_i before, both at room temperature

out to investigate the dependence of this mass loss, the porosity increase and the Young's modulus change on the particle size and the graphite content (see paragraph A.1.1 for exact ANOVA tables).

The graphite content as well as the particle size were found to be a significant influence on the retained Young's modulus after one measurement. Furthermore, the interaction of both was significant, too. Due to the high amount of experiments, pairwise comparisons were omitted. Instead, the means of Young's modulus variation were plotted against the graphite content (shown in Figure 4.25). Clearly, the significance of the particle size influence can be observed. Furthermore, an influence of the graphite content was visible, however the data scattering was quite high. Apparently, higher graphite contents led to less Young's modulus reduction. This was only true up to 20 wt % graphite. Above, $\Delta E/E_i$ was reduced. The particle size affected $\Delta E/E_i$ significantly, too. But only the levels 0.045 mm and 1/3 mm differed significantly from each other. The coarser the maximum particles were, the bigger was the observed Young's modulus reduction after one cycle.

The influence of the graphite content on the mass loss and the porosity was tested, too. There was no significance found for the graphite content at the particle size levels of 1 and 3 mm. Only at a level of 0.045 mm the graphite content had a significant influence on the retained mass and porosity. In Tables 4.9a and 4.9b the results of a comparison of means are shown. Only the zero graphite content composition showed a significantly

Tab. 4.9.: Results of the multiple comparison of means ad-hoc test (Tukey-HSD) for the graphite content influence on the retained porosity and mass loss after a high temperature measurement for the 0.045 mm compositions; for each pair a p-value is shown, $p < 0.05$ indicates a significant difference

(a) Test for the porosity change

	0	10	20
10	0.923	–	–
20	0.879	0.999	–
30	0.001	0.002	0.002

(b) Test for the mass loss

	0	10	20
10	0.018	–	–
20	0.0135	0.995	–
30	0.0145	0.997	0.999

different mass change compared to the other compositions (0.60 % lower porosity change compared to all other compositions). However, this tendency was not found for the porosity change (see Table 4.9b) as it could be expected since the mass loss was assumed to be caused by oxidation. Instead, the 30 wt % graphite composition exhibited a higher porosity increase than the other compositions.
In conclusion it can be said, that the oxidation influence could be registered by a mass loss. Nevertheless, a clear dependence of the retained Young's modulus values on the mass loss could not be demonstrated.

Discussion

In the discussion part of section 4.1, a model describing the high temperature changes of $E(T)$ of carbon-bonded alumina was suggested. The results presented above will be discussed according to that model.
Regardless of the graphite content and the particle size, an increase of E up to the former pyrolysis temperature was observed for all compositions. Furthermore, a strong hysteresis was found between heating and cooling. This behavior was explained earlier. Due to preexisting gaps between the constituents, which were closed at reheating, E increased. The hysteresis during cooling was explained by the occurrence of sintering (stiffening effect) and stretching of the matrix (decreasing E) due to different thermal expansion coefficients of the contained materials and temperatures above the former pyrolysis temperature. The sintering effect was proved due to an increase of E during the soak time and the occurrence of slight shrinkage during the holding time. Therefore, in general the results of the reference compositions support the described model.
Nevertheless the approach of this study was to determine the influence of certain factors on the high temperature Young's modulus. Therefore, the graphite content and the maximum particle size were introduced as factors. The influence of the graphite content was shown above at each particle size level. It was no consistent relationship between the

Young's modulus in dependence on the temperature and the graphite content found. At the smallest particle size the non graphite material showed the lowest overall E increase (also of all compositions). No significant difference was found for the graphite containing compositions between each other. Adding graphite to the composite reduces the volume fraction of alumina and binder. Thus, a mismatch between the thermal expansion coefficients of the material can be assumed and could contribute to microcracking and gap development in the material. These gaps and microcracks could be assumed to be numerously and even bigger than for the zero graphite composition. Therefore, the Young's modulus at reheating (during the measurement) increased strongly for the graphite containing compositions at a particle size of 0.045 mm. However, the contribution of the porosity to this behavior is not really understood yet. The results from the section 4.1 suggest that the porosity influence on the normalized Young's modulus could be omitted within a porosity range of 14 to 21 %. The 0.045 mm compositions had a porosity between 29 and 38 %. The range between highest and lowest porosity is comparable. Therefore, a possible porosity influence was omitted in this discussion.
It might be assumed, that at the other particle size levels the same relationship will be evident. However, different results were obtained. The 3 mm and zero graphite containing composition also comprised the lowest increase of E up to the former pyrolysis temperature. But, at a particle size of 1 mm and the same graphite level (zero), the increase of E was the highest found at this particle size level. Furthermore, differences between the graphite levels were found at these two particle size levels. These results show that there was an interaction effect between the graphite content and the maximum particle size. For example at a maximum particle size of 3 mm the strongest increase of E was found for the 30 wt % graphite composition, whereas at a particle size of 1 mm this graphite level caused the lowest E increase. According to the model suggested earlier, the addition of graphite would disturb the microstructure bit by bit resulting in a stronger increase of E due to the gap closure and crack healing. Nevertheless, too much graphite apparently caused so many microcracks that they could not be completely closed during reheating. This might be one reason for the phenomena observed. A second one could be the contribution of the particle size of the graphite. Alternating the alumina particle size, changes automatically the relation between the graphite and alumina particles. Therefore, the quite coarse graphite could exhibit more microcracks within the composite material, whereas at a bigger alumina particle size, the graphite could be better gathered in the gaps between the alumina particles.

Obviously, the maximum alumina particle size contributed significantly to the high temperature Young's modulus. In Figure 4.26 the previously shown results of the high

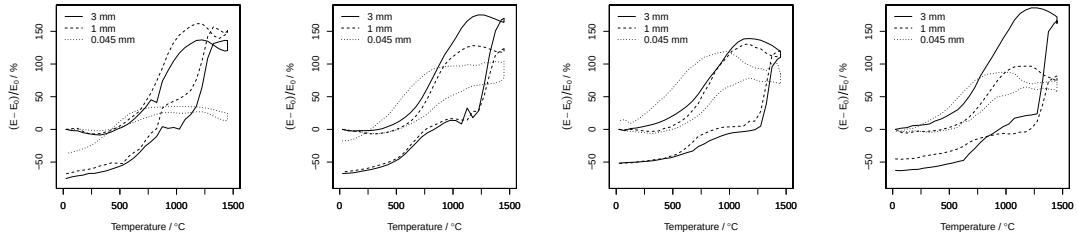

(a) 0 wt % **(b)** 10 wt % **(c)** 20 wt % **(d)** 30 wt %

Fig. 4.26.: Young's modulus measurement up to 1450 °C sorted by graphite content

temperature E measurement are sorted by the maximum particle size for each graphite content level. Thus, it is easier to obtain an influence of the particle size on the high temperature E. Clearly, the coarse particle containing compositions (1 and 3 mm) exhibited steeper and higher increases of E up to the former pyrolysis temperature. Furthermore, the hysteresis between cooling and heating was different for the finest particle size composition (0.045). Besides for the zero graphite composition there was almost no E reduction during one cycle for these compositions. The 3 mm compositions showed the strongest increase of E during heating and the steepest decrease during cooling. Besides these differences the 3 mm and 1 mm compositions showed an almost equal high temperature behavior.

Thus, the maximum particle size effect was greatest between 0.045 mm and 1 mm. Coarser particles are expanding and shrinking more in absolute values than smaller particles. Therefore, the coarse particle containing compositions might be regarded as stronger disturbed before a measurement. Again these defects could be healed during the reheating resulting in the strong increase observed. Also the strong decrease of the residual E supports this theory.

The sintering of the compositions at the holding time can be regarded as proven. All of the fine particle compositions showed a significant increase of E during the holding time, supporting the sintering theory. Furthermore, with increasing particle size that increase of E decreased until no effect for the 3 mm composition. Furthermore, this sintering influenced the hysteresis behavior which can be seen in Figures 4.26a - 4.26d. The finest particle size compositions were found to exhibit the strongest increase of E during soaking. At cooling these compositions then showed higher values of E than during heating. Only at graphite contents of 0 and 10 wt % the residual E was smaller than the initial.

Concluding, the introduced model from section 4.1 was proven by the results of the reference compositions. Furthermore, a significant influence of the graphite content, the

maximum particle size and their interaction on the high temperature Young's modulus was obtained. The effect of the graphite content was influenced by the level of the maximum particle size. Therefore, a main conclusion of the influence of the graphite content on E could not be made. However, there was a quite clear influence of the maximum particle size on E up to 1450 °C. The finer the alumina particles were the lower was the overall increase of E and the less strong was the hysteresis between cooling and heating. Thus, the fine particles did not disturb the material during pyrolysis as strong as the coarse particles.
Furthermore, a mild oxidation during a measurement was observed due to a mass loss of the samples. This mass loss was not dependent on the graphite content of the samples but on the particle size. This oxidation could not be avoided, however a clear influence on the retained Young's modulus could not be proven. Therefore, the shown results above contain a contribution of this oxygen attack which has to be considered.
The thermal expansion measurement supported the results obtained already in the previous section. In Table 4.10 a shift of the thermal expansion slope in the temperature range of $25 - 825\,°C$ and $1025 - 1450\,°C$ clearly was proven. This shift was dependent on the graphite content as well as on on the maximum particle size. For the smallest particle size of 0.045 mm the shift from a lower expansion coeffiecient to a higher above the former pyrolysis temperature was reversed. Below the pyrolysis temperature α was higher than above which shows the particle influence on the microstructure. For the 30 wt % graphite composition of this small particle size the expansion shift was found to be positive as for all other compositions. Thus, the bigger graphite flakes influenced the microstructure in a comparable way as the alumina particle. At the 1 and 3 mm particle size the shift was always positive. With higher graphite contents the difference between the expansion below and above the pyrolysis temperature increased. Therefore, again the graphite particle size influenced the result due to higher microcracks which were introduced during the pyrolysis. After closing these microcracks during reheating up to the former pyrolysis temperature, the expansion coefficient increased strongly due to an undisturbed expansion of the now "defect free" composite. These results support greatly the model suggested in section 4.1 and correlate to the results of the high temperature Young's modulus measurement.

Tab. 4.10.: Coefficients of thermal expansion below and above the pyrolysis temperature of 1000 °C in dependence on the graphite content and maximum particle size

max. particle size	3 mm		1 mm		0.045 mm	
Graphite content	α_{25-825}	$\alpha_{1025-1450}$	α_{25-825}	$\alpha_{1025-1450}$	α_{25-825}	$\alpha_{1025-1450}$
	$\times 10^{-6}\,K^{-1}$		$\times 10^{-6}\,K^{-1}$		$\times 10^{-6}\,K^{-1}$	
0 %	7.23	9.27	7.00	9.79	7.33	5.33
10 %	5.95	6.70	6.16	9.05	–	–
20 %	4.10	7.44	4.35	9.22	7.00	6.24
30 %	4.15	10.60	4.39	11.20	7.49	10.00

Tab. 4.11.: The factorial design for the investigation of the influence of carbon filler type and maximum particle size on the elastic and additional properties, the used filler types were **AF** = fine natural graphite, **NFL** = coarse natural graphite, **CB** = carbon black and **Mix** = 1:1 AF/NFL

Factor	−	+
A - Carbon filler type	Mix	AF
	Mix	NFL
	Mix	CB
B - Particle size / mm	0.045	3

4.2.2. Influence of the maximum alumina particle size and the carbon filler type

Since different types of carbon filler are applied often in the refractory industry, their influence on the elastic properties was investigated, too. Therefore, three 2^2 full factorial experiments were carried out (see Table 4.11). The maximum alumina particle size was varied in three steps (0.045 mm, 1 mm, 3 mm). Four different carbon filler types were investigated. Considering the filler type as a factor, the ”- level” was always defined as ”Mix” because this was the condition for all the previously discussed compositions. The 1 mm level of the particle size factor was omitted, though the results can be found in the appendix A.1.2.

Comparison of fine graphite (AF) to AF/NFL mix (fine/coarse)

In Figure 4.27 the effects of changing the filler type on the apparent porosity and bulk density are shown. Clearly, there was no effect of changing the carbon filler from a mixture of fine and coarse graphite to the fine graphite on its own on the porosity and the bulk density. Again, the effect of increasing the maximum particle size was a

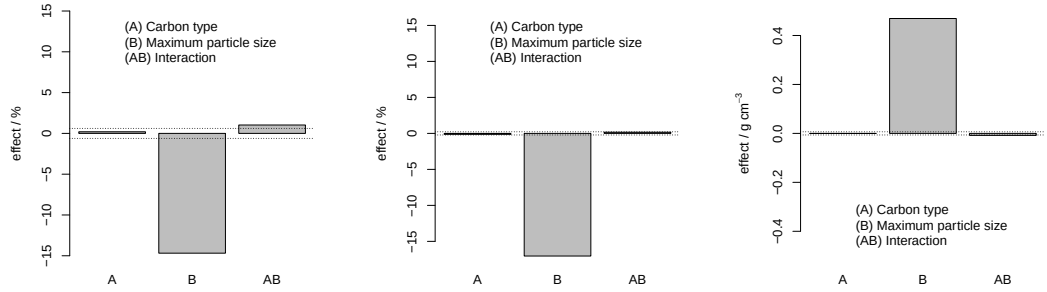

(a) Apparent porosity after the pressing

(b) Apparent porosity after the pyrolysis

(c) Bulk density

Fig. 4.27.: Effect of the carbon filler type (AF) and the maximum particle size (0.045 mm to 3 mm) on the Apparent porosity and bulk density of the reference compositions, the dotted horizontal lines represent the confidence levels

reduction of apparent porosity and an increase of bulk density. This effect was already found in the previous experiment described above.

Nevertheless, the elastic properties were influenced by both factors significantly (see Figure 4.28). Surprisingly, the influence of the graphite filler was stronger than that of the maximum particle size. Increasing the particle size resulted in a significant decrease of E and G (see Figures 4.28a and 4.28b). Considering the porosity results, this reduction effect was not caused by the pressing process, since there was no influence of the filler change found. Therefore, this reduction of E and G has to be related to a change in grain and phase boundaries.

The Poisson's ratio was influenced by both factors and their interaction, too. Therefore the means of the Poisson's ratio are considered (see Figure A.5c in the appendix). It was found that the maximum particle size effect on Poisson's ratio clearly influenced the effect of changing the filler type. Due to this strong interaction, the main effects shown in Figure A.5c should be ignored. Changing the carbon filler showed either no effect on Poisson's ratio for the coarse particle size (3 mm) or an increase for the fine grained composition. Furthermore, the change of the maximum particle size showed only an effect with the fine grained carbon filler.

Thus, it can be concluded that the change from a mixture of fine/coarse graphite to a singular fine graphite resulted in a remarkable decrease of E and G and showed no effect on the porosity or bulk density. There was no influence on the elastic properties of the particle size change.

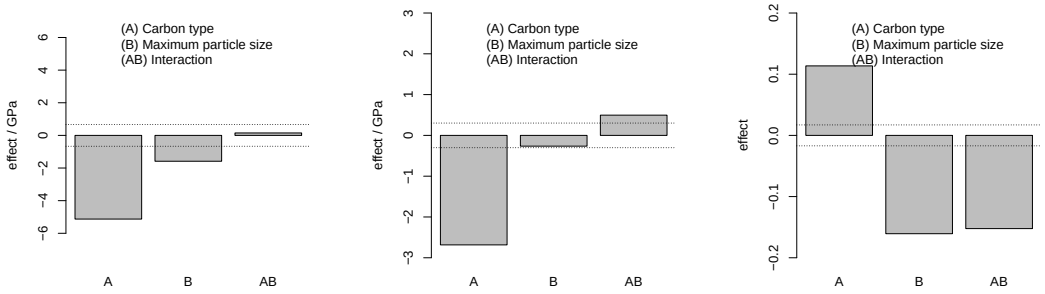

(a) Young's modulus **(b)** Shear modulus **(c)** Poisson's ratio

Fig. 4.28.: Effect of the carbon filler type (AF) and the maximum particle size (0.045 mm to 3 mm) on the Young's and shear modulus and Poisson's ratio of the reference compositions, the dotted horizontal lines represent the confidence levels

Comparison of coarse graphite (NFL) to AF/NFL mix (fine/coarse)

The results for the carbon filler change from "Mix" to "NFL" are shown in Figures 4.29 and 4.30. It is apparent that their was no effect of the filler change on the porosity and bulk density, as observed for the "Mix" to "AF" change.
The elastic properties were influenced in the same manner as for the change from mix to fine. However, the absolute effect values were found to be much smaller than for the change from "mix" to "AF".
Poisson's ratio was influenced in the same way as described above. In conclusion, the change from a mixture of graphite to a coarse graphite affected the elastic properties less than for the change from a mixture to fine graphite.

Comparison of carbon black (991) to AF/NFL mix (fine/coarse)

The last tested carbon filler type was carbon black. The results of its influence on the apparent porosity and bulk density are shown in Figure 4.31. Again, the influence of the filler type was non existent or very low compared to the influence of the maximum particle size. The porosity was reduced due to the change in the maximum particle size and furthermore this factor had an increasing effect on the bulk density.
Young's and shear modulus were mainly affected by the change in maximum particle size (see Figure 4.32). However, the interaction of both factors was significant, too. Therefore, the mean values from the appendix will be described here (see Figure A.5). The effect of the maximum particle size on the elastic properties E and G was influenced

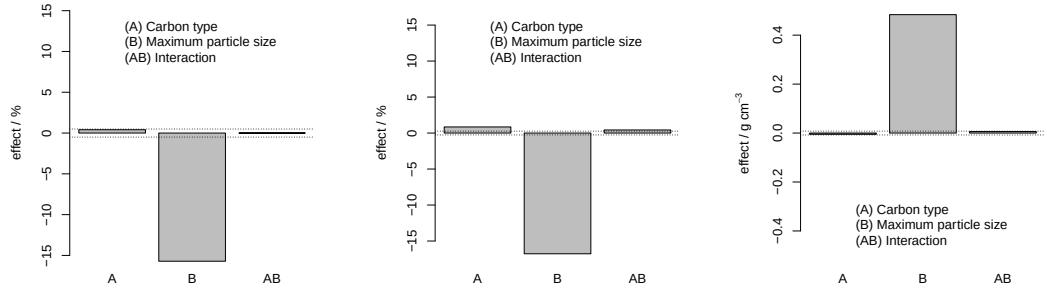

(a) Apparent porosity after the pressing **(b)** Apparent porosity after the pyrolysis **(c)** Bulk density

Fig. 4.29.: Effect of the carbon filler type (NFL) and the maximum particle size (0.045 mm to 3 mm) on the Apparent porosity and bulk density of the reference compositions, the dotted horizontal lines represent the confidence levels

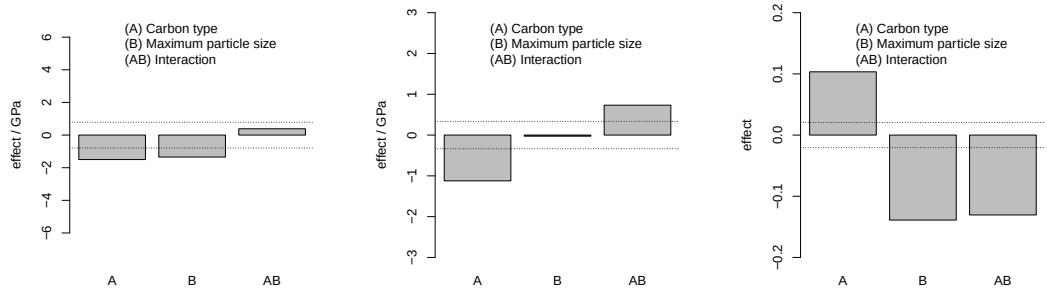

(a) Young's modulus **(b)** Shear modulus **(c)** Poisson's ratio

Fig. 4.30.: Effect of the carbon filler type (NFL) and the maximum particle size (0.045 mm to 3 mm) on the Young's and shear modulus and Poisson's ratio of the reference compositions, the dotted horizontal lines represent the confidence levels

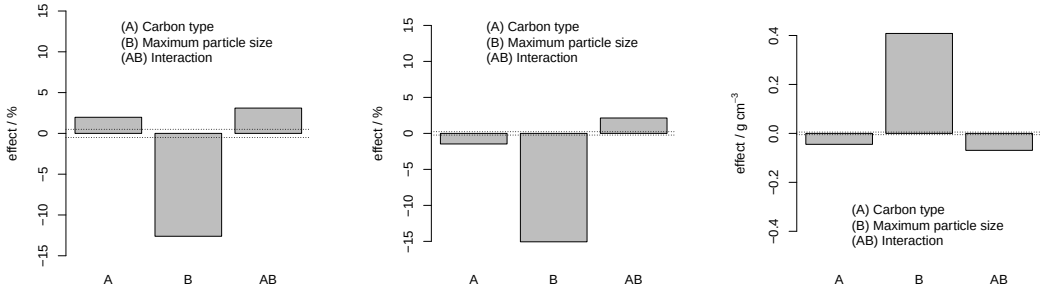

(a) Apparent porosity after the pressing

(b) Apparent porosity after the pyrolysis

(c) Bulk density

Fig. 4.31.: Effect of the carbon filler type (991) and the maximum particle size (0.045 mm to 3 mm) on the Apparent porosity and bulk density of the reference compositions, the dotted horizontal lines represent the confidence levels

by the level of the graphite filler type. With carbon black as a filler the effect of the particle size on E was bigger than for the mix composition. Nevertheless, the Poisson's ratio was affected only by the graphite filler type. Changing it to carbon black resulted in a strong increase of E.

Discussion

The influence of the carbon filler on the elastic properties was found to be less than the effect of the graphite content. The only significant influence on the elastic properties was found for the carbon black and fine graphite substitution. The change from a mix of coarse and fine graphite to coarse graphite on its own showed little to almost no effect. The decrease of the graphite flake size showed a strong decreasing effect on E and G but almost no effect on the apparent porosity and bulk density. Thus, the porosity did not influence these results. The smaller graphite flake size certainly contributed to the decreasing effect by dispersing energy due to the increase in grain boundaries between the graphite and alumina particles. Furthermore, the decrease of elasticity could be due to the increase in the specific surface area of the graphite. The additional surface had to be wet by the resin binder. Thus less binder certainly will be found between the alumina and graphite particle which led to a decrease of elasticity.
Other than graphite, carbon black is an amorphous carbon. Therefore its properties are considerably different to those of graphite [Pierson, 1993a]. Thus, the addition of carbon black to the composition considerably changed the nature of elastic response of the

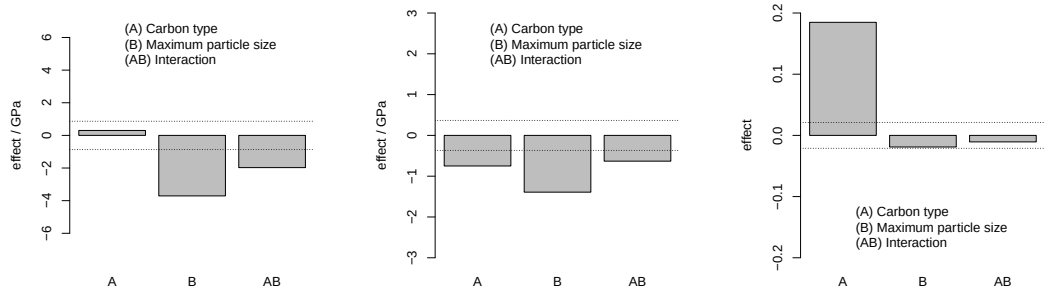

(a) Young's modulus **(b)** Shear modulus **(c)** Poisson's ratio

Fig. 4.32.: Effect of the carbon filler type (991) and the maximum particle size (0.045 mm to 3 mm) on the Young's and shear modulus and Poisson's ratio of the reference compositions, the dotted horizontal lines represent the confidence levels

material. The strong influence of the carbon black addition on Poisson's ratio illustrates this very well.

Besides the graphite or carbon filler content, the type of filler also contributed considerably to the elastic properties of carbon-bonded alumina. This should be investigated deeper, especially the influence on the high temperature behavior.

4.3. Young's modulus of carbon-bonded open cell foam structures

4.3.1. Room temperature observations

Foam structures are state of the art materials in many industries. The carbon-bonded open cell foam structures investigated will be used for steel melt filtration. Therefore, their thermal shock behavior is from a crucial interest to the material engineer. According to the approach of Gibson and Ashby, the so called strut material (bulk material) was investigated regarding its elastic behavior first. Afterwards, foams of the same compositions were investigated and the results will be compared to findings from the literature. The influence of the binder content (Carbores®) on the porosity and the elastic moduli (E and G) was investigated at room temperature. In Figure 4.33a the results are illustrated. The porosity clearly was dependent on the Carbores® content after the pressing as well as after the pyrolysis. With an increase of the Carbores® content the porosity was linearly reduced. After the pyrolysis this dependence was no longer linear. Still with an increase of the Carbores® content the porosity was decreased, however stronger at higher binder amounts.
The Young's modulus and shear modulus results are shown in Figure 4.33b. Increasing the Carbores® amount led from 5 to 10 wt % Carbores® to an increase of E and G. At higher binder contents there was no change of G and a slight increase of E observed. However, according to a comparison of means of the Carbores® levels (see Table 4.12) there were only significant differences between the 5 wt % and all other levels. ANOVA tests were carried out to obtain these influences. The exact result tables can be found in the appendix A.1.3.

The influence of the apparent porosity of the pyrolyzed material with 20 wt % Carbores® was investigated to compare the findings with the porosity models proposed by Spriggs [1961]; Phani and Niyogi [1986]; Nielsen [1984] and Gibson and Ashby [1997]. The Carbores® content was chosen according to the content of the foam structures. The results are shown in Figure 4.34. The obtained porosity range by alternating either the forming technology (pressing or slip casting) or adding a pore forming agent was from 35 to 61 % for the bulk material. Furthermore, results from carbon-bonded foams were added to extend this range (macroscopic porosity of 85 to 91 %). The measured Young's modulus values were in the range of 0.5 to 29 GPa. Within that broad porosity range all of the models fit the experimental data quite well. However, it was evident that the

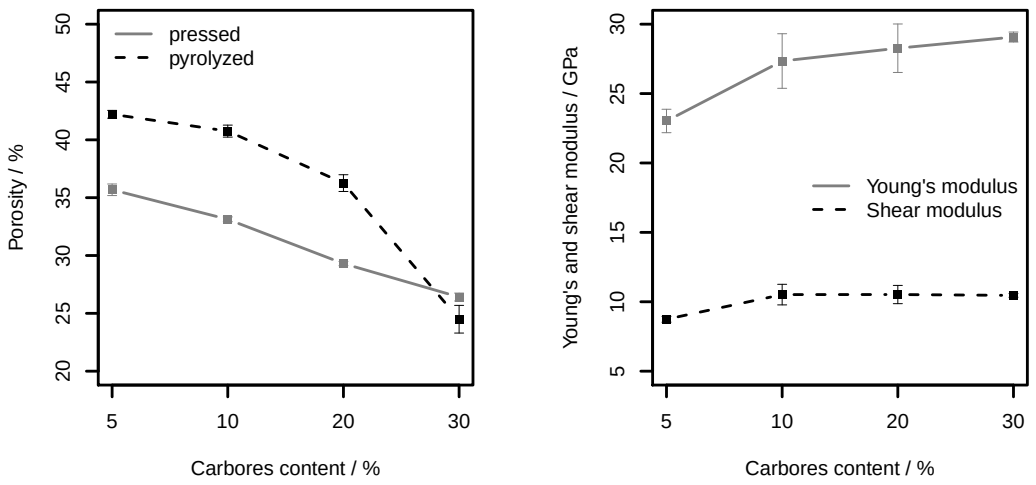

(a) Young's modulus **(b)** Shear modulus

Fig. 4.33.: Influence of the Carbores® content on the apparent porosity after the pressing / pyrolysis, on the Young's and shear modulus of a filter bulk material

Tab. 4.12.: Results of the Tukey range test with a p-value of 0.05 for the different Carbores® contents and response values (E, G); the values tested were evaluated at room temperature, $p < 0.05$ indicates significant differences between the tested pair

Carbores® pairs	p_E	p_G
$10 - 5$	0.0000805	0.0000111
$20 - 5$	0.0000016	0.0000070
$30 - 5$	0.0000001	0.0000134
$20 - 10$	**0.7236276**	**0.9999991**
$30 - 10$	**0.2187615**	**0.9979442**
$30 - 20$	**0.7860770**	**0.9972654**

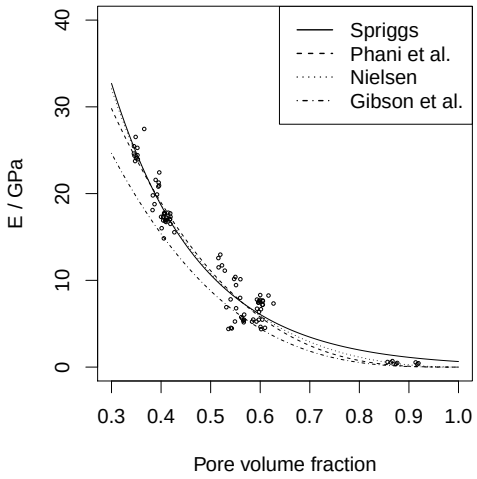

Fig. 4.34.: Young's modulus of the bulk and foam material (20 wt % Carbores® content) in dependence on the porosity; Models found in the literature were fitted against the experimental data to analyze their applicability for this composite material

Tab. 4.13.: Estimates of the model fits on the experimental data of $E(P)$ for the carbon-bonded bulk and foam material (20 wt % Carbores® content), $p < 0.05$ indicates significance of the estimates

Model	E_0 / GPa	p	Estimate 2	p
Spriggs [1961]	176.32	$< 2e-16$	5.62	$< 2e-16$
Nielsen [1984]	283.91	0.0519	0.08	0.08
Phani and Niyogi [1986]	84.84	$< 2e-16$	2.93	$< 2e-16$
Gibson and Ashby [1997]	73.51	$< 2e-16$	3.06	$< 2e-16$

Spriggs model did not fit the highest porosity well. The reason therefore was explained in the chapter "State of the art". This model does not fulfill the boarder condition $p = 0 \longrightarrow E = 0$. On the other hand did the Gibson and Ashby model not fit the lower porosity data well, which was not surprising since it was proposed for cellular materials.

Furthermore, the estimates of the model fits (see Table 4.13) were quite different. The Nielsen and Spriggs model returned very high E_0 values whereas the Gibson and Ashby and Phani and Niyogi model returned significant lower values. The significance of these estimates was below 0.05 for all models except for Nielsen's model.

4.3.2. High temperature observations

The high temperature measurements were carried out only for the 20 wt % Carbores® content bulk samples, because this was the used amount for the foam structures as well.

Tab. 4.14.: Absolute Young's modulus values of the bulk material and the filter structure before the high temperature measurement (pyrolyzed at 800 °C)

Material	E / GPa
Bulk	≈ 20.0
Foam	≈ 0.5

The initial values of E are shown in Table 4.14. The Young's modulus of the foam structure should only be regarded as an approximate value since the equations for the calculation of E only are valid for homogeneous, isotropic materials. In Figure 4.35a the Young's modulus (normalized to the initial room temperature value) in dependence on the temperature is shown. Two measurement sets were carried out; one up to 1000 °C and the second up to 1450 °C. Two samples each set were investigated. The filter structure was also measured up to 1000 °C and only one sample was observed. The maximum temperature of 1000 °C was defined due to an increasing oxidation and further microstructural changes above this temperature which would disturb the analysis of the measurement especially of the filter structures.

The change of E for the bulk material is quite comparable to the evolution of E of the reference and industry related compositions discussed above. There was a slight decrease of E up to 500 °C. Above E increase up to the samples former pyrolysis temperature which was in this case 800°C. Above 800°C a small decrease was registered which was superimposed for the 1000°C measurement by an increase of E during the holding time. After holding at 1000 °C E remained almost constant 5 % above the initial value. Increasing the temperature above 1000 °C resulted in a strong decrease of E (-10 %) up to 1450 °C. In Figure 4.35c $E(T)$ of alumina is shown, to compare that decrease of the carbon-bonded alumina with the one obtained for pure alumina above 1200 °C.

During the holding time at 1450 °C E of the carbon-bonded alumina increased significantly, as seen also in the sections above. After the holding time there was an increase of E up to approximately 1000 °C. Below E remained constant at around 5 % of the initial value.

The values obtained for the filter structure were very strong scattered. Especially during holding a strong scattering could be observed. The trend of $E(T)$ however was comparable to that of the bulk samples. A decrease of E during heating up to 500 °C, followed by an increase up to the former pyrolysis and a small decrease up to 1000 °C. Nevertheless, during cooling E decreased instead of remaining constant. Thus, the residual E was around 15 % below the initial value.

Several problems came up during this experiment. Besides the mentioned oxygen attack

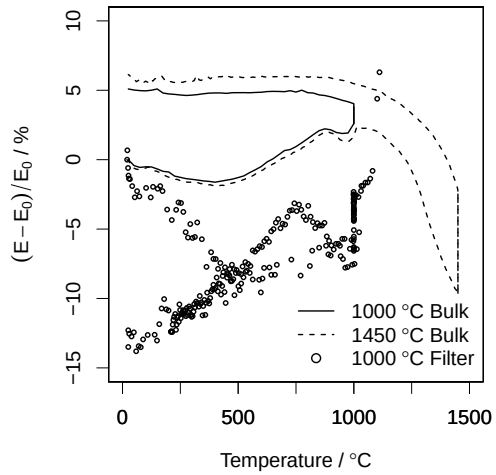

(a) Young's modulus

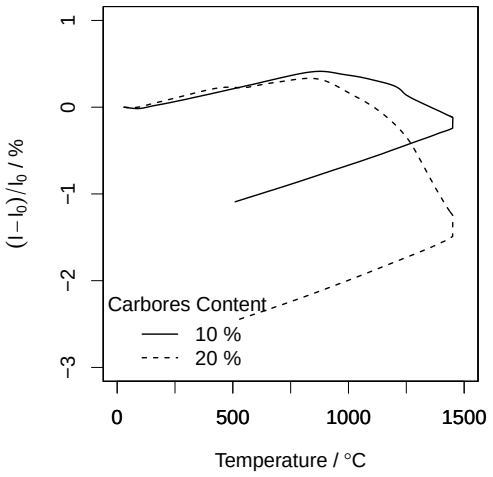

(b) Thermal expansion measurement

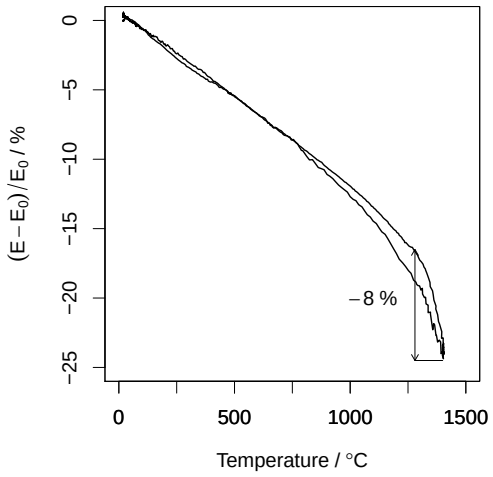

(c) HT E of alumina

Fig. 4.35.: Influence of the temperature on the Young's modulus and linear change of the bulk material and filter structures which were pyrolyzed at 800 °C; the Young's modulus dependent on the temperature of alumina is shown at the bottom for a comparison of the nonlinear decrease of E above 1200 °C of the alumina and the carbon-bonded alumina

due to residual oxygen within the furnace, the area of excitation of the filter was not even. Thus, the impact energy was not equal each time. Furthermore, it is not assured that a rectangular foam structure vibrates in the same way as a dense rectangular bar does. Additionally, the measurement of the foam dimensions added uncertainty.

Thermal expansion measurements were carried out for a 20 wt % and a 10 wt % Carbores® bulk material sample. The lower amount of binder was investigated to obtain the contribution of the binder on the thermal expansion of this composite material (see Figure 4.35b).
Both compositions showed a similar almost linear expansion behavior up to the former pyrolysis temperature ($0.3 - 0.4\,\%$). Above, the expansion turned into a shrinkage and the intensity of shrinkage was dependent on the Carbores® content because the 20 wt % sample shrunk 1.5 % up to 1450 °C while the shrinkage was only 0.24 % for the 10 wt % composition. The cooling behavior was similar again for both compositions. A linear decrease with the same slope.

4.3.3. Discussion

The influence of the Carbores® content on the elasticity of the bulk material at room temperature is important for the filter design and probable finite element computation. To exclude an influence of the Carbores® content on the porosity of the samples, their apparent porosity after the pressing was investigated. A clear linear decrease of the porosity with increasing Carbores® content revealed its significant influence on the pressing behavior. The Carbores® improved the compaction of the material either by optimizing the particle size distribution (filling the space particles) or by acting as a lubricant during pressing. Likely, both mechanism contributed to this result.
The results revealed a slight increase of E with increasing the binder content. However, the lower porosity of the higher Carbores® containing compositions contributed certainly to this effect. Therefore, it can be concluded that an increase of E was not only affected by an increase of the binder but also by an enhancement of the compaction process due to the higher binder amount. Klemm et al. [2013] found a relationship between the cold modulus of rupture (CMOR) and the Carbores® content. With increasing binder content CMOR increased, too. The same conclusion was found by Soltysiak et al. [2013] for the effective strength evaluated by means of a small punch test. These results are quite contrary to the Young's modulus results in dependence on the binder content. However, the material investigated in those studies contained additional graphite and

carbon black. Furthermore, no porosity results were reported by Soltysiak et al. which complicates a comparison. Nevertheless, an increase of the strength of this material could be possible even without an increase of E. Since the bonding phase (coke like structure) was still the same, its stiffness has not to be changed by increasing its amount. But the strength could be improved due to a higher amount of bonds between the composite constituents.

The porosity dependence of the 20 wt % Carbores® bulk material and foam structure followed the assumed exponential like relationship. The different models fitted the experimental data in a very broad porosity range. As already explained in the literature, the model by Spriggs [1961] did not fit the data as well as the others. Furthermore, the estimates of the model by Nielsen [1984] were not significant. Therefore, both models might not be suitable for a prediction of E within the investigated porosity range. The models by Gibson and Ashby [1997] and Phani and Niyogi [1986] fitted the data quite well. Furthermore, the estimation of E_0, the Young's modulus of the pore free material, was quite in the same range (73 and 84 GPa). Therefore, these two models might be appropriate for E prediction within the investigated temperature range of this material. Furthermore, the power factor n of the Gibson and Ashby model was computed and found to be approximately 3. This parameter describes the cell structure of the foam and was found to be 2 for open cell foams. The constant C_1 was assumed to be 1 according to Gibson and Ashby [1997].

These results could be used for the design of foam structures or thermal shock prediction within the observed porosity range. A big drawback is still the uncertainty of E_0 and the problem of forming samples with different porosity without influencing the microstructure (for example due to organic pore forming agents). Further investigations should be made to clear this up.

The high temperature Young's modulus of the bulk material of the filter coating was found to be in accordance to the model introduced earlier (see section 4.1). A small decrease of E up to 500 °C was followed by an increase up to the former pyrolysis temperature. However, compared to the amount of E increase of the reference and industry compositions (70 to 150 %) the change of E for the bulk material was very small (2 %). Still it seems like some preexisting gaps or pores were closed up to the former pyrolysis temperature. A big difference between those earlier compositions and the bulk composition (AC4) was the maximum alumina particle size of $\approx 3\mu$m compared to 0.045 mm (the lowest maximum particle size of the reference compositions). This result confirms the theory of gap closing during reheating. Smaller particles retain smaller gaps and therefore lead to less E increase during reheating.

Above that, the behavior of the bulk and filter material differed significantly from that of the earlier compositions. E decreased very strong above 1000 °C up to 1450 °C. During cooling E increased in the same way as it decreased during heating. From about 1000 °C down to room temperature E remained constant. This cooling behavior was completely similar to that of common oxides like alumina or magnesia [Wachtman and Lam, 1959]. The nonlinear decrease above the former pyrolysis temperature might be induced due to two different mechanisms. Wachtman and Lam [1959] observed such a phenomena for polycrystalline alumina and attributed it to a "viscous slip of grain boundaries". Comparing $E(T)$ of alumina and the carbon-bonded bulk material shows a similar decrease of approximately 8 % down to 1400 °C. The second possible effect contributing to this nonlinear decrease would be a further transformation of the Carbores®. According to Dopita et al. [2014] in the temperature range of 800 to 1400 °C a significant increase of atoms within one graphitic layer (retained from the Carbores®), as well as an increase of these layers was observed. This on the other hand could be interpreted as a kind of densification since atoms were more ordered than before. Thus, a densification of one constituent could also lead to higher porosity inside a composite due to a volume shrinkage. These two mechanisms are likely to be the main reasons for the nonlinear decrease of E above the former pyrolysis temperature. Furthermore, the influence of the Carbores® on E was illustrated by the 1000 °C measurement of the bulk material. There was a similar increase of E after the measurement as for the 1450 °C cycle. This could be probably affected due to a further transformation of the Carbores® during the holding time. The thermal expansion measurement underlined the influence of the Carbores®. Above the former pyrolysis temperature the material started shrinking which was much stronger for the high Carbores® containing sample (20 wt %). This shrinkage might be a sign of densification either of the Carbores® or the alumina. Certainly this fine alumina could sinter already above 1000 °C. Therefore, it can not be determined exactly which phase densified.

The relative Young's modulus of the foam structure followed the same trend as the bulk material. This result is in accordance with the findings of Gibson and Ashby. They described E as a function of the bulk or strut material. Furthermore, they included the well known $E(T)$ equation by Wachtman et al. [1961] into their model, a linear dependence of E on T. However, due to the composite character of the strut material, which was described and explained earlier, such a linear dependence of E on T for the foam structure investigated in this study was not found. The difference between the bulk material and the filter structure during cooling might be caused by a slight oxidation attack, which could be much stronger for the foam structure since the attack-able surface

is much higher than that of the bulk material. Furthermore, the result revealed a strong scattering of the data since the response signal of the foam structure was damped very strong and the impulse area was quite uneven. Nevertheless, the measurement revealed clearly a link between bulk and foam material.

5. Experimental errors and error analysis

Generally, there are two different kinds of errors to distinguish. Systematic and random errors. Systematic errors often appear due to a wrong measurement setup for example using a not calibrated caliper (i.e. +1 mm). This means every measurement will be 1 mm above the true value. Often this is described as the accuracy of an experiment. It is not possible to increase the accuracy by a bigger amount of samples.
Random errors represent the uncertainty of an experiment and are often referred to in terms of precision. For example setting up an experiment with always the same initial conditions may be impossible (i.e. exact sample dimensions). Random errors can be calculated and mathematically expressed by a standard deviation or confidence interval of 95 %. In this case the presented values of a variable represent estimates. These estimates are equal to the true value with a certain probability (95 % for a confidence interval with $p < 0.05$).

In case of this study the main experiment carried out was the measurement of Young's modulus, shear modulus and Poisson's ratio. Systematic errors arising from this experiment could be:

- a wrong support distance which would affect the damping behavior
- a flawed thermocouple resulting in an erroneous temperature measurement
- residual oxygen within the furnace during the measurement under argon atmosphere

The last systematic error definitely was evident during the experiments of this study. The mass of the samples was measured before and after a measurement. Therefore, a mass loss could be connected to an oxidation caused by that residual oxygen. However, it was found that even a very small oxidation did affect the result of the high temperature measurement in a significant way.

Classical random errors like the measurement of the specimen dimensions and mass certainly contributed to the results presented above. At room temperature these errors

were taken into account due to the presentation of a mean value and a confidence interval for this value. Furthermore, many of the room temperature measurements were planned and carried out using design of experiments and the analysis formulas according to Montgomery [2001]. Within the presented effect diagrams a confidence interval was presented taking random errors into account. Furthermore, these effects were calculated using an effect matrix according to the principles of the design of experiments. Due to addition and subtraction with different algebraic pre signs a systematic error would be automatically eliminated. The introduced effect of residual oxygen within the furnace was a source of random errors, too. Even though the atmosphere provided within the furnace was always the same, due to the application of the same evacuation and purge cycles for all measurements, the samples differed. For example samples without graphite only contained a carbonaceous, amorphous carbon phase which was more prone for oxidation than graphite. Therefore, the same amount of oxygen affected the samples in a different way. This effect only could be suppressed by using an oxygen free atmosphere which is almost impossible using a furnace with highly porous lining material.

6. Summary and outlook

Thermal shock resistance is a key property of refractory materials. Its determination and prediction is essential for the design of structural refractories as well as lining materials. Young's modulus of elasticity is a crucial parameter for the calculation of thermal shock resistance. Providing information regarding high temperature elasticity could promote the design of new refractories.

In this study the elasticity of carbon bonded refractories was investigated. At first a series of industry related compositions was investigated to obtain an overview of the general high temperature elasticity of this material class. It was found that the pyrolysis temperature of these materials determined the Young's modulus. During reheating Young's modulus always increased up to the former pyrolysis temperature independently of the composition and porosity. Furthermore, at the maximum temperature of 1450°C an increase of E, attributed to sintering, was observed. Also characteristic for carbon-bonded materials was a hysteresis during cooling. After one measurement the residual Young's modulus was mostly lower than the initial one. A similar behavior was also found for the additionally carried out thermal expansion measurements. Below the former pyrolysis temperature the coefficient of thermal expansion (CTE) was lower than that above this temperature. This typical behavior was more or less found for all compositions and technological treatments.
A model was described based on literature findings and supported by the carried out experiments. Basically the behavior described above was a result of the composite nature of carbon bonded materials comprised from alumina, amorphous carbon and graphite. The coarse alumina and graphite particles are embedded in a matrix of fine alumina and amorphous carbon. Due to the CTE mismatch of these constituents, gaps were assumed around the coarse particles. These gaps formed during cooling after the pyrolysis since the alumina as well as the graphite were assumed to contract faster than the surrounding matrix. After reheating (during the $E(T)$-measurement) the constituents expanded again. Near the former pyrolysis temperature the former gaps were closed bit by bit.

Due to this closure the Young's modulus increased and also the expansion of the macroscopic sample increased because now the stronger expanding constituents contributed to the measured expansion behavior. It has to be emphasized that the porosity of the composite is assumed to remain open. The gaps between two materials (matrix/alumina) are assumed to be closed.

Besides this similar behavior significant influences of the composition and porosity on the Young's modulus were obtained. The type of binder (resin or modified pitch tar) did not influence the high temperature elasticity significantly, whereas the amount of binder affected that behavior remarkably. Increasing the binder content resulted in a decrease of the maximum E and lower residual E values after a measurement. The higher binder amount contributed to a lower volume fraction of coarse particles which affected the amount of gaps introduced in the matrix. Thus, less gaps were closed during reheating resulting in a lower E increase. Furthermore, the higher amount of amorphous carbon contributed to a lower overall expansion correlating with the $E(T)$ measurement.
The influence of the graphite amount and maximum alumina particle size on the elasticity was investigated at room and high temperature. It was found that both factors interact with each other. Thus, the main effects were dependent on the level of the second factor. The obtained results were compared to calculated Hashin and Shtrikman [1963] (HS) bounds. There was a big discrepancy between the calculated and measured values due to the heterogeneous nature of the material. The decreasing tendency of E was not represented in the direct measured values. However, the porosity contributed to these results whereas the HS-bounds did not take the porosity into account. Furthermore, the parameter b of the $E(P)$ model of Spriggs [1961] was calculated using the lower HS-bound and the experimental data. This parameter showed a clear dependence on the maximum alumina particle size but almost not on the graphite content. Therefore, it is assumed that the pore shape contributed to this result because different particle size distributions cause different pore shapes. Furthermore, other models from the literature already showed the pore shape influence. This is a possible task for future work to obtain the exact influence of the pore shape on the Young's modulus of carbon-bonded alumina.
The influence of the carbon amount and maximum particle size on the high temperature Young's modulus was not consistent as already observed at room temperature. The effect of the graphite content on $E(T)$ was dependent on the maximum particle size. Nevertheless, the maximum particle size had a global effect on $E(T)$. The overall increase of E during heating was lowest for the smallest particle size. In terms of thermal shock resistance it could be concluded that a lower elasticity during reheating might improve the thermal shock resistance. However, the initial values of E have to be considered

since the discussed Young's modulus evolution was always relative. Therefore, a global statement was not possible regarding the influence of both factors on the thermal shock resistance. Furthermore, the elasticity is just one part contributing to the thermal shock behavior.

In addition to the composition influence on the elastic behavior the contribution of different porosities was investigated, too. At room temperature, models found in the literature were applied to the experimental data. The fits of these models were satisfactory within the investigated porosity range ($14 - 21\,\%$ and $35 - 95\,\%$). Outside the investigated range the models differed remarkably. Furthermore, it was found that there is no model which describes the porosity of carbon bonded compositions within a porosity range of 0 to $90\,\%$ accurately. However, this was also found for oxide materials. Therefore, the appropriate model for the investigated porosity range has to be chosen carefully.
At high temperatures, the behavior described above was found for all porosities. The curves only differed quantitatively since the initial E values differed in dependence on the porosity. Thus, the porosity did not significantly influence the high temperature elasticity of the investigated materials.

Finally, the portability of the results obtained for coarse particle carbon-bonded refractories to fine grained bulk material and filter structures was investigated. The evolution of $E(T)$ of the bulk material as well as of the filter structures was comparable to the coarse particle samples. However, the overall change of $E(T)$ was in the range of $\pm 10\,\%$ which was very low compared to the coarse compositions (at least $\pm 50\,\%$). Compared to that compositions, this material might be regarded as more stable in terms of thermal shock resistance, however again the initial elasticity was quite high compared to the coarse samples. Furthermore, the measurement of a foam structure was successfully carried out. However, several problems occurred with that measurement questioning the results obtained for the foam structures. These problems should be addressed in further research projects.

These findings support the understanding of the microstructure evolution of carbon-bonded alumina in the temperature range of $25 - 1450°\mathrm{C}$. Furthermore, they might prepare the ground for further research connecting the high temperature Young's modulus measurement with the modeling of thermal shock resistance.

Bibliography

Andersson, C. A. (1996). Derivation of the exponential relation for the effect of ellipsoidal porosity on eleastic modulus. *Journal of the American Ceramic Society 79*(8), 2181–2184.

Aneziris, C. G., U. Klippel, W. Schärfl, V. Stein, and Y. Li (2007). Functional refractory material design for advanced thermal shock performance due to titania additions. *International Journal of Applied Ceramic Technology 4*(6), 481–489.

Auvray, J. M., C. Gault, M. Huger, and H. Lemercier (2001). Ultrasonic investigation of the mechanical behaviour at high temperature of alumina-spinel castables. *Key Engineering Materials 206-213*(213 PART 3), 1667–1670.

Bancroft, D. (1941, 04). The velocity of longitudinal waves in cylindrical bars. *Physical Review 59*(7), 588–593.

Baudson, H., F. Debucquoy, M. Huger, C. Gault, and M. Rigaud (1999). Ultrasonic measurement of Young's modulus of MgO-C refractories at high temperatures. *Journal of the European Ceramic Society 19*(10), 1895 – 1901.

Belrhiti, Y., A. Germaneau, P. Doumalin, J. Dupré, O. Pop, M. Huger, and T. Chotard (2013, September). Characterization of the mechanical behavior of magnesia spinel refractories using image correlation. In D. Gosky and J. Smith (Eds.), *UNITECR*, Volume 13, Victoria, B.C., Canada, pp. 36–41.

Boccaccini, D. N. and A. R. Boccaccini (1997). Dependence of ultrasonic velocity on porosity and pore shape in sintered materials. *Journal of Nondestructive Evaluation 16*, 187–192. 10.1023/A:1021891813782.

Boccaccini, D. N., M. Cannio, T. D. Volkov-Husoviae, E. Kamseu, M. Romagnoli, P. Veronesi, C. Leonelli, I. Dlouhy, and A. R. Boccaccini (2008). Service life prediction for refractory materials. *Journal of Materials Science 43*(12), 4079–4090.

Böhm, A., E. Skiera, C. Aneziris, S. Dudczig, and J. Malzbendera (2013, September). Temperature dependent thermo-mechanical behavior of novel alumina based refractories. In D. Gosky and J. Smith (Eds.), *UNITECR*, Volume 13, Victoria, B.C., Canada, pp. 42–47.

Bourret, J., N. Tessier-Doyen, B. Nait-Ali, F. Pennec, A. Alzina, C. S. Peyratout, and D. S. Smith (2013, 8). Effect of the pore volume fraction on the thermal conductivity and mechanical properties of kaolin-based foams. *Journal of the European Ceramic Society 33*(9), 1487–1495.

Bradt, R. C. (1993). Elastic moduli, strength and fracture characteristics of refractories. *Key Engineering Materials 88*, 165–192.

Brochen, E. (2011). *Measuring and modeling of thermal shock resistance of refractory materials*. Ph. D. thesis, TU Bergakademie Freiberg.

Buchebner, G., R. Neuböck, J. Eder, and J. Studnicka (2008). Thermomechanical design of magnesia-carbon bricks for steel ladles. In *51st international colloquium on refractories Aachen (Germany)*, pp. 70–72. European Centre for Refractories.

Carreon, H., A. Ruiz, A. Medina, G. Barrera, and J. Zarate (2009, 8). Characterization of the alumina-zirconia ceramic system by ultrasonic velocity measurements. *Materials Characterization 60*(8), 875–881.

Carter, C. and M.G.Norton (2007a). *Ceramic Materials, Science and Engineering*, Chapter 4, pp. 51–70. Springer Science and Business Media, LCC.

Carter, C. and M.G.Norton (2007b). *Ceramic Materials, Science and Engineering*, Chapter 16, pp. 294. Springer Science and Business Media, LCC.

Case, E. D., J. R. Smyth, and O. Hunter Jr. (1981, 12). Microcracking in large-grain Al_2O_3. *Materials Science and Engineering 51*(2), 175–179.

Chang, R. (1959, 7). High temperature creep and anelastic phenomena in polycrystalline refractory oxides. *Journal of Nuclear Materials 1*(2), 174–181.

Chotard, T., J. Soro, H. Lemercier, M. Huger, and C. Gault (2008). High temperature characterization of cordierite-mullite refractory by ultrasonic means. *Journal of the European Ceramic Society 28*(11), 2129 – 2135.

Coble, R. L. and W. D. Kingery (1956). Effect of porosity on physical properties of sintered alumina. *Journal of the American Ceramic Society 39*(11), 377–385.

Cowlard, F. C. and J. C. Lewis (1967). Vitreous carbon - a new form of carbon. *Journal of Materials Science 2*(6), 507–512.

Davies, R. M. (1948). A critical study of the Hopkinson pressure bar. *Philosophical Transactions of the Royal Society of London. Series A, Mathematical and Physical Sciences 240*(821), 375–457.

de Silva, C. W. (2005). *Vibration Damping, Control, and Design*, Chapter 1.2, pp. 2–4. CRC Press.

Dopita, M., M. Emmel, A. Salomon, M. Rudolph, Z. Matěj, C. G. Aneziris, and D. Rafaja (submitted 2014). Temperature evolution of microstructure of turbostratic high melting coal-tar resin carbores p studied using the x-ray scattering method. *Carbon*.

Dupuy, D., M. Huger, and T. Chotard (2013, September). Basic understanding of physical properties of carbon bonded refractory composites. In D. Gosky and J. Smith (Eds.), *UNITECR*, Volume 13, Victoria, B.C., Canada, pp. 64–67.

Emmel, M. and C. G. Aneziris (2012). Development of novel carbon bonded filter compositions for steel melt filtration. *Ceramics International 38*(6), 5165–5173.

Eto, M., T. Oku, and T. Konishi (1991). High temperature Young's modulus of a fine-grained nuclear graphite oxidized or prestressed to various levels. *Carbon 29*(1), 11–21.

Fitzer, E., W. Schaefer, and S. Yamada (1969, 12). The formation of glasslike carbon by pyrolysis of polyfurfuryl alcohol and phenolic resin. *Carbon 7*(6), 643–648.

Fogaing, E. Y., Y. Lorgouilloux, M. Huger, and C. P. Gault (2006). Young's modulus of zirconia at high temperature. *Journal of Materials Science 41*(22), 7663–7666.

Förster, F. (1937, April). Ein neues Messverfahren zur Bestimmung des Elastizitätsmoduls und der Dämpfung. *Zeitschrift fuer Metallkunde 29*(4), 109–115.

Franklin, S. and B. Tucker (1995). Hot strength and thermal shock resistance of magnesia-carbon refractories. *British Ceramic Transactions 94*(4), 151–156.

Gardziella, A. and J. Suren (1992). Carbon from phenolic resins: Carbon yield and volatile components - recent studies. *Interceram 41*(7/8), 461–467.

Gault, C., F. Platon, and D. Le Bras (1985, 9). Ultrasonic measurements of Young's modulus of Al_2O_3-based refractories at high temperatures. *Materials Science and Engineering 74*(1), 105–111.

Gerlich, D. and E. Fisher (1969). The high temperature elastic moduli of aluminum. *Journal of Physics and Chemistry of Solids 30*(5), 1197 – 1205.

Gibson, L. and M. Ashby (1997). *Cellular solids : structure and properties*. Cambridge University Press.

Guyer, R. A. and P. A. Johnson (2009). *Nonlinear mesoscopic elasticity*. Wiley-VCH Verlag GmbH & Co. KGaA.

Hampel, M. (2010). *Beitrag zur Eigenschaftsbewertung von feuerfesten Magnesiakohlenstofferzeugnissen*. Ph. D. thesis, TU Bergakademie Freiberg.

Hashin, Z. and S. Shtrikman (1963, 1963/4//). A variational approach to the theory of the elastic behaviour of multiphase materials. *Journal of the Mechanics and Physics of Solids 11*(2), 127–140.

Hasselman, D. (1969). Unified theory of thermal shock fracture initiation and crack propagation in brittle ceramics. *Journal of the American Ceramic Society 52*(11), 600–604.

Hasselman, D. P. H. (1963). Elastic energy at fracture and surface energy as design criteria for thermal shock. *Journal of the American Ceramic Society 46*(11), 535–540.

Holm, S. (1979). A simple sequentially rejective multiple test procedure. *Scandinavian Journal of Statistics 6*(2), 65–70.

Hudson, G. E. (1943, 01). Dispersion of elastic waves in solid circular cylinders. *Physical Review 63*(1-2), 46–51.

Iacono, S. T., M. W. Perpall, P. G. Wapner, W. P. Hoffman, and D. W. Smith Jr. (2007, 4). Carbonization and thermal expansion of glassy carbon derived from bis-ortho-diynylarenes. *Carbon 45*(5), 931–935.

Ide, J. M. (1936). Comparison of statically and dynamically determined Young's modulus of rocks. In *Proceedings of the National Academy of Sciences*, Volume 22, pp. 81–92.

Itoh, K. (1998, June). *Refactories Handbook*, Chapter II Alumina carbon (for steel casting), pp. 191–201. Japan: The Technical Association of Refractories.

Jain, A., A. Kathuria, A. Kumar, Y. Verma, and K. Murari (2013). Combined use of non-destructive tests for assessment of strength of concrete in structure. *Procedia Engineering 54*(0), 241–251.

Kingery, W. D. (1955). Factors affecting thermal stress resistance of ceramic materials. *Journal of the American Ceramic Society 38*(1), 3–15.

Kingery, W. D., H. K. Bowen, and D. Uhlmann (1976). *Introduction to ceramics, second edition*, Chapter Elasticity, anelasticity and strength, pp. 768–813. John Wiley & Sons, Inc.

Klemm, Y., H. Biermann, and C. G. Aneziris (2013, September). Different fabrication routes for carbon-bonded Al_2O_3-C and their influence on the physical and mechanical properties. In D. Gosky and J. Smith (Eds.), *UNITECR*, Volume 13, Victoria, B.C., Canada, pp. 543–548.

Knackstedt, M., C. Arns, M. Saadatfar, T. Senden, A. Sakellariou, A. Sheppard, R. Sok, W. Schrof, and H. Steininger (2005). Virtual materials design: Properties of cellular solids derived from 3D tomographic images. *Advanced Engineering Materials 7*(4), 238–243.

Knudsen, F. P. (1962). Effect of porosity on Young's modulus of alumina. *Journal of the American Ceramic Society 45*(2), 94–95.

Landau, L. D. and E. M. Lifshitz (1970). *Theory of elasticity* (2nd ed.). Pergamon Press.

Lee, W. E. (2012, August). Possible future applications of ceramics in the nuclear sector. In *Summer School on Inorganic Materials for Energy Conversion and Storage*, California, USA. UC Santa Barbara.

Li, X. and M. Rigaud (1993). Anisotropy of the properties of magnesia-graphite refractories – linear thermal change and carbon oxidation resistance. *Journal of the Canadian Ceramic Society 63*(3), 197–205.

Luz, A. P., T. Santos Jr., J. Medeiros, and V. C. Pandolfelli (2013, 8). Thermal shock damage evaluation of refractory castables via hot elastic modulus measurements. *Ceramics International 39*(6), 6189–6197.

MacKenzie, J. K. (1950). The elastic constants of a solid containing spherical holes. *Proceedings of the Physical Society. Section B 63*(1), 2–11.

Manhart, C. and H. Harmuth (2009). Resonant frequency and damping analysis of refractories with and without reduced brittleness. In *Unified International Technical Conference on Refractories*, Volume 11, Salvador, Bahia, Brazil.

Manhart, C., H. Harmuth, and G. Buchebner (2005). Elastic moduli of carbon-bonded magnesia refractories at elevated temperatures. In *UNITECR*, Volume 9, Orlando, Florida, USA, pp. 288–290.

Mason, I. B. and R. H. Knibbs (1960, 10). Variation with temperature of Young's modulus of polycrystalline graphite. *Nature 188*(4744), 33–35.

McKee, D. W. (1973, 2014/04/04). Carbon and graphite science. *Annual Review of Materials Science 3*(1), 195–231.

McSkimin, H. J. (1959). Measurement of ultrasonic wave velocities and elastic moduli for small solid specimens at high temperatures. *Journal of Acoustical Society of America 31*, 287.

Mileiko, S. T. (1997). Deformation and failure of composites. In S. Mileiko (Ed.), *Metal and Ceramic Based Composites*, Volume 12 of *Composite Materials Series*, Chapter 3, pp. 77 – 145. Elsevier.

Montgomery, D. C. (2001). *Design and Analysis of Experiments* (5th ed.). Wiley & Sons, Inc.

Munro, R. G. (1997). Evaluated material properties for a sintered alpha-alumina. *Journal of the American Ceramic Society 80*(8), 1919–1928.

Munro, R. G. (2004). Analytical representations of elastic moduli data with simultaneous dependence on temperature and porosity. *Journal of Research of the National Institute of Standards and Technology 109*(5), 497–503.

Nielsen, L. F. (1984). Elasticity and damping of porous materials and impregnated materials. *Journal of the American Ceramic Society 67*(2), 93–98.

Oshima, T. and F. McCarty (2012). *Factorial Analysis of Variance Statistically Significant Interactions: What's the next step?* (http://tinyurl.com/md72kr7 ed.). Atlanta, USA: Georgia State University.

Panteliou, S. D., T. G. Chondros, V. C. Argyrakis, and A. D. Dimarogonas (2001, 3). Damping factor as an indicator of crack severity. *Journal of Sound and Vibration 241*(2), 235–245.

Patapy, C., N. Gey, A. Hazotte, M. Humbert, D. Chateigner, R. Guinebretiere, M. Huger, and T. Chotard (2012, 11). Mechanical behavior characterization of high zirconia

fused-cast refractories at high temperature: Influence of the cooling stage on microstructural changes. *Journal of the European Ceramic Society 32*(15), 3929–3939.

Patapy, C., A. Proust, D. Marlot, M. Huger, and T. Chotard (2010, 11). Characterization by acoustic emission pattern recognition of microstructure evolution in a fused-cast refractory during high temperature cycling. *Journal of the European Ceramic Society 30*(15), 3093–3101.

Paul, A., D. Jayaseelan, S. Venugopal, E. Zapata-Solvas, J. Binner, B. Vaidhyanathan, A. Heaton, P. Brown, and W. Lee (2012). UHTC composites for hypersonic applications. *American Ceramic Society Bulletin 91*(1), 22–28.

Pereira, A. H., A. R. Nascimento, and J. d.A. Rodrigues (2010). Effect of non-linearity on Young's modulus and damping characterisation of high alumina refractory castables through the impuls excitation technique. In *53rd international colloquium on refractories Aachen (Germany)*, pp. 90–93. European Centre for Refractories.

Pereira, A. H. A., A. R. C. Nascimento, L. B. Otani, and J. de Anchieta Rodrigues (2011, October). The evaluation of thermal shock damage in refractory castables through non-linear resonance acoustic spectroscopy. In *UNITECR*, Volume 12, Kyoto, Japan.

Pereira, A. H. A., L. B. Otani, J. De Anchieta Rodrigues, N. Traon, T. Tonnesen, and R. Telle (2011). The influence of nonlinear elasticity on the accuracy of thermal shock damage evaluation by the impulse excitation technique. *InterCeram: International Ceramic Review 60*(6), 388–392.

Phani, K. K. and S. K. Niyogi (1986). Porosity dependence of ultrasonic velocity and elastic modulus in sintered uranium dioxide - a discussion. *Journal of Materials Science Letters 5*(4), 427–430.

Pickett, G. (1945a). Equations for computing elastic constants from flexural and torsional resonant frequencies of vibration of prisms and cylinders. In *Proceedings of the american society for testing materials*, Volume 45, pp. 846.

Pickett, G. (1945b). Flexural vibration of unrestrained cylinders and disks. *Journal of Applied Physics 16*, 820.

Pierson, H. (1997, Dec). *Handbook of refractory carbides and nitrides: Properties, characteristics, processing and applications*. Noyes Publications.

Pierson, H. O. (1993a). *Handbook of carbon, graphite, diamond, and fullerenes*, pp. 226–229. Park Ridges: Noyes Publications.

Pierson, H. O. (1993b). *Handbook of carbon, graphite, diamond, and fullerenes*, pp. 58 – 60. Park Ridges: Noyes Publications.

Poirier, J., A. Gasser, and P. Boisse (2005). Thermo-mechanical modelling of steel ladle refractory structures. *Interceram 54*(3), 182–188.

Puškár, A. (2001). *Internal friction of materials.* Cambridge International Science Publishing.

Quadling, A., L. Vandeperre, W. Lee, and P. Myers (2013, September). High temperature characteristics of refractory zirconia crucibles used for vacuum induction melting. In D. Gosky and J. Smith (Eds.), *UNITECR*, Volume 13, Victoria, B.C., Canada, pp. 102–107.

R Core Team (2013). *R: A Language and Environment for Statistical Computing.* Vienna, Austria: R Foundation for Statistical Computing.

Reed, J. S. (1995). *Principles of ceramics processing* (second ed.)., Chapter 8, pp. 426. Hoboken, USA: John Wiley & Sons Inc.

Reuss, A. (1929). Berechnung der Fließgrenze von Mischkristallen auf Grund der Plastizitätsbedingung für Einkristalle. *Journal of Applied Mathematics and Mechanics / Zeitschrift für Angewandte Mathematik und Mechanik 9*(1), 49–58.

Roebben, G., B. Bollen, A. Brebels, J. van Humbeeck, and O. van der Biest (1997). Impulse excitation apparatus to measure resonant frequencies, elastic moduli, and internal friction at room and high temperature. *Review of Scientific Instruments 68*(12), 4511–4515.

Roungos, V. and C. G. Aneziris (2012). Improved thermal shock performance of refractories due to nanoscaled additives. *Ceramics International 38*(2), 919–927.

Sabbagh, J., J. Vreven, and G. Leloup (2002). Dynamic and static moduli of elasticity of resin-based materials. *Dental Materials 18*, 64–71.

Salmang, H. and H. Scholze (2007). *Keramik*, Chapter Eigenschaften keramischer Werkstoffe, pp. 381–463. Springer Berlin Heidelberg.

Salvini, V. R., V. C. Pandolfelli, and R. C. Bradt (2012, 9). Extension of Hasselman's thermal shock theory for crack/microstructure interactions in refractories. *Ceramics International 38*(7), 5369–5375.

Savich, A. (1984). Generalized relations between static and dynamic indices of rock deformability. *Gidrotekhnieheskoe Stroitel'stvo 8*, 50–54.

Scheiner, S. M. and J. Gurevitch (Eds.) (1993). *Design and analysis of ecological experiments* (2nd ed.). London, England: Chapman & Hall.

Schmitt, N., Y. Berthaud, and J. Poirier (2000). Tensile behaviour of magnesia carbon refractories. *Journal of the European Ceramic Society 20*(12), 2239 – 2248.

Schulle, W., F. Tomsu, and J. Ulbricht (2000). Evaluation of the modulus of elasticity of refractories. *Ceramic Forum International 77*(4), 36–38.

Schwartz, B. (1952). Thermal stress failure of pure refractory oxides. *Journal of the American Ceramic Society 35*(12), 325–333.

Schwartzwalder, K. (1963). *Method of making porous ceramic articles.* Patent US 3,090,094.

Semler, C. E. (2014, March). Refractories - The world's most important but least known products. *American Ceramic Society Bulletin 93*(2), 34–39.

Shultz, R. L., R. Engel, R. G. Brenneman, and B. H. Baker (1986, October). Refractories for the steel industry - A diagnosis and prognosis. In *Fall Meeting of the Refractories Division of the American Ceramic Society.*

Soga, N. and O. L. Anderson (1966). High-temperature elastic properties of polycrystalline MgO and Al_2O_3. *Journal of The American Ceramic Society 49*(7), 355–359.

Soltysiak, S., M. Abendroth, and M. Kuna (2013, September). Influence of the cabores content on the strength of carbon bonded alumina obtained by means of small punch test. In D. Gosky and J. Smith (Eds.), *UNITECR*, Volume 13, Victoria, B.C., Canada, pp. 127–132.

Souza, T. M., A. P. M. Mati, M. A. M. Brito, and V. C. Pandolfelli (2014, 6). Oxidation protection system for hot elastic modulus evaluation of refractory ceramics. *Ceramics International 40*(5), 7595–7600.

Spinner, S. and W. Tefft (1961). A method for determining mechanical resonance frequencies and for calculating elastic moduli from these frequencies. In *Proceedings of the american society for testing materials*, Volume 61, pp. 1221–1238.

Spriggs, R. M. (1961). Expression for effect of porosity on elastic modulus of polycrystalline refractory materials, particularly aluminum oxide. *Journal of the American Ceramic Society 44*(12), 628–629.

Spriggs, R. M., L. A. Brisette, and T. Vasilos (1962). Effect of porosity on elastic and shear moduli of polycrystalline magnesium oxide. *Journal of the American Ceramic Society - Discussions and Notes 45*(8), 400.

Spriggs, R. M., J. B. Mitchell, and T. Vasilos (1964). Mechanical properties of pure, dense aluminum oxide as a function of temperature and grain size. *Journal of the American Ceramic Society 47*(7), 323–327.

Stanford, E. G. (1950). A contribution on the velocity of longitudinal elastic vibrations in cylindrical rods, and on the relationship between Young's modulus and temperature for aluminium. *Il Nuovo Cimento 7*(2), 332–340.

Stiffler, R. C. and D. P. H. Hasselman (1983). Shear moduli of composites with elliptical inclusions. *Journal of the American Ceramic Society 66*(3), C–52–C–53.

Tomšu, F. and J. Ulbricht (2009). Thermal shock resistance of refractory materials. *Keramische Zeitschrift 61*(4), 190–194.

Traon, N., T. Tonnesen, and R. Telle (2011, October). Correlation of different quenching techniques and resulting elastic properties of refractory castable formulations. In *UNITECR*, Volume 12, Kyoto, Japan.

Traon, N., T. Tonnesen, R. Telle, B. Myszka, and R. Silva (2013, September). Influence of the pore shape on the internal friction of refractory castables. In D. Gosky and J. Smith (Eds.), *UNITECR*, Volume 13, Victoria, B.C., Canada, pp. 133–138.

Tu, L. Y., J. N. Brennan, and J. A. Sauer (1955). Dispersion of ultrasonic pulse velocity in cylindrical rods. *Journal of Acoustical Society of America 27*, 550.

van Heerden, W. (1987). General relations between static and dynamic moduli of rocks. *International Journal of Rock Mechanics and Mining Sciences & Geomechanics Abstracts 24*(6), 381–385.

Voigt, W. (1889). Über die Beziehung zwischen den beiden Elasticitätsconstanten isotroper Körper. *Annalen der Physik 274*(12), 573–587.

Wachtman, J. and D. Lam (1959). Young's modulus of various refractory materials as a function of temperature. *Journal of the American Ceramic Society 42*(5), 255–260.

Wachtman, J. B. (Ed.) (1969, May). *Mechanical and Thermal Properties of Ceramics*, Volume 303. U.S. Department of Commerce, National Bureau of Standards.

Wachtman, Jr, J. B., W. Tefft, D. Lam, Jr., and C. Apstein (1961, 06). Exponential temperature dependence of Young's modulus for several oxides. *Physical Review 122*(6), 1754–1759.

Werner, J. and C. G. Aneziris (2012, September). Measurement of the young's modulus of elasticity of carbon-bonded alumina at elevated temperatures with the aid of the impulse excitation technique. In *International Colloquium on Refractories*, Volume 55, Aachen, Germany, pp. 82–84.

Werner, J. and C. G. Aneziris (2013, September). Contribution of different binder systems to young's modulus of elasticity of carbon-bonded alumina at elevated temperatures. In D. Gosky and J. Smith (Eds.), *UNITECR*, Volume 13, Victoria, B.C., Canada, pp. 139–144.

Werner, J., C. G. Aneziris, and S. Dudczig (2013). Young's modulus of elasticity of carbon-bonded alumina materials up to 1450 °C. *Journal of the American Ceramic Society 96*(9), 2958–2965.

Werner, J., C. G. Aneziris, and S. Schafföner (2014, 11). Influence of porosity on Young's modulus of carbon-bonded alumina from room temperature up to 1450 °C. *Ceramics International 40*(9, Part A), 14439–14445.

Werner, J., C. G. Aneziris, S. Schafföner, J. Fruhstorfer, M. Oppelt, and S. Dudczig (2013, September). Impulse excitation measurement up to 1600 °C - an advanced analysis technique for refractories. In *International Colloquium on Refractories*, Volume 56, Aachen, Germany, pp. 138–140.

Wolfenden, A. (Ed.) (1990). *Dynamic Elastic Modulus Measurements in Materials*, pp. 198. American Society for Testing Materials.

Yamaguchi, A. (2007). Self-repairing function in the carbon-containing refractory. *International Journal of Applied Ceramic Technology 4*(6), 490–495.

Zhang, L., J. M. F. Ferreira, S. Olhero, L. Courtois, T. Zhang, E. Maire, and J. C. Rauhe (2012, 6). Modeling the mechanical properties of optimally processed cordierite-mullite-alumina ceramic foams by x-ray computed tomography and finite element analysis. *Acta Materialia 60*(10), 4235–4246.

Zhang, S. W. (2006). Next generation carbon-containing refractory composites. In *Advances in Science and Technology*, Volume 45, pp. 2246.

A. Appendix

A.1. Additional results

Complete confidential plots and ANOVA tables can be found within this section.

A.1.1. Influence of graphite content and maximum particle size

Room temperature results

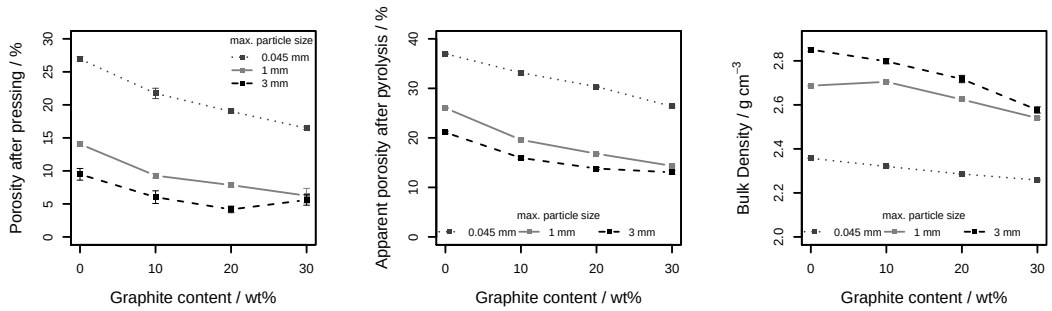

(a) Porosity after pressing **(b)** Apparent porosity **(c)** Bulk density

Fig. A.1.: Effect of the graphite content and maximum particle size on the porosity after pressing, apparent porosity and bulk density after pyrolysis at room temperature

Tab. A.1.: ANOVA statistic for the factors graphite content and maximum particle size on the porosity after pressing (PP) and after the pyrolysis (AP), as well as for the bulk density (BD)

Response	PP	AP	BD
Factor	p-value	p-value	p-value
Graphite amount	$< 2e-16$	$< 2e-16$	$< 2e-16$
max. particle size	$< 2e-16$	$< 2e-16$	$< 2e-16$
Interaction of both	$< 2e-16$	$< 2e-16$	$< 2e-16$

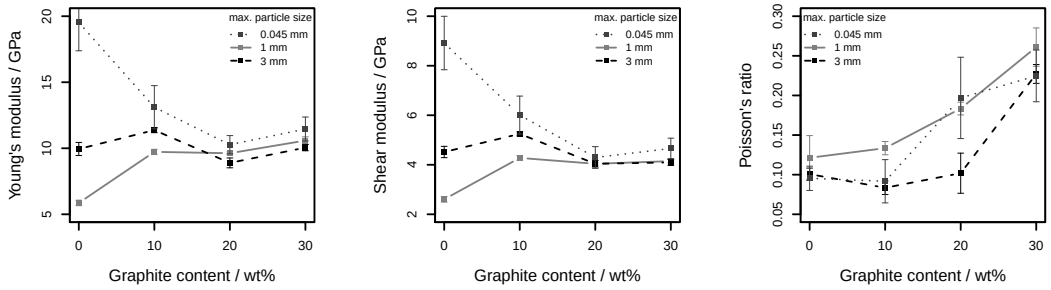

(a) Young's modulus **(b)** Shear modulus **(c)** Poisson's ratio

Fig. A.2.: Effect of the graphite content and maximum particle size on the Young's modulus, shear modulus and Poisson's ratio at room temperature

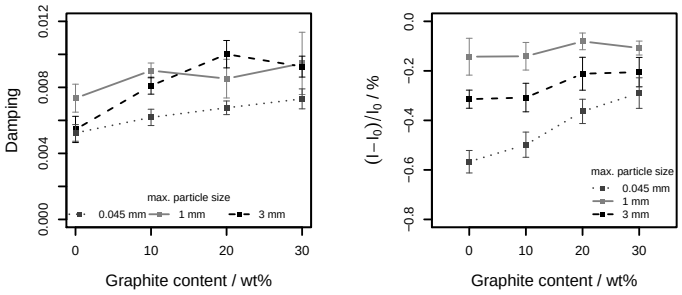

(a) Damping **(b)** $l - l_0/l_0$

Fig. A.3.: Effect of the graphite content and maximum particle size on the damping behavior and change in length of the sample at room temperature

Tab. A.2.: ANOVA summary of the Young's modulus in dependence on the factors A - graphite content and B - maximum particle size as well as on their interaction

```
             Df Sum Sq Mean Sq F value   Pr(>F)
A             3   82.8   27.62   18.41 1.02e-09 ***
B             2  469.5  234.75  156.50  < 2e-16 ***
A:B           6  591.1   98.52   65.68  < 2e-16 ***
Residuals   108  162.0    1.50
---
Signif. codes:  0 '***' 0.001 '**' 0.01 '*' 0.05 '.' 0.1 ' ' 1
```

Tab. A.3.: ANOVA summary of the shear modulus in dependence on the factors A - graphite content and B - maximum particle size as well as on their interaction

```
             Df Sum Sq Mean Sq F value   Pr(>F)
A             3  33.92   11.31   31.01 1.54e-14 ***
B             2 101.10   50.55  138.61  < 2e-16 ***
A:B           6 125.91   20.99   57.54  < 2e-16 ***
Residuals   108  39.39    0.36
---
Signif. codes:  0 '***' 0.001 '**' 0.01 '*' 0.05 '.' 0.1 ' ' 1
```

Tab. A.4.: ANOVA summary of the Poisson's ratio in dependence on the factors A - graphite content and B - maximum particle size as well as on their interaction

```
             Df Sum Sq Mean Sq F value   Pr(>F)
A             3 0.3586 0.11953 103.435  < 2e-16 ***
B             2 0.0433 0.02167  18.751 1.02e-07 ***
A:B           6 0.0360 0.00599   5.188 0.000101 ***
Residuals   108 0.1248 0.00116
---
Signif. codes:  0 '***' 0.001 '**' 0.01 '*' 0.05 '.' 0.1 ' ' 1
```

Tab. A.5.: ANOVA summary of the damping in dependence on the factors A - graphite content and B - maximum particle size as well as on their interaction

```
             Df    Sum Sq   Mean Sq F value   Pr(>F)
A             3 1.317e-04 4.389e-05  30.679 2.17e-14 ***
B             2 1.106e-04 5.528e-05  38.641 2.34e-13 ***
A:B           6 3.759e-05 6.270e-06   4.379 0.000539 ***
Residuals   107 1.531e-04 1.430e-06
---
Signif. codes:  0 '***' 0.001 '**' 0.01 '*' 0.05 '.' 0.1 ' ' 1
1 observation deleted due to missingness
```

Tab. A.6.: ANOVA summary of the apparent porosity in dependence on the factors A - graphite content and B - maximum particle size as well as on their interaction

```
             Df Sum Sq Mean Sq F value Pr(>F)
A             3   1691   563.7  5187.3 <2e-16 ***
B             2   5526  2763.2 25429.7 <2e-16 ***
A:B           6     68    11.3   103.6 <2e-16 ***
Residuals   108     12     0.1
---
Signif. codes:  0 '***' 0.001 '**' 0.01 '*' 0.05 '.' 0.1 ' ' 1
```

Tab. A.7.: ANOVA summary of the bulk density in dependence on the factors A - graphite content and B - maximum particle size as well as on their interaction

```
             Df Sum Sq Mean Sq F value Pr(>F)
A             3  0.541  0.1803  1453.1 <2e-16 ***
B             2  4.078  2.0388 16432.5 <2e-16 ***
A:B           6  0.108  0.0179   144.5 <2e-16 ***
Residuals   108  0.013  0.0001
---
Signif. codes:  0 '***' 0.001 '**' 0.01 '*' 0.05 '.' 0.1 ' ' 1
```

Tab. A.8.: ANOVA summary of the porosity after pressing in dependence on the factors A - graphite content and B - maximum particle size as well as on their interaction

```
             Df Sum Sq Mean Sq F value Pr(>F)
A             3    964   321.2  399.98 <2e-16 ***
B             2   4825  2412.7 3004.72 <2e-16 ***
A:B           6    121    20.1   25.09 <2e-16 ***
Residuals   107     86     0.8
---
Signif. codes:  0 '***' 0.001 '**' 0.01 '*' 0.05 '.' 0.1 ' ' 1
1 observation deleted due to missingness
```

Tab. A.9.: ANOVA summary of the linear change in length of the samples after the pyrolysis in dependence on the factors A - graphite content and B - maximum particle size as well as on their interaction

```
             Df Sum Sq Mean Sq F value   Pr(>F)
A             3 0.4450  0.1483  27.505 3.31e-13 ***
B             2 1.8870  0.9435 174.949  < 2e-16 ***
A:B           6 0.1667  0.0278   5.151 0.000112 ***
Residuals   105 0.5663  0.0054
---
Signif. codes:  0 '***' 0.001 '**' 0.01 '*' 0.05 '.' 0.1 ' ' 1
3 observations deleted due to missingness
```

Tab. A.10.: ANOVA summary of the Young's modulus from room temperature to 1450°C of the 0.045 mm compositions in dependence on the factors B - graphite content and D - temperature as well as on their interaction

```
Error: C
  Df Sum Sq Mean Sq
B  2  837.9   418.9

Error: Within
           Df Sum Sq Mean Sq F value Pr(>F)
B           3  20160    6720  329.32 <2e-16 ***
D          29 227323    7839  384.15 <2e-16 ***
B:D        87  35229     405   19.84 <2e-16 ***
Residuals 232   4734      20
---
Signif. codes:  0 '***' 0.001 '**' 0.01 '*' 0.05 '.' 0.1 ' ' 1
```

High temperature measurement results

Tab. A.11.: Results of the pairwise Student's t-test (adjusted p-value according to the Holm-Bonferroni method [Holm, 1979]) of the temperature influence on E for the 0.045 mm compositions at heating; for each pair a p-value is shown, $p < 0.05$ indicates a significant difference

```
        Pairwise comparisons using paired t tests

data:  joern.up.0.045$E and joern.up.0.045$B

   0       10    20
10 7.3e-08 -     -
20 1.6e-10 0.057 -
30 1.1e-09 0.014 3.0e-07

P value adjustment method: holm
```

Tab. A.12.: ANOVA summary of the Young's modulus from 1450°C to room temperature of the 0.045 mm compositions in dependence on the factors B - graphite content and D - temperature as well as on their interaction

```
Error: C
  Df Sum Sq Mean Sq
B  2   1596   798.2

Error: Within
           Df Sum Sq Mean Sq F value   Pr(>F)
B           3 190678   63559 468.564  < 2e-16 ***
D          29 372837   12856  94.778  < 2e-16 ***
B:D        87  23982     276   2.032 2.53e-05 ***
Residuals 196  26587     136
---
Signif. codes:  0 '***' 0.001 '**' 0.01 '*' 0.05 '.' 0.1 ' ' 1
```

Tab. A.13.: Results of the pairwise Student's t-test (adjusted p-value according to the Holm-Bonferroni method [Holm, 1979]) of the temperature influence on E for the 0.045 mm compositions at cooling; for each pair a p-value is shown, $p < 0.05$ indicates a significant difference

```
        Pairwise comparisons using paired t tests

data:  joern.down.0.045$E and joern.down.0.045$B

   0       10      20
10 < 2e-16 -       -
20 < 2e-16 0.00035 -
30 < 2e-16 0.00045 4.5e-13

P value adjustment method: holm
```

Tab. A.14.: ANOVA summary of the Young's modulus during the soak time of the 0.045 mm compositions in dependence on the factors B - graphite content and D - time as well as on their interaction

```
Error: C
          Df Sum Sq Mean Sq F value Pr(>F)
Residuals  2   89.7   44.85

Error: Within
          Df Sum Sq Mean Sq F value   Pr(>F)
B          3   93.9   31.29   2.182   0.0953 .
D         11 1476.4  134.22   9.359 3.87e-11 ***
B:D       33  100.1    3.03   0.212   1.0000
Residuals 94 1348.0   14.34
---
Signif. codes:  0 '***' 0.001 '**' 0.01 '*' 0.05 '.' 0.1 ' ' 1
```

Tab. A.15.: Results of the pairwise Student's t-test (adjusted p-value according to the Holm-Bonferroni method [Holm, 1979]) of the graphite content influence on the soak time behavior of E for the 0.045 mm compositions; for each pair a p-value is shown, $p < 0.05$ indicates a significant difference

```
        Pairwise comparisons using paired t tests

data:  soak.0.045$E and soak.0.045$B

   0     10    20
10 0.011 -     -
20 1.000 0.145 -
30 1.000 0.027 1.000

P value adjustment method: holm
```

Tab. A.16.: ANOVA summary of the Young's modulus from room temperature to 1450°C of the 3 mm compositions in dependence on the factors B - graphite content and D - temperature as well as on their interaction

```
Error: C
          Df Sum Sq Mean Sq F value Pr(>F)
B          1  19.31   19.31    0.27  0.695
Residuals  1  71.61   71.61

Error: Within
           Df  Sum Sq Mean Sq F value Pr(>F)
B           3   55343   18448 1345.68 <2e-16 ***
D          29 1445427   49842 3635.82 <2e-16 ***
B:D        87   33355     383   27.97 <2e-16 ***
Residuals 237    3249      14
---
Signif. codes:  0 '***' 0.001 '**' 0.01 '*' 0.05 '.' 0.1 ' ' 1
```

Tab. A.17.: Results of the pairwise Student's t-test (adjusted p-value according to the Holm-Bonferroni method [Holm, 1979]) of the temperature influence on E for the 3 mm compositions at heating; for each pair a p-value is shown, $p < 0.05$ indicates a significant difference

```
        Pairwise comparisons using paired t tests

data:  joern.up.3$E and joern.up.3$B

   0       10      20
10 < 2e-16 -       -
20 < 2e-16 5.2e-05 -
30 < 2e-16 < 2e-16 1.9e-14

P value adjustment method: holm
```

Tab. A.18.: ANOVA summary of the Young's modulus from 1450°C to room temperature of the 3 mm compositions in dependence on the factors B - graphite content and D - temperature as well as on their interaction

```
Error: C
          Df Sum Sq Mean Sq F value Pr(>F)
B          1  596.9   596.9   0.835  0.529
Residuals  1  715.1   715.1

Error: Within
           Df  Sum Sq Mean Sq F value Pr(>F)
B           3   10223    3408   37.28 <2e-16 ***
D          29 1286356   44357  485.22 <2e-16 ***
B:D        87   63944     735    8.04 <2e-16 ***
Residuals 236   21574      91
---
Signif. codes:  0 '***' 0.001 '**' 0.01 '*' 0.05 '.' 0.1 ' ' 1
```

Tab. A.19.: Results of the pairwise Student's t-test (adjusted p-value according to the Holm-Bonferroni method [Holm, 1979]) of the temperature influence on E for the 3 mm compositions at cooling; for each pair a p-value is shown, $p < 0.05$ indicates a significant difference

```
        Pairwise comparisons using paired t tests

data:  joern.down.3$E and joern.down.3$B

   0      10      20
10 0.0054 -       -
20 0.1284 9.2e-05 -
30 0.8996 0.0034  0.0114

P value adjustment method: holm
```

Tab. A.20.: ANOVA summary of the Young's modulus during the soak time of the 3 mm compositions in dependence on the factors B - graphite content and D - time as well as on their interaction

```
Error: C
  Df Sum Sq Mean Sq
B  1  33.27   33.27

Error: Within
          Df Sum Sq Mean Sq F value   Pr(>F)
B          3  540.2  180.07 186.479  < 2e-16 ***
D         11    8.9    0.81   0.841    0.602
B:D       33  106.6    3.23   3.345 9.86e-05 ***
Residuals 45   43.5    0.97
---
Signif. codes:  0 '***' 0.001 '**' 0.01 '*' 0.05 '.' 0.1 ' ' 1
```

Tab. A.21.: Results of the pairwise Student's t-test (adjusted p-value according to the Holm-Bonferroni method [Holm, 1979]) of the graphite content influence on the soak time behavior of E for the 3 mm compositions; for each pair a p-value is shown, $p < 0.05$ indicates a significant difference

```
        Pairwise comparisons using paired t tests

data:  soak.3$E and soak.3$B

   0       10      20
10 8.2e-08 -       -
20 3.0e-10 1.9e-09 -
30 5.4e-08 1.2e-05 1.2e-05

P value adjustment method: holm
```

Tab. A.22.: ANOVA summary of the Young's modulus from room temperature to 1450°C of the 1 mm compositions in dependence on the factors B - graphite content and D - temperature as well as on their interaction

```
Error: C
          Df Sum Sq Mean Sq F value Pr(>F)
Residuals  2   83.6    41.8

Error: Within
           Df  Sum Sq Mean Sq F value Pr(>F)
B           3   34661   11554  914.47 <2e-16 ***
D          29 1064931   36722 2906.49 <2e-16 ***
B:D        87   35455     408   32.26 <2e-16 ***
Residuals 238    3007      13
---
Signif. codes:  0 '***' 0.001 '**' 0.01 '*' 0.05 '.' 0.1 ' ' 1
```

Tab. A.23.: Results of the pairwise Student's t-test (adjusted p-value according to the Holm-Bonferroni method [Holm, 1979]) of the temperature influence on E for the 1 mm compositions at heating; for each pair a p-value is shown, $p < 0.05$ indicates a significant difference

```
        Pairwise comparisons using paired t tests

data:  joern.up.1$E and joern.up.1$B

   0       10      20
10 3.8e-16 -       -
20 1.2e-09 0.00029 -
30 4.1e-14 4.9e-11 < 2e-16

P value adjustment method: holm
```

Tab. A.24.: ANOVA summary of the Young's modulus from 1450°C to room temperature of the 1 mm compositions in dependence on the factors B - graphite content and D - temperature as well as on their interaction

```
Error: C
  Df Sum Sq Mean Sq
B  2  13730    6865

Error: Within
           Df Sum Sq Mean Sq F value Pr(>F)
B           3  36919   12306  73.754 <2e-16 ***
D          29 807772   27854 166.934 <2e-16 ***
B:D        87 104879    1206   7.225 <2e-16 ***
Residuals 177  29534     167
---
Signif. codes:  0 '***' 0.001 '**' 0.01 '*' 0.05 '.' 0.1 ' ' 1
```

Tab. A.25.: ANOVA summary of the Young's modulus during the soak time of the 1 mm compositions in dependence on the factors B - graphite content and D - time as well as on their interaction

```
Error: C
          Df Sum Sq Mean Sq F value Pr(>F)
Residuals  1  15.45   15.45

Error: Within
          Df Sum Sq Mean Sq F value   Pr(>F)
B          3  65.96  21.985   9.338 0.000211 ***
D          6  29.58   4.930   2.094 0.087206 .
B:D       18  27.82   1.545   0.656 0.821742
Residuals 27  63.57   2.354
---
Signif. codes:  0 '***' 0.001 '**' 0.01 '*' 0.05 '.' 0.1 ' ' 1
```

Tab. A.26.: Results of the pairwise Student's t-test (adjusted p-value according to the Holm-Bonferroni method [Holm, 1979]) of the graphite content influence on the soak time behavior of E for the 1 mm compositions; for each pair a p-value is shown, $p < 0.05$ indicates a significant difference

```
        Pairwise comparisons using paired t tests

data:  soak.1$E and soak.1$B

   0      10      20
10 0.1813 -       -
20 0.0205 9.4e-05 -
30 0.0205 0.0049  0.1813

P value adjustment method: holm
```

Tab. A.27.: ANOVA summary of the Young's modulus in dependence on the factors A - particle size and B - graphite content as well as on their interaction after the high temperature measurement

```
            Df Sum Sq Mean Sq F value   Pr(>F)
A            2  15403    7701 142.007 5.01e-14 ***
B            3   5168    1723  31.763 1.60e-08 ***
A:B          6   1183     197   3.634   0.0104 *
Residuals   24   1302      54
---
Signif. codes:  0 '***' 0.001 '**' 0.01 '*' 0.05 '.' 0.1 ' ' 1
```

Tab. A.28.: ANOVA summary of the mass loss in dependence on the factors A - particle size and B - graphite content as well as on their interaction after the high temperature measurement

```
            Df Sum Sq Mean Sq F value   Pr(>F)
A            2 1.2129  0.6064  19.364 9.84e-06 ***
B            3 0.4258  0.1419   4.532   0.0118 *
A:B          6 0.5951  0.0992   3.167   0.0197 *
Residuals   24 0.7516  0.0313
---
Signif. codes:  0 '***' 0.001 '**' 0.01 '*' 0.05 '.' 0.1 ' ' 1
```

Tab. A.29.: ANOVA summary of the porosity change in dependence on the factors A - particle size and B - graphite content as well as on their interaction after the high temperature measurement

```
            Df Sum Sq Mean Sq F value   Pr(>F)
            Df Sum Sq Mean Sq F value   Pr(>F)
A            2  5.913  2.9565  18.254 1.52e-05 ***
B            3  4.641  1.5470   9.552 0.000246 ***
A:B          6  2.854  0.4756   2.937 0.027120 *
Residuals   24  3.887  0.1620
---
Signif. codes:  0 '***' 0.001 '**' 0.01 '*' 0.05 '.' 0.1 ' ' 1
```

A.1.2. Influence of carbon filler type and maximum particle size

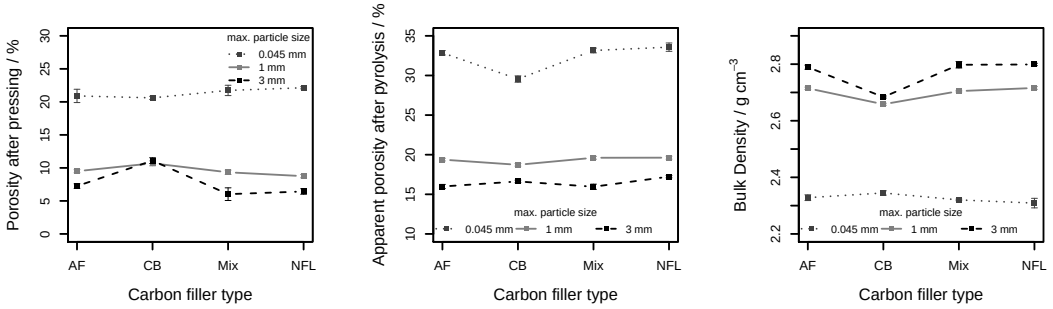

(a) Porosity after pressing **(b)** Apparent porosity **(c)** Bulk density

Fig. A.4.: Effect of the carbon filler type and maximum particle size on the porosity after pressing, apparent porosity and bulk density after pyrolysis at room temperature

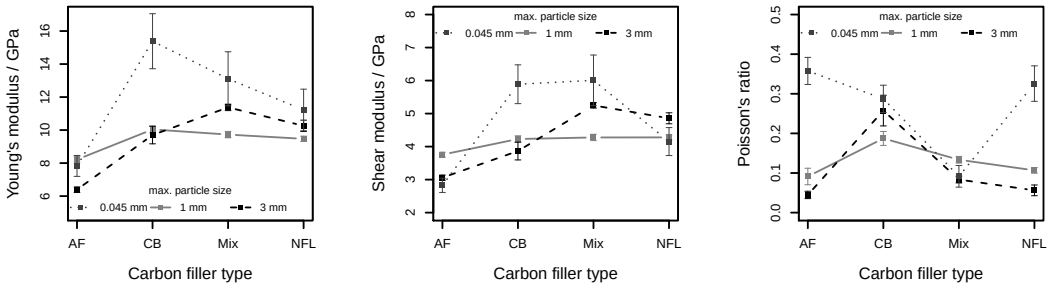

(a) Young's modulus **(b)** Shear modulus **(c)** Poisson's ratio

Fig. A.5.: Effect of the carbon filler type and maximum particle size on the Young's modulus, shear modulus and Poisson's ratio at room temperature

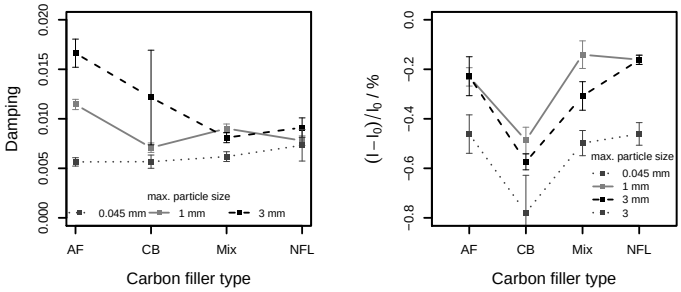

(a) Damping **(b)** $l - l_0/l_0$

Fig. A.6.: Effect of the carbon filler type and maximum particle size on the damping behavior and change in length of the sample at room temperature

Tab. A.30.: ANOVA summary of the Young's modulus in dependence on the factors A - carbon filler type and B - maximum particle size as well as on their interaction

```
             Df Sum Sq Mean Sq F value   Pr(>F)
A             3  324.6  108.21   88.74  < 2e-16 ***
B             2  153.2   76.58   62.80  < 2e-16 ***
A:B           6  123.4   20.56   16.86 1.39e-13 ***
Residuals   106  129.3    1.22
---
Signif. codes:  0 '***' 0.001 '**' 0.01 '*' 0.05 '.' 0.1 ' ' 1
2 observations deleted due to missingness
```

Tab. A.31.: ANOVA summary of the shear modulus in dependence on the factors A - carbon filler type and B - maximum particle size as well as on their interaction

```
             Df Sum Sq Mean Sq F value   Pr(>F)
A             3  61.86  20.619  103.11  < 2e-16 ***
B             2   6.69   3.347   16.74 4.81e-07 ***
A:B           6  36.98   6.163   30.82  < 2e-16 ***
Residuals   106  21.20   0.200
---
Signif. codes:  0 '***' 0.001 '**' 0.01 '*' 0.05 '.' 0.1 ' ' 1
2 observations deleted due to missingness
```

Tab. A.32.: ANOVA summary of the Poisson's ratio in dependence on the factors A - carbon filler type and B - maximum particle size as well as on their interaction

```
             Df Sum Sq Mean Sq F value Pr(>F)
A             3 0.2815 0.09384   78.66 <2e-16 ***
B             2 0.5780 0.28900  242.26 <2e-16 ***
A:B           6 0.4680 0.07800   65.38 <2e-16 ***
Residuals   106 0.1265 0.00119
---
Signif. codes:  0 '***' 0.001 '**' 0.01 '*' 0.05 '.' 0.1 ' ' 1
2 observations deleted due to missingness
```

Tab. A.33.: ANOVA summary of the damping in dependence on the factors A - carbon filler type and B - maximum particle size as well as on their interaction

```
             Df    Sum Sq   Mean Sq F value   Pr(>F)
A             3 0.0002343 7.811e-05   18.80 7.47e-10 ***
B             2 0.0005397 2.699e-04   64.97  < 2e-16 ***
A:B           6 0.0003330 5.549e-05   13.36 3.15e-11 ***
Residuals   106 0.0004403 4.150e-06
---
Signif. codes:  0 '***' 0.001 '**' 0.01 '*' 0.05 '.' 0.1 ' ' 1
2 observations deleted due to missingness
```

Tab. A.34.: ANOVA summary of the apparent porosity in dependence on the factors A - carbon filler type and B - maximum particle size as well as on their interaction

```
             Df Sum Sq Mean Sq  F value Pr(>F)
A             3     54    17.9   115.72 <2e-16 ***
B             2   5690  2845.0 18417.76 <2e-16 ***
A:B           6     65    10.9    70.25 <2e-16 ***
Residuals   108     17     0.2
---
Signif. codes:  0 '***' 0.001 '**' 0.01 '*' 0.05 '.' 0.1 ' ' 1
```

Tab. A.35.: ANOVA summary of the bulk density in dependence on the factors A - carbon filler type and B - maximum particle size as well as on their interaction

```
             Df Sum Sq Mean Sq F value Pr(>F)
A             3  0.049  0.0162   136.4 <2e-16 ***
B             2  4.522  2.2608 18977.7 <2e-16 ***
A:B           6  0.074  0.0124   103.7 <2e-16 ***
Residuals   108  0.013  0.0001
---
Signif. codes:  0 '***' 0.001 '**' 0.01 '*' 0.05 '.' 0.1 ' ' 1
```

Tab. A.36.: ANOVA summary of the porosity after pressing in dependence on the factors A - carbon filler type and B - maximum particle size as well as on their interaction

```
             Df Sum Sq Mean Sq F value Pr(>F)
A             3     64    21.4   37.71 <2e-16 ***
B             2   4379  2189.7 3859.96 <2e-16 ***
A:B           6    133    22.1   39.02 <2e-16 ***
Residuals   108     61     0.6
---
Signif. codes:  0 '***' 0.001 '**' 0.01 '*' 0.05 '.' 0.1 ' ' 1
```

Tab. A.37.: ANOVA summary of the linear change in length of the samples after the pyrolysis in dependence on the factors A - carbon filler type and B - maximum particle size as well as on their interaction

```
             Df Sum Sq Mean Sq F value Pr(>F)
A             3 2.2964  0.7655  90.224 <2e-16 ***
B             2 1.9285  0.9642 113.652 <2e-16 ***
A:B           6 0.1147  0.0191   2.254 0.0435 *
Residuals   107 0.9078  0.0085
---
Signif. codes:  0 '***' 0.001 '**' 0.01 '*' 0.05 '.' 0.1 ' ' 1
1 observation deleted due to missingness
```

Tab. A.38.: ANOVA summary of the porosity after the pressing in dependence on the factor A - Carbores® content

```
            Df Sum Sq Mean Sq F value Pr(>F)
A            3 2300.1   766.7   528.5 <2e-16 ***
Residuals   43   62.4     1.5
---
Signif. codes:  0 '***' 0.001 '**' 0.01 '*' 0.05 '.' 0.1 ' ' 1
1 observation deleted due to missingness
```

Tab. A.39.: Results of the Tukey range test with a p-value of 0.05 for the influence of the different Carbores® contents on the apparent porosity after the pressing; the values tested were evaluated at room temperature, $p < 0.05$ indicates significant differences between the tested pair

```
  Tukey multiple comparisons of means
    95% family-wise confidence level

Fit: aov(formula = AP ~ A, data = joern.charge1)

$A
            diff        lwr        upr     p adj
10-5   -1.455455  -2.799121  -0.111788 0.0291863
20-5   -5.950000  -7.264132  -4.635868 0.0000000
30-5  -17.718333 -19.032465 -16.404202 0.0000000
20-10  -4.494545  -5.838212  -3.150879 0.0000000
30-10 -16.262879 -17.606545 -14.919212 0.0000000
30-20 -11.768333 -13.082465 -10.454202 0.0000000
```

A.1.3. Young's modulus of carbon-bonded open cell foam structures

Tab. A.40.: ANOVA summary of the porosity after the pyrolysis in dependence on the factor A - Carbores® content

```
            Df Sum Sq Mean Sq F value Pr(>F)
A            3  503.4  167.79   775.7 <2e-16 ***
Residuals   36    7.8    0.22
---
Signif. codes:  0 '***' 0.001 '**' 0.01 '*' 0.05 '.' 0.1 ' ' 1
8 observations deleted due to missingness
```

Tab. A.41.: Results of the Tukey range test with a p-value of 0.05 for the influence of the different Carbores® contents on the porosity after the pyrolysis; the values tested were evaluated at room temperature, $p < 0.05$ indicates significant differences between the tested pair

```
  Tukey multiple comparisons of means
    95% family-wise confidence level

Fit: aov(formula = AP1 ~ A, data = joern.charge1)

$A
           diff       lwr       upr p adj
10-5  -2.554865 -3.115033 -1.994697     0
20-5  -6.380383 -6.940551 -5.820215     0
30-5  -9.272631 -9.832799 -8.712462     0
20-10 -3.825518 -4.385686 -3.265350     0
30-10 -6.717766 -7.277934 -6.157598     0
30-20 -2.892248 -3.452416 -2.332080     0
```